NTNU – Trondheim
Norwegian University of
Science and Technology

Ice-Induced Loads on Ship Hulls

Herman Holm

Marine Technology
Submission date: June 2012
Supervisor: Bernt Johan Leira, IMT

Norwegian University of Science and Technology
Department of Marine Technology

NTNU
Norwegian University of Science and Technology
Department of Marine Technology

Master Thesis, Spring 2012
for
Stud. Techn. Herman Holm

Ice-Induced Loads on Ship Hulls

Is-induserte Belastninger på Skipsskrog

There is an increasing need for transport and exploitation of resources in the northern areas. The climatic conditions in these areas represent a challenge both to the operation and design of ships under these conditions.

The presence of sea ice is the main factor hindering the operations in Arctic. Sea ice is a complex material and induces high pressures in contact with ships or structures. To understand how ice force is developed and acting, the ice physics and ice mechanics have to be studied. Methods for computation of ice loads are important in Arctic design and to ensure safe operation in ice covered areas.

The following subjects are to be examined:

1. Different types of sea ice and their mechanical/physical properties are to be described.

2. A review of DNV ice-class and IACS class rules and the corresponding procedures for calculation of ice pressure and hull scantlings is to be given.

3. Example calculations of ice pressure and resulting hull member design are to be performed to the extent that time allows. Comparison of ice classes e.g. in the DNV ICE/DNV POLAR/PC/Russian set of rules (or a selected subset of these rules) is to be made.

4. A finite element model for a part of the hull of KV Svalbard is to be established (based on modification of an existing model). Response analysis (i.e. stress calculations) are performed for this numerical model by application of relevant load cases which represent the ice pressure as obtained from item 3.

5. Comparison is made between computed and measured strains for a selected set of load cases for the vessel KV Svalbard. Estimation is to be made of the contributions from each of the selected load cases to the measured strain signals.

The work scope may prove to be larger than initially anticipated. Subject to approval from the supervisor, topics may be deleted from the list above or reduced in extent.

In the thesis the candidate shall present his personal contribution to the resolution of problems within the scope of the thesis work.

Theories and conclusions should be based on mathematical derivations and/or logic reasoning identifying the various steps in the deduction.

The candidate should utilise the existing possibilities for obtaining relevant literature.

The thesis should be organised in a rational manner to give a clear exposition of results, assessments, and conclusions. The text should be brief and to the point, with a clear language. Telegraphic language should be avoided.

The thesis shall contain the following elements: A text defining the scope, preface, list of contents, summary, main body of thesis, conclusions with recommendations for further work, list of symbols and acronyms, references and (optional) appendices. All figures, tables and equations shall be numbered.

The supervisor may require that the candidate, in an early stage of the work, presents a written plan for the completion of the work. The plan should include a budget for the use of computer and laboratory resources which will be charged to the department. Overruns shall be reported to the supervisor.

The original contribution of the candidate and material taken from other sources shall be clearly defined. Work from other sources shall be properly referenced using an acknowledged referencing system.

The thesis shall be submitted in 3 copies:

- Signed by the candidate
- The text defining the scope included
- In bound volume(s)
- Drawings and/or computer prints which cannot be bound should be organised in a separate folder.

Supervisor: Professor Bernt J. Leira

Deadline: June 10th 2012

Trondheim, January 16th, 2012

Bernt J. Leira

Preface

This report is an individual master thesis carried out during spring semester 2012 at the Department of Marine Technology, Norwegian University of Technology and Science, Trondheim. This master thesis followed up the project thesis in the fall semester of 2011

I would like to thank my supervisor Bernt J. Leira for helpful guidance and the willingness to discuss different aspects of the project. I would also like to thank fellow student Ivar Stange for helping me with the development of the Matlab script close to the deadline of this thesis and fellow students with the help with LaTeXcode.

Trondheim, June 10th, 2012

Herman Holm

Summary

The calculation of ice-induced loads on ships is still mainly based on empirical models. In order to gain a better physical understanding of the loading on ice-going vessels, Det Norske Veritas launched an *ice load monitoring* project involving full scale trials with the coastguard vessel KV Svalbard during the winters 2006, 2007 and 2011. The results from the full scale measurements conducted with KV Svalbard has been topic of several earlier master's thesis at NTNU,

The master thesis consists of four parts. The first part is a literature review of the mechanical and physical properties of sea ice.

The second part is a review of the rule sets developed by DNV and the IACS regarding vessels operating in ice infested waters. Both design principles and numerical values have been evaluated. The main difference between the designs principles used, is that IACS base their rules on a plastic method of approach, while DNV uses an elastic method. Despite the difference in the design principles, when comparing their numerical values turned out to be quite similar. The DNV rules are in general most conservative for the smaller vessels and the IACS rules the most conservative for large vessels.

The third part consists of a finite element study of a part of the bow on KV Svalbard. A systematic load scheme is used, consisting of 102 load cases. For each of the stress factors there where made graphs that showed the stress at the sensor location when moving the patch load. The sensor mounted on the frame were able to measure load that was within the frame loading area and sensor mounted on the stringer could measure stress for all of the load cases in the horizontal directions. One of the explanations for this is that the stringer transfers stress from the load patch area that could be measured by the sensors.

The last part consists of a comparison between measurements from the full scale trials and the results from the 102 load cases. This comparison is done through a weighted summation method where 5 different load cases are combined to represent the measured result, and a load factor is calculated for each load case for its contribution of the measured results. The stress component used in this comparison is the shear stress τ_{xy}.

The load cases were tested against the 11 measurements from the full scale trials. There were in total 11 load cases that gave positive factors for all of the 11 measurements at the same time. A figure was made to show which load cases were likely to contribute in the solution of the load cases. Load cases inside the frame loading area have the largest load factors for the solution of measurements.

This load decision scheme is very sensitive to the selection of load cases and boundary conditions. A change of the boundary conditions for the model was tried out for 7 load cases, and with changed boundary conditions, only 5 gave positive load factors.

The results of this thesis shows that is possible to find many solution to the measured result by combining many load case, but is it not possible to decide *the* solution.

Sammendrag

Beregningen av isinduserte belastninger på skip er fortsatt i hovedsak basert på empiriske modeller. For å få en bedre fysisk forståelse av de påførte lastene på isgående fartøy, lanserte Det Norske Veritas et *islast monteringen* prosjekt med fullskala forsøk på kystvaktfartøyet KV Svalbard i løpet av vinterene 2006, 2007 og 2011. Resultatene fra fullskala målinger utført med KV Svalbard har vært tema for flere tidligere masteroppgaver ved NTNU.

Masteroppgaven består av fire deler. Den første delen er en litteraturstudie av mekaniske og fysiske egenskaper av havis.

Den andre delen er en gjennomgang av regelsett utviklet av DNV og IACS om fartøy som opererer i isinfiserte farvann. Både designprinsipper og numeriske verdier har blitt evaluert. Hovedforskjellen mellom designprinsipper som brukes, er at IACS baserer sine regler på et plastisk tilnærmingsmåte, mens DNV benytter en elastisk metode. Til tross for forskjellen i designprinsipper er forskjellen liten når man sammenligner de nummerike effektene av regelsettene. DNVs Reglene er generelt mest konservative for de mindre fartøyene og IACS er den mest konservative for store fartøy.

Den tredje delen består av en "finite element" analyse av en del av baugen på KV Svalbard. Et systematisk belastningsskjema brukes, bestående 102 lasttilfeller. For hver av de ulike spenningsfaktorene er det laget grafer som viser den målte spenningen for hver sensor når man flytter lasttilfellet. Sensorer som monteres på rammen var i stand til å måle belastningen som var innenfor lasteområdet til rammen og sensorene montert på stringer kan måle spenninninger for alle lastetilfeller i den horisontale retningen. En av forklaringene på dette er det at stringer overfører spenninger fra lasttilfellet området som kan måles av sensorene.

Den siste delen består av en sammenligning mellom målinger fra fullskala forsøk og resultatene fra de 102 lastetilfellene. Denne sammenligningen er gjort gjennom en vektet summeringsmetode der 5 forskjellige lasttilfeller er kombinert for å kunne representere målt resultat, og en lastfaktor beregnes for hvert lasttilfelle sitt bidrag av de målte resultatene. Spenningskomponent som brukes i sammenligningene er skjærspenningen τ_{xy}.

Lasttilfellene ble testet mot de 11 målingene fra fullskala forsøk. Det var 11 lastetilfeller som ga positive lastfaktorer for alle de 11 målingene samtidig. En figur ble laget for å vise hvilke lasttilfeller som var egnet til å bidra i løsningen av de målte resultatene. Lasttilfeller innenfor i rammens belastningsområde har de største lastfaktorer for løsninger av de ulike målinger.

Denne vektede summeringsmetode er følsom for valg av lasttilfeller og grensebetingelser. En endring av grensebetingelser for modellen ble prøvd ut for 7 lasttilfeller som gav positive lastfaktorer, og kun 5 av dem gav dette etter nye grensebteingelser for modellen.

Resultatene av denne oppgaven viser at det er mulig å finne løsninger på de målte resultatene ved å kombinere mange lasttilfeller, men det er ikke mulig å bestemme *den ene* løsningen.

Contents

List of Figures

List of Tables

Chapter 1

Introduction

Over the recent years the activities related to exploitation of oil and gas resources activities in the Polar areas have a significant increased. A rapidly extending maritime transport industry has also pursued more efficient trading routes between Eastern Asia and Europe. The climatic conditions in these areas makes it challenging to design ships to operate in conditions. The presence of ice is the main factor for the complexity for operations in these regions.

At the present, the calculation of ice-induced loads on ships is mainly based on empirical methods due to the lack of a unified theory that is able to properly explaining the underlying physical mechanisms. As a response to these challenges Det Norske Veritas introduced the *Ice Load Monitoring* project. During the winters of 2006, 2007 and 2001 the coast guard vessel KV Svalbard was instrumented with strain gauges to enable a continuous monitoring of ice loads on the ship. One of the superior goals is to be able to create a decision support system that is cheap enough to be installed on all vessels operating in ice infested waters.

The intention of this thesis is to study the physical and mechanical properties of ice and review the present design rules. To be able to quantify these rules, a numerical comparison of these two sets of rules on design loads and plate thickness on different parts of the hull. Further, a finite element analysis is preformed to investigate stress response over a large area in the bow area of KV Svalbard. The final task is to apply the load decision scheme. The purpose of applying this scheme is to be able to identify the location and magnitude of the load acting on the hull based on the measured data from the strain sensors, by using the load cases from a finite element analysis.

Chapter 2

The Arctic Area

The Arctic areas have many different definitions, such as the Arctic Circle (66° 33' N). The most commonly used today is the 10 °C isotherm in July and this corresponds roughly to the tree line in the most of the arctic. (Riska, 2011)

Sea ice is found in many areas in the northern hemisphere. Most of this is found in the Arctic areas, where the Arctic Basin is mostly covered ice during the winter. The thickness of the sea ice here varies a lot from sea to sea. Where the ice is present the whole year, Multi-year ice, we could get ice thickness of 3-4 meters, and where the ice is only present during the winter we could expect 1-2m ice thickness. This type of first-year ice is also present in other areas of the northern hemisphere. Such as Baltic Sea, Bohai Bay, Sea of Okhotsk in Russia, Caspian Sea of Kazakhstan, Cook inlet in Alaska, and other rivers and lakes in the countries around the Arctic region. (Furnes, 2011)

The ice extent in the Arctic has changed a lot during the last centuries. The first ice charts dates back to 1553, but the following 3 centuries the observation of ice conditions remained irregular and infrequent. From the second half of the 19th century the collection of data has been sufficient enough to make continuous time series of ice maps for the summer season due to whale and seal hunting. But it's only the last 2-3 decades there been paid a substantial amount of attention to study the sea ice using satellites, aircraft, in situ observations and modelling.

The sea ice cover in the Arctic was in the summer of 2007 on its lowest point as long as we have measured the extent. There are many reasons for studying the sea ice in the Arctic. The increased research over the last couple of decades is done within many fields.

- Navigation
- Oil developments and transport of petroleum
- Exploration of mineral deposits in the Arctic
- The use of ice bergs as a source of fresh water

- Fisheries – The ice edge areas are very productive
- Climate studies

It is expected that there are a large reserve of undiscovered oil and gas resources in the Arctic area underneath the ice pack. If the ice pack melts, this area would be of high interest for oil companies and countries that could claim to own this area. This will also open up new shipping routes and possibly new fishing grounds. Many of the countries around the Arctic region try to claim as much of the area as they could, but there is no international agreement that formally agrees on how to divide the Arctic region between the neighbouring countries.

There is also challenging to develop and operate the arctic area because of the harsh and cold environment. Compared to other offshore oilfields, the arctic area offers lack of infrastructure, lower temperatures, ice and reduced daylight. Also the environment is much more sensitive to external influence such as oil spills and other hazards. To get an international accept to operate in this area, an arctic engineer requires designing a "bulletproof" system and needs knowledge about the ice behavior, physics and mechanical properties.

Chapter 3

Mechanical and Physical Properties of Sea Ice

The activity in the Arctic regions is increasing with the interest of expansion in the oil and gas exploration and shortened shipping routes through the arctic. But the presence of sea ice is the main factor for restricting these operations. To ensure safe and economical activities in these areas, this requires very careful and insightful engineering in these hostile and unusual operating conditions. Sea ice properties are depending on the environmental factors affecting the properties of the ice. This makes it challenging to design with respects to the ice properties and we have to study the different mechanical and physical properties and its variations within the different regions we want to operate in.

Some of the physical properties we will look at are microstructure, thickness, salinity and density. For the mechanical properties are tensile, flexural, shear and compressive strength (Weeks, 2009).

3.1 Microstructure and growth of sea ice

Sea ice is a material composed of solid ice, gas, brine and various types of solid salts depending on the temperature. Depending on different variations in the environmental conditions we could get very different grain structures. The common grain structures are granular, columnar and discontinuous columnar. When seawater freezes to ice, it tries to reject the salt present in the water. But it does not succeed to completely reject it all and some salt is trapped in brine pockets within the growing ice sheet. The amount of brine trapped is determined by different environmental factors such as salinity and growth rate, and if it is first-year ice or multi-year ice. Ice sheets usually m during the summer time, and some of the brine pockets are released. This makes multi-year to have less salinity than first year ice.

3.2 Ice Thickness

The thickness of ice is one of the most important parameters to determining ice loads on structures. The strength and how it fails are directly correlated to its thickness and heavily influence the size and thickness of pressure ridges. For engineering purposes, this is one of most important parameters to measure and predict.

For first-year ice, the thickness is directly coupled to the air temperature, freezing time, wind speed, snow type and thickness, surface radiation balance and ocean heat flux. The air temperature and freezing time is the governing factors, so areas as the Arctic would get the thickest ice. Through a winter season the maximum ice thickness could reach to about 2 meters. For multi-year ice, we could get very thick ice through a combination of thermal growth and consolidation of pressure-ridges.

3.3 Ice density

Ice density is another parameter that is important for many applications. Density determines the weight and the difference in density between the ice and sea water also determines the buoyancy force of the ice. The buoyancy force is one of the important factors when a vessel is moving through the ice cover and the loads a ridge keel could exert on a structure. But for structures it is also important to be able to estimate the weight in conditions where we could get ice pile-ups or pressure ridges against the structure.

3.4 Tensile strength

Tensile strength is a key property for sea ice and defines the maximum tensile stress the ice could sustain before failure. This is the key failure mode when ships and offshore interacts with ice. For level ice, ice is best broken in bending downwards and the necessary bending forces are related to the vertical tensile strength.

Measuring the true tensile strength is very difficult, unreliable and time consuming, and such test haven't been done in large extent. But those measured values that are taken, lays in the region between 0.2 and 2 MPa.

3.5 Flexural strength

The flexure strength of sea ice is not a basic material property, but it is important to know since many real sea ice failures occurs in this fashion. In pressure ridge formation, ice breaking vessels and bending of ice on conical-shaped structures, the flexural strength is of importance. Since flexural strength is easy to measure, there have been a large

number of experiments. The flexural strength ranges from 1 MPa and decreases with larger brine volume.

3.6 Shear strength

Shear strength is not frequently used in engineering practice since ice tends to fail in tension rather than in shear because of the tensile strength is normally lower. But it still is an important factor since ice interacting with structures is often subjected to a biaxial stress condition with tensile and compressive stresses or a shear stress.

3.7 Compressive strength

Since ice often tends to fail in compression, the compressive strength is another important material factor for ice. The failure mechanism can occur during the formation of large compression pressure ridges and by crushing against ship side or offshore structures. The factors that affects the compressive strength, as many as the other sea ice properties; are temperature, density, salinity, ice type, crystal size and orientation.

3.8 Different types of sea ice

(Furnes, 2011)

First-year ice: ice with more than 1 year's growth that develops from young ice. Thickness 30 cm to 2 m. Level when undeformed, but where ridges and hummocks occur, it is rough and sharply angular.

Multi-year ice: Ice more than 1 year's growth with thickness over 2 m. Hummocks and ridges are smooth and the ice is almost salt-free. Fast ice: Sea ice that remains fast along the coast, over shoals, or between grounded icebergs.

Pancake ice: Pieces of new ice, usually near circular shaped, about 30 cm to 3 m across. Upturned edges due to wave action (close to ice edge)

Ice floe: Flat piece of ice, typical >20 m across and >1 m thick

Level ice: Sea ice that is unaffected by deformation

Rafted ice: A form of pressure ice in which one floes overrides another

Brash ice: Accumulations of ice made up of fragments no more than 2 m across. Often found in channels where icebreakers have made fairways for other ships

Ridges: A ridge or wall of broken ice forced up by pressure. The upper-above water level-part is called SAIL and the lower part KEEL

Chapter 4

Classification of Ships Operating in Ice Infested Waters

4.1 Introdution

All commercial vessels, including most icebreakers are classified to rules develop by different classifications societies. Most of the class societies have divided their rules for Ships Navigation into two different categories, being Ice classes for Arctic and Icebreaking service, and for Baltic ice classes. Baltic Ice class rules are for the most based on the "Finnish-Swedish Ice Class Rules". (Riska, 2011)

The Russian Maritime Register of Shipping (RS) does not have specific rules for the Baltic areas, but instead have created a general set of rules valid for all ships operating in ice infested areas. International Association of Classification Societies (IACS) has developed the IACS Polar code based on these general rules from RS. Det Norske Veritas (DNV) has incorporated both these set of rules into their rule "Ships for Navigation in Ice" in addition to their own rules (DNV, 2011). These three categories are:

1. Ice Strengthening for the Northern Baltic Pt.5 Ch.1 Sec. 3
2. Vessels for Arctic and Ice Breaking Service Pt.5 Ch.1 Sec. 4
3. Polar Class Pt.5 Ch.1 Sec. 8

DNV Ice class notation	Equivalent Finnish-Swedish Ice Class
ICE-1A*	1A Super
ICE-1A	1A
ICE-1B	1B
ICE-1C	1C

Table 4.1: Correlation between DNV and Finnish-Swedish ice class rules

High speed ferries that complies with the class notation ICE-1A* could acquire the notation ICE-1A*F with extra requirements.

DNV Ice class notation	Ice Conditions	Ice Thickness h_0	Ice Thickness h
ICE-1A*	Extreme	1	0.35
ICE-1A	Severe	0.8	0.30
ICE-1B	Medium	0.6	0.25
ICE-1C	Light	0.4	0.22

Table 4.2: Ice strengthening for the Northern Baltic

Class notation	Type of ice encountered	Normal ice strength $\sigma_{ice}(N/mm^2)$	Nominal Ice Thickness $h_{ice}(m)$	Limiting impact conditions
ICE-05 ICE-10 ICE-15	Extreme Winter ice with pressure ridges	4.2 5.6 7.0	0.5 1.0 1.5	No ramming anticipated
POLAR-10 POLAR-20 POLAR-30	Winter ice with pressure ridges and multi-year ice-floes and glacial ice inclusions	7.0 8.5 10.0	1.0 2.0 3.0	Occasional ramming
Icebreaker	As above	As above	As above	Repeated Ramming

Table 4.3: Vessels for Arctic and Ice Breaking Service

Polar Class	**Ice Description**
PC 1	Year-round operation in Polar waters
PC 2	Year-round operation in moderate multi-year ice conditions
PC 3	Year-round operation in second-year ice which may include multi-year ice inclusions
PC 4	Year-round operation in thick first-year ice which may include old ice inclusions
PC 5	Year-round operation in medium first-year ice which may include old ice inclusions
PC 6	Summer/autumn operation in medium first-year ice which may include old ice inclusions
PC 7	Summer/autumn operation in thin first-year ice which may include old ice inclusions

Table 4.4: Polar Class Description

4.2 Structural Requirements

The common way to determining the structural requirements has historically been with an elastic method. Both the Finnish-Swedish Ice class rules and DNVs Vessels for Arctic and Ice Breaking Service had been based on this theory. But also the use of plastic limit state design has been used such as Russian Register of shipping have used in their rules. And since the Polar class is partly derived from these rules, Polar class is also a plastic limit state design. When the action effects are dominated by a few extremes and are not cyclic of nature the use of plastic design methods are accepted.

In the following chapters both these 2 rules will be presented and we will look closer onto plate requirements.

The elastic method of analysis is well developed and easy to use. Using the ordinary mechanics it is easy to calculate stress, strain and moments for plate fields and girders. The usual design limit state is to consider the combined multi-axial stresses and applying the von Mises equivalent stress criteria

$$\sigma_j = \sqrt{\sigma_1^2 + \sigma_2^2 + \sigma_3^2 - \sigma_1\sigma_2 - \sigma_2\sigma_3 - \sigma_3\sigma_1} \tag{4.1}$$

The criteria for the von Mises equivalent stress is the yield stress of the applied material The plastic design approach is often more complex to apply since there are several possible limit states in the range from yield to final rupture. But there are many key elements that speak in favour of using plastic design in ice-structure interactions.

4.3 Polar Class design Ice Loads (IACS)

The derivation of Polar Class ice loads that forms the basis for plating and framing design are based on a glancing impact on the shoulder of the bow. The maximum impact force can be found by equating the total kinetic energy of the ship with the energy needed to crush the ice. In the Polar rules the ice loads are only explicitly calculated at the bow and are dependent of the hull shape. Loads on other parts of the hull are independent of the bow shape, but are based on empirical hull area factors. (DNV, 2011)

In figure 4.1 , β' is the normal frame angle at upper ice waterline, α is the upper ice waterline angle and γ is the buttock angle at upper ice waterline. All angles are in degree.

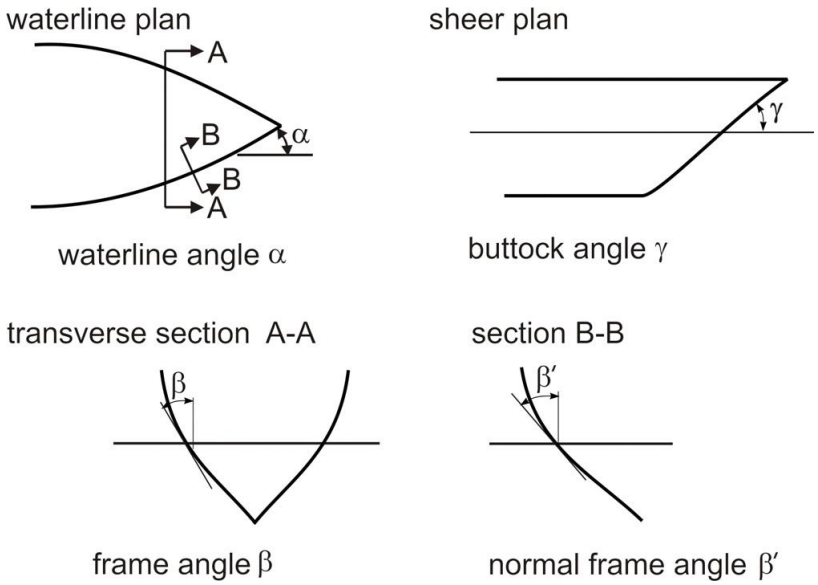

Figure 4.1: Definition of hull angles

Polar Class	Crushing Failure Class Factor CF_C	Flexural Failure Class Factor (CF_F)	Load Patch Dimensions Class Factors (CF_D)	Displacement Class Factors (CF_{DIS})	Longitudinal Class Factors (CF_L)
PC1	17.69	68.60	2.01	250	7.46
PC2	9.89	46.80	1.75	210	5.46
PC3	6.06	21.17	1.53	180	4.17
PC4	4.50	13.48	1.42	130	3.15
PC5	3.10	9.00	1.31	70	2.50
PC6	2.40	5.49	1.17	40	2.37
PC7	1.80	4.06	1.11	22	1.81

Table 4.5: Polar class factors

The bow area load characteristics are determined by the factor f_a. This shape factor is determined by

$$f_a = minimum(f_{a_{i,1}}; f_{a_{i,2}}; f_{a_{i,3}}) \tag{4.2}$$

where

$$f_{a_{i,1}} = (0.097 - 0.068(\frac{x}{L_{wl}} - 0.15)^2) \cdot \frac{\alpha_i}{(\beta_i')^{0.5}} \tag{4.3}$$

$$f_{a_{i,2}} = 1.2 \cdot \frac{CF_F}{(\sin\beta_i' \cdot CF_C \cdot \Delta_{tk}^{0.64})} \tag{4.4}$$

$$f_{a_{i,3}} = 0.60 \tag{4.5}$$

where

i = sub-region considered

L_{wl} = ship length measured at the upper ice waterline

x = distance from the forward perpendicular to station under consideration

α = water angle

β' = normal frame angle

Δ_{tk} = ship displacement

CF_C = Crushing failure class from table (see table 4.5)

CF_F = Flexural failure class from table (see table 4.5)

When the class factors are known we can express the total bow force as:

$$F_n = f_{a,i} \cdot CF_C \Delta_{tk}^{0.64} \qquad [MN] \tag{4.6}$$

For other areas the total force is given as

$$F_{NonBow} = f_{a,i} \cdot CF_C \cdot DF \tag{4.7}$$

where DF is ship displacement factor:

$$DF = \begin{cases} \Delta_{tk}^{0.64} & \text{if } \Delta_{tk} \leq CF_{DIS} \\ CF_{DIS} + 0.10(\Delta_{tk} - CF_{DIS}) & \text{if } \Delta_{tk} > CF_{DIS} \end{cases} \tag{4.8}$$

After finding the total force we need to find the load patch aspect ratio. This is for the bow defined as:

$$AR_i = 7.46 \cdot \sin(\beta_i') \geq 1.3 \tag{4.9}$$

The line load is given as:

$$Q_i = F_i^{0.61} \cdot \frac{CF_D}{AR_i^{0.35}} \qquad [MN] \tag{4.10}$$

$$Q_{NonBow} = 0.639 F_{NonBow}^{0.61} CF_D \qquad [MN] \tag{4.11}$$

and the patch pressure is:

$$p = F_n^{0.22} \cdot CF_D^2 \cdot AR^{0.3} \qquad [MPa] \tag{4.12}$$

4.4 DNV design ice loads for Arctic and ice breaking vessels

The derivation of the Arctic design (DNV, 2011) ice loads is only based on finding a local nominal pressure. Contact area assumptions in the Arctic rules area are incorporated in the plate and stiffener/girder requirement and therefore difficult to give a direct interpretation of the different effects. The ship speed ramming in ice V_{ram} is giving a vertical bow impact design for the hull girder. The kinetic energy from the impact of the bow is transferred to a sliding/lifting motion of the bow, initially considered as a ridged body motion. The impact with the ice will also crush the ice over a certain contact area, and the impact force will give elastic deflection and vibration of the hull girder.

The elastic energy model equation is simplified and combined with the expression for crushing energy and related input energy.

4.4.1 Vertical design force

The vertical design force component due to head ramming is given by:

$$P_{ZR} = P_R F_{EL} \qquad [kN] \tag{4.13}$$

$$P_R = 28 \left(\frac{C_R E_{IMP}}{\tan \gamma} \right)^{0.6} (\sigma_{ice} \tan \alpha)^{0.4} \tag{4.14}$$

For spoon bow:

$$\tan \alpha = 1.2 \frac{B^{0.1}}{\sqrt{\cos \gamma}} \tag{4.15}$$

To take into account for the geometry of the bow with a stem angle γ, the impact energy is given by:

$$E_{IMP} = E_k \frac{\tan^2 \gamma}{\tan^2 \gamma + 2.5} \tag{4.16}$$

$$F_{EL} = \sqrt{\frac{E_{IMP}}{E_{IMP} + C_L P_R^2}} \tag{4.17}$$

$$C_L = \frac{L^3}{3x10^10 I_V} \tag{4.18}$$

E_{KE} is given as the kinetic energy before ramming:

$$E_{KE} = \frac{1}{2} \Delta V_{ram}^2 \qquad (kNm) \tag{4.19}$$

I_V is the moment of inertia in m^4 about the neutral axis of the midship section. Where C_R is 1 for the class notation POLAR and 2 for Icebreaker

4.4.2 Total design force normal to shell plating

The total design force normal to the shell plating in the bow area due to an oblique impact with an ice feature is based on the ratio between side forces and the vertical force P_{ZR}

$$P_{OI} = \frac{P_{ZR} F_{SIDE}}{\cos\gamma} \qquad [kN] \tag{4.20}$$

$$F_{side} = \frac{1.9}{(\tan\alpha)^{0.4}} \left(\frac{\sigma_{ice}}{E_{KE}}\right)^{0.05} \tag{4.21}$$

4.4.3 Ice compression loads midships

When a vessel is trapped between moving ice floes, it should be able to withstand line loads acting simultaneously in the horizontal plane at the water level on both side of the hull.

$$q = \frac{165}{\sin\beta_f} (h_{ice})^{1.5} \qquad (\frac{kN}{m}) \tag{4.22}$$

$$= 950(h_{ice})^{1.5} \qquad (\frac{kN}{m}) \qquad \text{for vertical side shells } (\beta_f < 10^\circ) \tag{4.23}$$

h_{ice} = average ice thickness β_f = angle of outboard flare at the water level

4.4.4 Local ice pressure

The local ice pressure is used in the calculations of local strength components such as plating, stiffeners and girders. The local ice pressure is directly proportional to the selected ice crushing strength, multiplied by a weighting factor F_A for the different parts of the hull.

$$p_0 = 1000 F_A \sigma_{ice} \qquad (\frac{kN}{m^2}) \tag{4.24}$$

F_A= 1 for bow and stem area in general and σ_{ice} is given in table 4.3

Other areas of the ship are given in the Arctic design code (DNV, 2011)

In the rules the effect of contact area has been incorporated by the factor F_B

$$F_B = \begin{cases} \frac{0.58}{A_C^{0.5}} & \text{if } A_C \leq 1.0m^2 \\ \frac{0.58}{A_C^{0.15}} & \text{if } A_C > 1.0m^2 \end{cases} \tag{4.25}$$

The final expression for design pressure can then be taken as

$$p = F_B p_0 \qquad (\frac{kN}{m^2}) \tag{4.26}$$

4.5 Plating requirements

The plating on ships contributes to the largest percentage of the structural weight. When combined with frames and stringers, it forms a stiffened panel to resist the load on the ship. When a plate is supported by frames on all four sides and loaded by a uniform pressure perpendicular to the surface, the deflection could be calculated by using small deflection theory of plate bending. This theory will neglect membrane stresses developed in the plate during yielding of material and large deflection of the plate. The result of ignoring membrane action is that the load carrying capacity estimated from small deflection theory is small compared to the actual capacity. The Polar Code utilizes a simplified collapse mechanism that neglects membrane stresses and strain hardening. This will also have a substantial reserve beyond its design limits. The DNV code for Vessels for Arctic and Ice Breaking Service base their analysis on an elastic method with some plastic capacity assumptions.

4.5.1 Polar Class plate thickness requirement

The required minimum shell plate thickness t in transversely-framed plating is given by:

$$t = 500s\sqrt{\frac{AF * PPF_P * P_{avg}}{\sigma_y}}\frac{1}{1+\frac{s}{2b}} + t_s \qquad (mm) \tag{4.27}$$

where AF and PPF_P are tabulated values, σ_y is material yield stress, t_k is corrosion allowance, s is frame or longitudinal spacing (m), b is height of design load patch (m) and P_{avg} is defined as:

$$P_{avg} = \frac{F}{b \cdot w} \tag{4.28}$$

4.5.2 Arctic and Ice Breaking Service plating requirements

The thickness of plating exposed to patch load is:

$$t = 23k_a\frac{s^{0.75}}{h_0^{0.25}}\sqrt{\frac{k_w p_0}{m_p \sigma_f}} + t_k \qquad [mm] \tag{4.29}$$

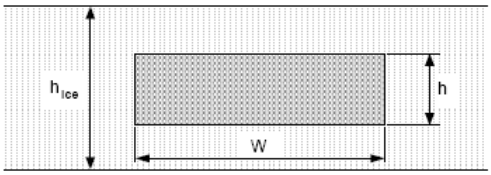

Figure 4.2: Design load patch size

where

k_a = aspect ratio factor

k_w = pressure distribution factor

p_0 = basic ice pressure

m_p = bending moment factor

$b = s$ in general (transverse frames)

$b = h_0$ for longitudinally stiffened plating

s = stiffener spacing

l = effective span of stiffener

For ice loads the patch area is limited to $h_0 = s$ as the maximum expansion of the patch area.

The aspect ratio factor can be described as:

$$k_a = 1.1 - 0.25\frac{s}{l} \qquad k_a \in [0.85 - 1.0] \tag{4.30}$$

The pressure distribution factor k_w is defined as:

$$k_w = 1.3 - \frac{4.2}{(a/s + 1.8)^2} \qquad k_w \in [0.85 - 1.0] \tag{4.31}$$

where

$a = s$ in general

$a = h_0$ for longitudinally stiffened plating

Chapter 5

Numerical Comparison of Rule Requirements

5.1 Introduction

In chapter 4 the different class rules for DNV Arctic and Ice Breaking Service and IACS Polar class where reviewed. To be able to compare these rules against each other, a numerical comparison of the rules are needed. This comparison will be done for the bow region, the midship and the stern area. The comparison is done with some similarity as in (Boersheim, 2007), but with updated rules and, extended range and some other considerations. The requirements will be a function of class, displacement, hull shape angles, frame spacing and frame span. The geometry used in the comparison is based on ships in this typical range, and will be presented as their used. The results will be presented in diagram with the requirements versus the vessel displacement. The displacement will be shown in interval between 5000 and 150 000 tons.

Since the Arctic rules are based on an elastic approach and the Polar rules on a plastic method, not all results are directly comparable. The requirements will be presented as net requirements and additional requirements such as corrosion have to be added to this.

5.2 Bow region

5.2.1 Design Loads

For the design loads the main focus will be the local ice pressure the different rules will give for the different classes. The basic ice pressure is given by equation 4.12 in the Polar Code:

$$p = F_n^{0.22} \cdot CF_D^2 \cdot AR^{0.3} \qquad [MPa]$$

and by equation 4.24 for the Arctic rules:

$$p_0 = 1000 F_A \sigma_{ice} \qquad (\frac{kN}{m^2})$$

5.2.2 Polar code design load

One can see from equations 4.6, 4.9 and 4.12 that the scantling requirements will be dependent on hull shape factors, class dependent ice thickness factors and the vessels displacement. The class factors are given in table 4.5. The hull shape factors for the bow used in this comparison is $\beta' = 35°$ and $\alpha = 30°$

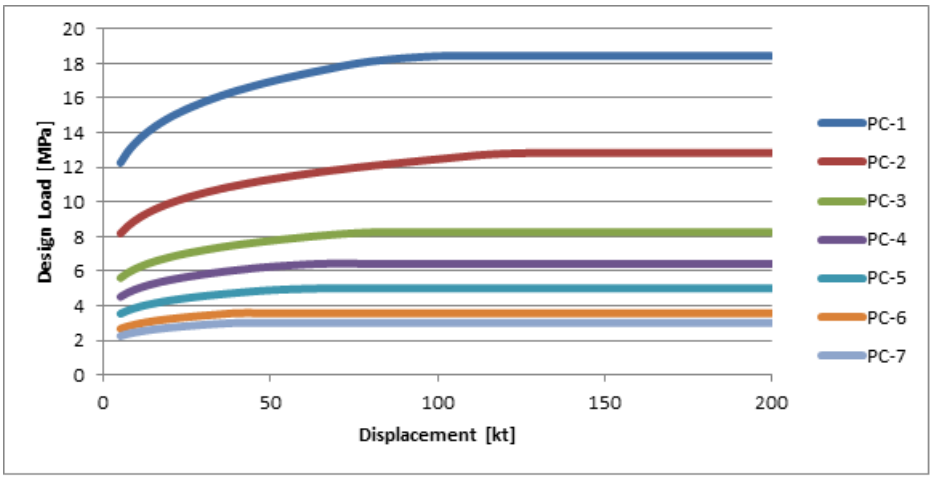

Figure 5.1: Load versus displacement for Polar Code

Figure 5.1 shows the relation between the applied design load and the vessel displacement. For each different class the displacement is the governing factor. But also the hull shape angles will have an effect on the local ice pressure. The hull shape factor $f_{a,i}$ and load patch area AR_i will change with different β' and α. Different angles has also been tested to see the effect they will make.

For β' increasing this will make the whole curve shift to a higher load value until we reach the maximum value of $f_{a,i} = 0.6$. $f_{a,i}$ is also dependent of α so here we there is a correlation. When we decrease the β', the local ice pressure will decrease until we reach the point when $\beta' \leq \arcsin(\frac{1.3}{7.46}) = 10.03°$. This could be taken from equation 4.9 when the lowest value of 1.3 is dominating the load patch area AR. Lowering the β' more will not decrease the load, but could in correlation with α increase the local ice pressure.

The α is only included in equation (4.3) for $f_{a_{i,1}}$ in the local ice pressure equation. Decreasing this angle would make the local ice pressure decrease, and could go to zero for very low angles. 0 angle will give zero load, but this is not physical possible to get. Increasing this value will increase the load until $f_{a_{i,1}}$ is larger than $f_{a_{i,2}}$ or $f_{a_{i,3}}$ This effect is also present in figure 5.1 were we get a plateau level for large displacements. The different classes reaches the plateau level at different displacement, because of the the different class factors.

5.2.3 Arctic and Ice Breaking Service design loads

From equation (4.26) we see that the ice design pressure is proportional to the basic local ice pressure p_0.

$$p = F_B p_0 \qquad (\frac{kN}{m^2})$$

This is again proportional to the ice crushing strength σ_{ice} that is defined for each class (see table 4.3). Then we can conclude that the applied design load is only related to the selected class. We could also see from equation (4.26) that the factor F_B is present.F_B incorporate the effect of the contact area and is defined in equation (4.25).

$$F_B = \begin{cases} \frac{0.58}{A_C^{0.5}} & \text{if } A_C \leq 1.0m^2 \\ \frac{0.58}{A_C^{0.15}} & \text{if } A_C > 1.0m^2 \end{cases}$$

This size could change for different size and class of ships, and influence the applied load. But when considering a specific plate field, the load is only dependent on class and will be constant for all displacements. Both POLAR-10 and ICE-15 have the same nominal ice strength.

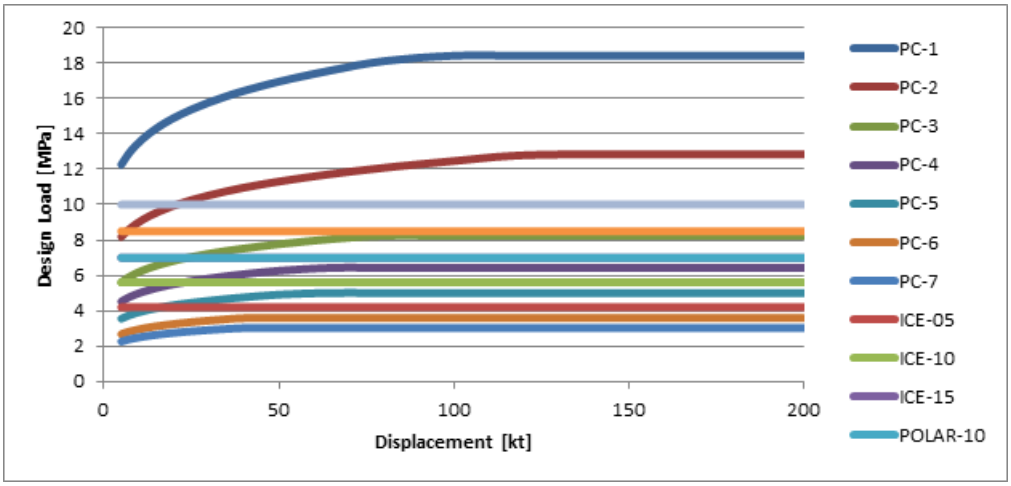

Figure 5.2: Arctic and Polar Class design loads

Figure 5.2 compares the Arctic and Polar Class design loads. We could see that despite the two rules are based on two different design principles, the values of the design loads seem to be close. The Polar Class has both the highest and lowest design loads. This could be related to that the Polar Class designs for all ice loads, but the Arctic rules also have a subset of Baltic rules for less severe ice loading. In addition could the Arctic rules give a ship the notation ICEBREAKER, giving it more strict requirements. Also the DNV loads for the upper classes seems to be somewhat smaller than the Polar Code loads, and therefore have a substantial excess of strength

5.2.4 Plating thickness requirements

The plating requirements for Polar Class rules are given by equation (4.27)

$$t = 500s\sqrt{\frac{AF * PPF_P * P_{avg}}{\sigma_y}}\frac{1}{1+\frac{s}{2b}} + t_s \qquad [mm]$$

and the Arctic by equation (4.29)

$$t = 23k_a\frac{s^{0.75}}{h_0^{0.25}}\sqrt{\frac{k_w p_0}{m_p \sigma_f}} + t_k \qquad [mm]$$

These are dependent of the plate geometry under consideration, and under this comparison the plate would have a length of 1300 mm and width of 400 mm. Also assume the material yield limit to be 355 MPa If we consider the lower classes in figure 5.3, we could see that the Polar rule requirements are lower than the Arctic rules for the most of the classes. The Arctic rules have a subset of rules for the Baltic area, and PC-6 and PC-7 could be seen as equivalents to the two highest classes in the Baltic rules. As we have seen for the design pressure, the Polar rules require more minimum plate thickness for higher displacement ships and Arctic rules have higher requirements for the lower displacement ships.

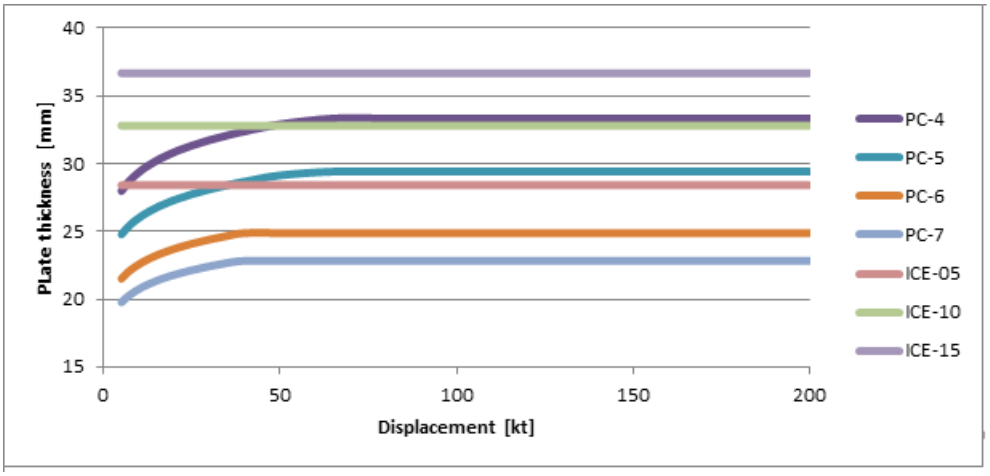

Figure 5.3: Plate thickness low classes, bow region

For the higher classes in figure 5.4 the Polar class rules are much more conservative than the Arctic rules for the larger vessels. We see also that PC-1 is always larger than POLAR-30 class. This could be different if we consider another plate strip, but generally the Polar rules are stricter since they are based on a plastic approach and does not have much excess of strength in this regime as the Arctic rule. From both figure 5.3 and 5.4 it is evident that the thickness requirement is governed by the design load.

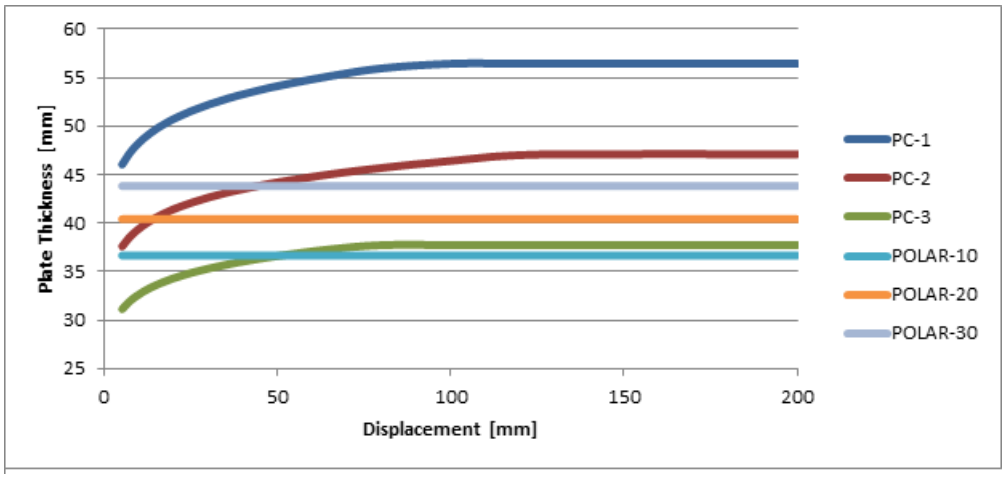

Figure 5.4: Plate thickness high classes, bow region

5.3 Midship region

5.3.1 Design load

The design load for the midship region is calculated in the same way as for the bow region. The difference is that is it scaled with a hull factor. For the Arctic rules the hull area factor $F_{a,mid} = 0.6$. The Polar class rules have a more complex approach to the hull area factor (AF) as seen in table 5.1 For the design load, the hull area factor is not included, but here the hull shape factor $f_a = 0.36$.

Hull Area		*Area*	*Polar Class*						
			PC-1	PC-2	PC-3	PC-4	PC-5	PC-6	PC-7
Bow (B)	All	B	1.00	1.00	1.00	1.00	1.00	1.00	1.00
Bow Intermediate (BI)	Ice belt	BI_i	0.90	0.85	0.85	0.80	0.80	1.00*	1.00*
	Lower	BI_l	0.70	0.65	0.65	0.60	0.55	0.55	0.50
	Bottom	BI_b	0.55	0.50	0.45	0.40	0.35	0.30	0.25
Midbody (M)	Ice belt	M_i	0.70	0.65	0.55	0.55	0.50	0.45	0.45
	Lower	M_l	0.50	0.45	0.40	0.35	0.30	0.25	0.25
	Bottom	M_b	0.30	0.30	0.25	**	**	**	**
Stern (S)	Ice belt	S_i	0.75	0.70	0.65	0.60	0.50	0.40	0.35
	Lower	S_l	0.45	0.40	0.35	0.30	0.25	0.25	0.25
	Bottom	S_b	0.35	0.30	0.30	0.25	0.15	**	**

Table 5.1: Hull Area factors

As shown in figure 5.5 there is a large difference between the Arctic rules and Polar class rules; this is mainly due to the fact that the Polar class does not include the hull area factor. In deciding the design load for Polar class, the rules defines $P_{avg} = \frac{F}{bw}$, where $w_{NonBow} = \frac{F_{NonBow}}{Q_{NonBow}}$ and $b_{NonBow} = \frac{w_{NonBow}}{3.6}$

5.3.2 Plate thickness

For the plate thickness, we get much of the same results as the bow region, except that the thickness is lowered some down. The Polar class is most strict for higher

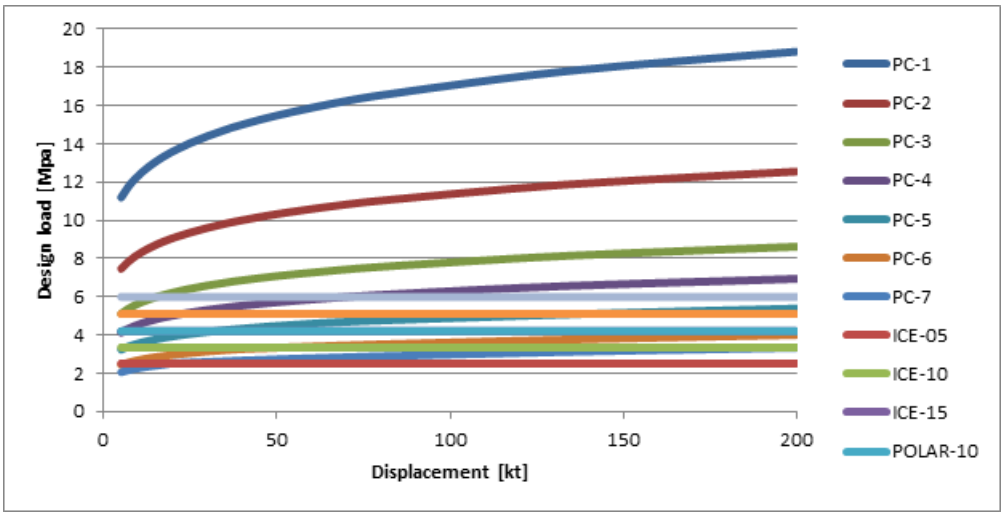

Figure 5.5: Design load midship

displacements and the Arctic rules are stricter for the lower displacements ships. This could be seen in Figure 5.6 and 5.7

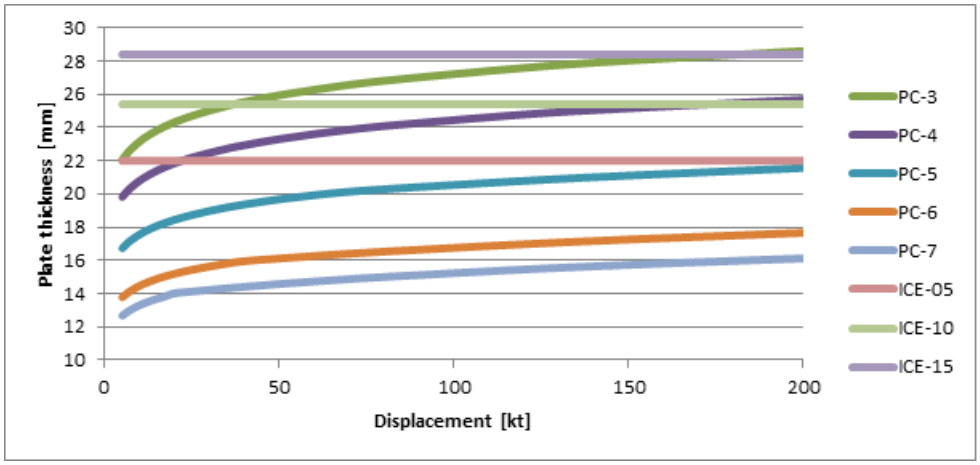

Figure 5.6: Plate thickness lower classes, midship

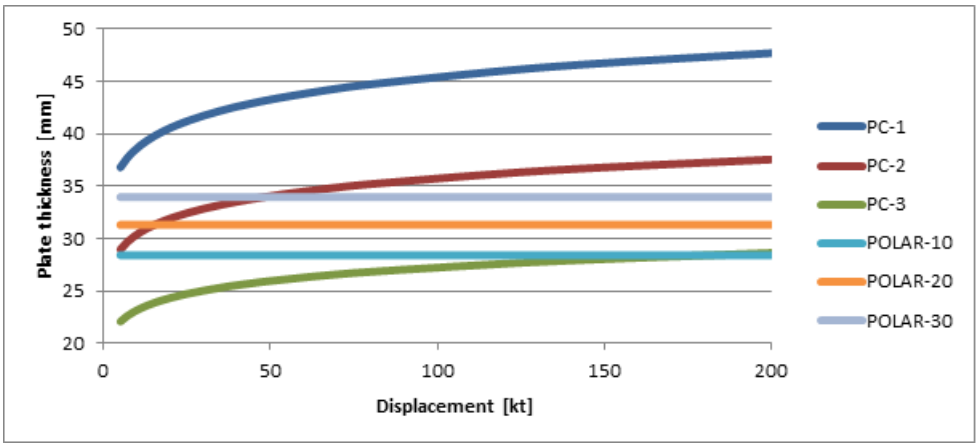

Figure 5.7: Plate thickness higher classes, midship

5.4 Stern region

For the stern region, I will only look at the hull factors and the resulting plate thickness since they are the only different factors from the midship region.

For Arctic rules the stern area is generally $F_A = 0.6$. For vessels fitted with podded propulsion or designed for continuous operation astern, POLAR $F_a = 1.0$ and ICE $F_a = 0.8$. In the Polar rules we have to look at table 5.1 again. In the ice belt area, the higher classes have a higher hull area factor, and a lower factor for lower classes. When the ship is intended to operate astern, the Polar class assign a hull area factor AF=1.0 for all classes. For ships intended for astern operation, both Polar class and Arctic class will have an increased plate thickness compared to midships (Se figures 5.8 and 5.9). They will be moved upwards and the only difference we will see on the figures is that ICE class will be some lower compared to the lower Polar Classes. Also worth mentioning is that POLAR-30 will be larger than PC-2 for the whole range

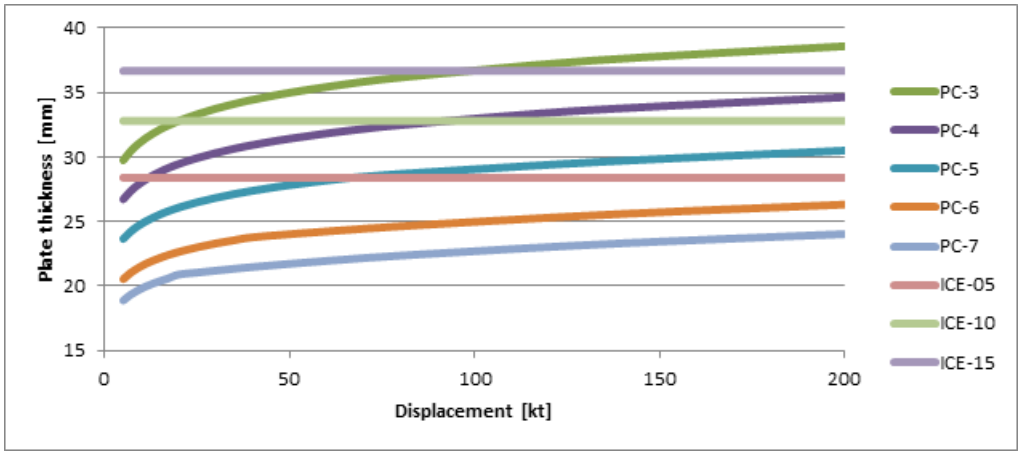

Figure 5.8: Plate thickness, lower classes, stern, with operations astern

For the stern area and not operating astern, there is some difference compared to midships for the Polar class. The Arctic class is exactly the same as midships. This could

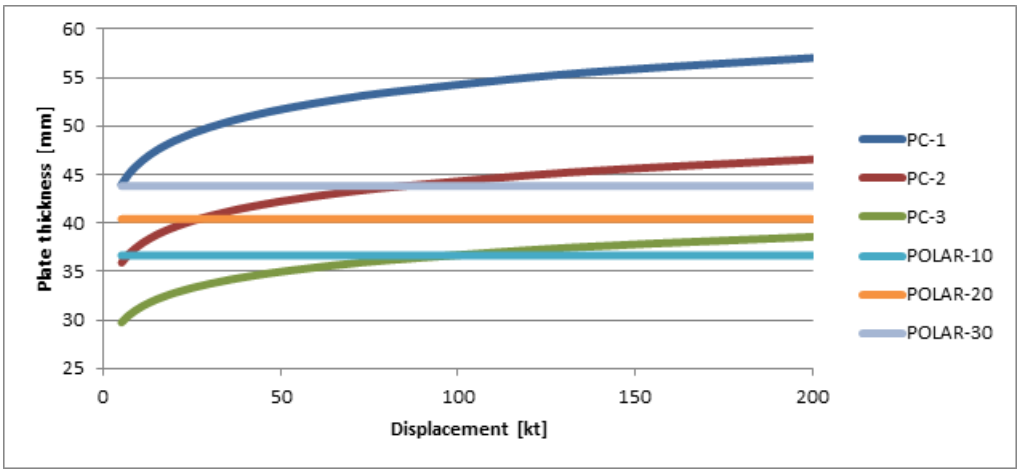

Figure 5.9: Plate thickness, higher classes, stern, with operations astern

be seen in figure 5.10 and 5.11 .

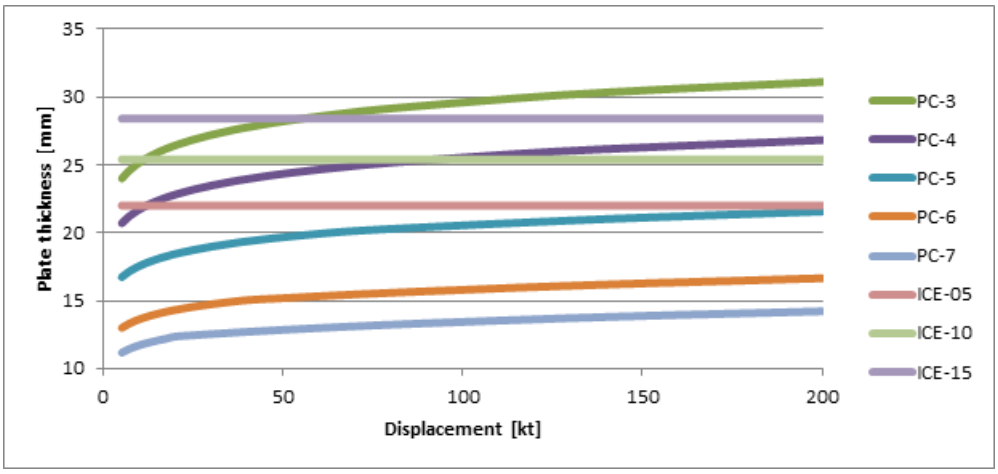

Figure 5.10: Plate thickness, lower classes, stern, no operations astern

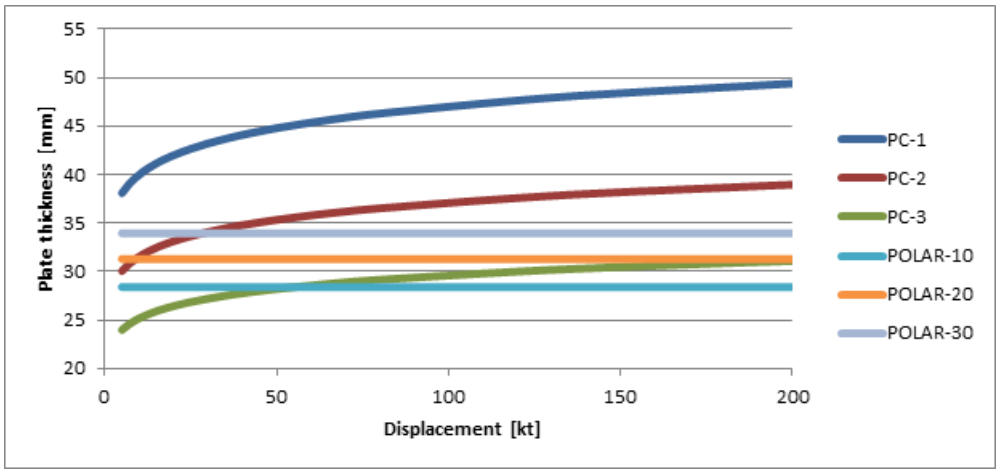

Figure 5.11: Plate thickness, higher classes, stern, no operations astern

5.5 Discussion and conclusion

This chapter presented a numerical comparison of the structural requirements regarding ships operating in ice infested waters. Since the rules are based on two different design principles, this numerical comparison is necessary to be able to say something definite about the differences between these class rules.

The conclusion we could draw from these calculations is that Polar class is more conservative for higher classes. (POLAR and PC-1 to 3) For the lower classes (ICE and PC-4 to 7) the Arctic rules are stricter. One of the explanations for this could be the subset of Baltic rules that is associated with Arctic rules for vessels operating in the Baltic areas, and that the Polar code is meant for all ice conditions.

The other major difference between Polar class and Arctic and ice breaking service rules are the dependency of displacement. Polar class is strongly dependent of displacement, making it more conservative for vessels with high displacement than the Arctic rules that are constant within their class. At the other end of the displacement scale, the Arctic rules are most conservative for smaller vessels.

Chapter 6

Finite Element Model and Measurements from KV Svalbard

6.1 Background

The calculation of ice-induced loads on ships is still mainly based on empirical models. In order to gain a better physical understanding of the loading on ice-going vessels, Det Norske Veritas launched an *ice load monitoring* project involving full scale trials with the coastguard vessel KV Svalbard during the winters 2007 and 2008. By instrumenting the vessel with strain gauges in bow region and a sensor system to detect the ice thickness, time series of ice-induced strains have been recorded for given ice conditions (Bernt Leira and Amdahl, 2009)

The results from the full scale measurements conducted with KV Svalbard has been topic of several earlier master thesis at NTNU, in which various finite element models have been developed.

6.2 The model

The finite element model used in this thesis was created by (Erland, 2006). This model was used to carry put a preliminary evaluation of the strain sensors by comparing the stress results from anticipated load cases with the strain measurements from KV Svalbard.

Figure 6.1 shows the part of the ship which is model. The model extends from transverse bulkhead 4 to 9 in the longitudinal direction, including all main and intermediate frames in between. The transverse extent of the model is from outer hull plating to center line. In the vertical directions, the model extends from 4500 ABL (above baseline) to 8300 ABL, including all longitudinal stringers in between. All degrees of freedom are fixed along the frames and bulkheads at the center line, as shown in figure 6.2

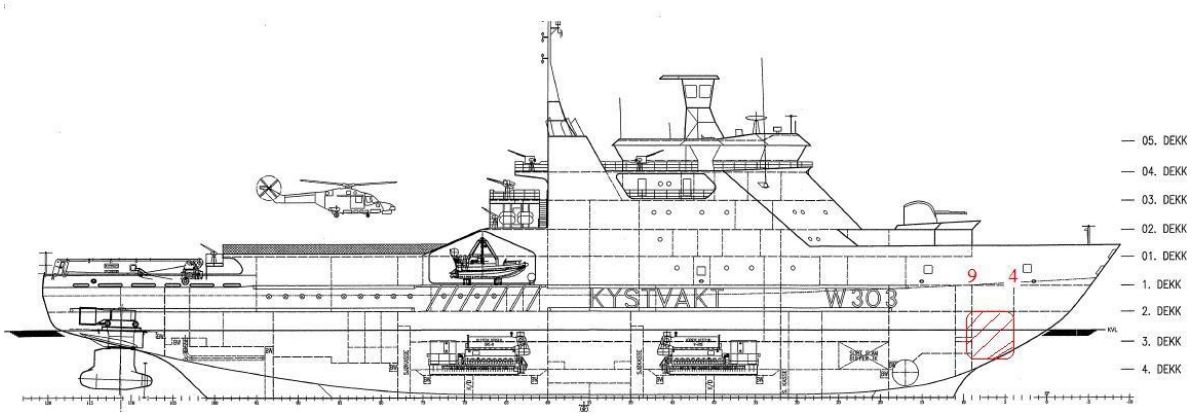

Figure 6.1: Part of KV Svalbard covered by model (Erland, 2006)

The model was made by modeling software *MSc. Patran-Pre*. The model consists of 60338 elements of type S4R5 and 59647 nodes. After the model has been applied for definition of load cases and boundary conditions, the model is exported from Patran-Pre as an input-file (.inp). This .inp is imported into the FEM software *Abaqus/CAE*. *Abaqus/CAE* is used for the linear static analysis (linear perturbation) and post-processing of the results.

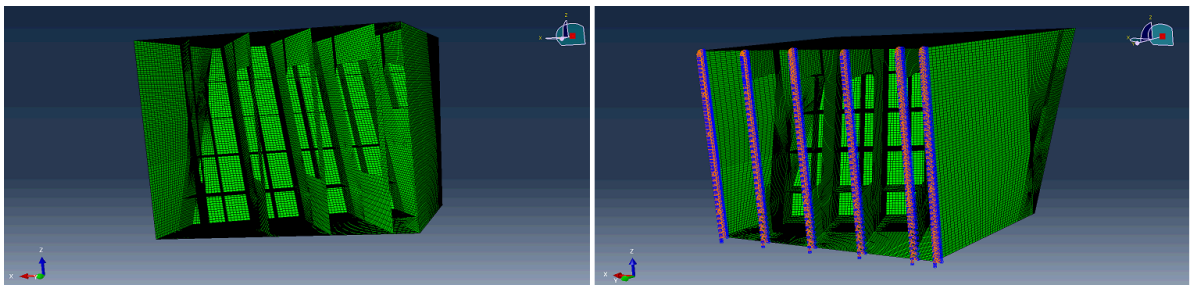

Figure 6.2: Finite Element Model by (Erland, 2006)

6.3 Instrumentation

The instrumentation configuration for the intermediate frame location L4 from Det Norske Veritas *ice load monitoring* project used in (Boersheim, 2007) master thesis is shown in figure 6.3

Gage 1 is located in frame 150 mm below stringer level 6700 and 112 mm from ship side plating. Gage 2 is located 150 mm above stringer level 5900 and 112 mm from ship side plating. Gages 3 and 4 located at each side of the frame on stringer level 5900, 200 mm in vertical direction and 140 mm from ship side plating. Gage 5 is located 150 mm above stringer level 5100 and 112 mm from ship side plating.

The strain locations are approximately located by these element- or node numbers in the finite element model in table 6.1

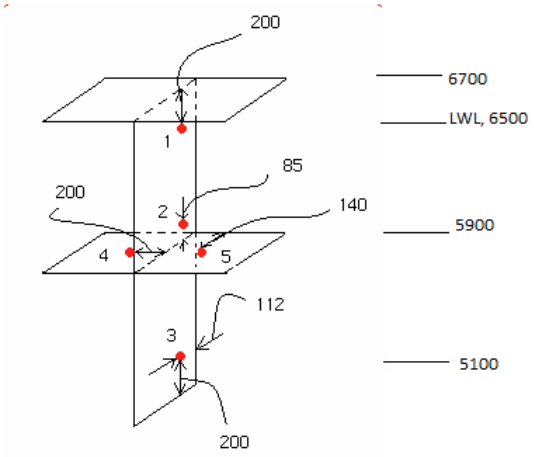

Figure 6.3: Strain gages mounted on intermediate frame

Gage	Element no	Node no
1	36726	47837
2	36843	47987
3	39011	50697
4	26220	3681
5	26102	3716

Table 6.1: Strain gages and element/node no in model

6.4 Measurements from KV Svalbard

6.4.1 Introduction

The following section contains the measurements from the *Ice Load Monitoring* project done with KV Svalbard carried out in March 2007. These measurements are collected from the Master thesis of Boersheim (2007). The main focus of data will be the measured results from March 25^{th}, between 16:30 and 17:00. In this time interval, the vessel speed, heading and ice thickness were relatively uniform and there were not too many unknown factors influencing the results. The location of interest will be sensor location L4 on figure 6.4.

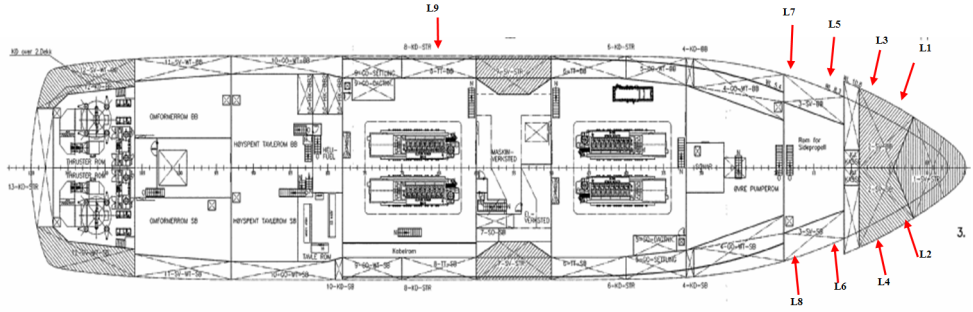

Figure 6.4: Labeling and sensor location on KV Svalbard

6.4.2 Calculating different stress components

The stress over a cross section of the stiffener is divided into axial, transverse and shear stress. To be able to calculate the three components three strain filaments are needed. To make the instrumentation system cheaper, most stiffeners are only mounted with two sensors. Thus it is not possible to calculate all stress components. Frame 4 was only instrumented with two filaments, but Frame 2 was mounted with three filaments at each sensor.

In appendix A.1 the procedure for using just 2 filaments is presented. If the strain gauges are mounted on the neutral axis of the stringer with 45 degree angle to the axial direction, the error of not using 3 filaments instead of 2 becomes small. But since the position of the neutral axis could change during loading, the error could affect the results.

The procedure of calculating the shear distribution and shear force is presented in appendix A.2 and the von Mises stress without axial contribution is presented in appendix A.1.2.

6.4.3 Loading on Frame 4 March 25^{th} between 16:30 and 17:00

In figure 6.5 we could see the heading, speed and ice thickness in the interval between 16:30 and 17:00 at March 25^{th} 2007. We could see that the heading, speed and ice thickness is relatively uniform in this area. The calculations of the loads are based on the load decision method developed by DNV (see appendix A.2). In this interval there are identified 91 peak loads over 30kN and 38 peak loads over 50 kN (Boersheim (2007) ch 6.6). In this section the focus will be on the peak loads above 50 kN

Figure 6.6 shows the relation between the ice thickness and the calculated max load on frame 4. It is not evident that there is a direct correlation between the ice thickness and the maximal loading. There are periods where the load increases with increasing ice thickness, and decreasing in the same way. There are also periods were the ice thickness or load increases very much without the other component reacts as much. There is no

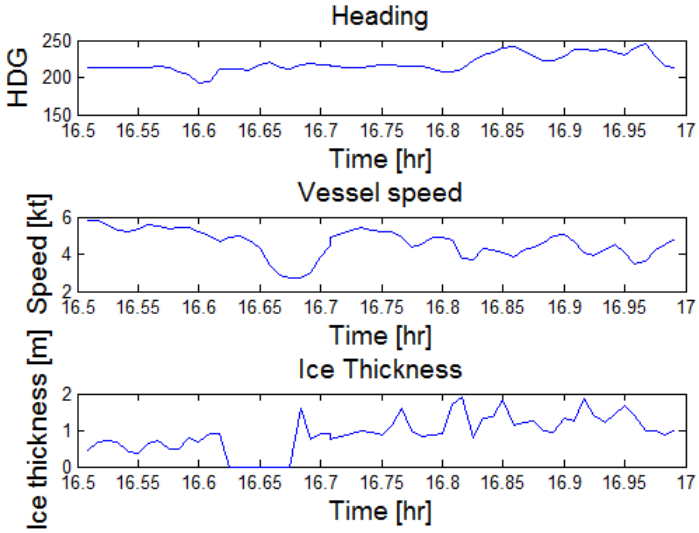

Figure 6.5: Heading, vessel speed and ice thickness measured on frame 4 March 25^{th} between 16:30 and 17:00

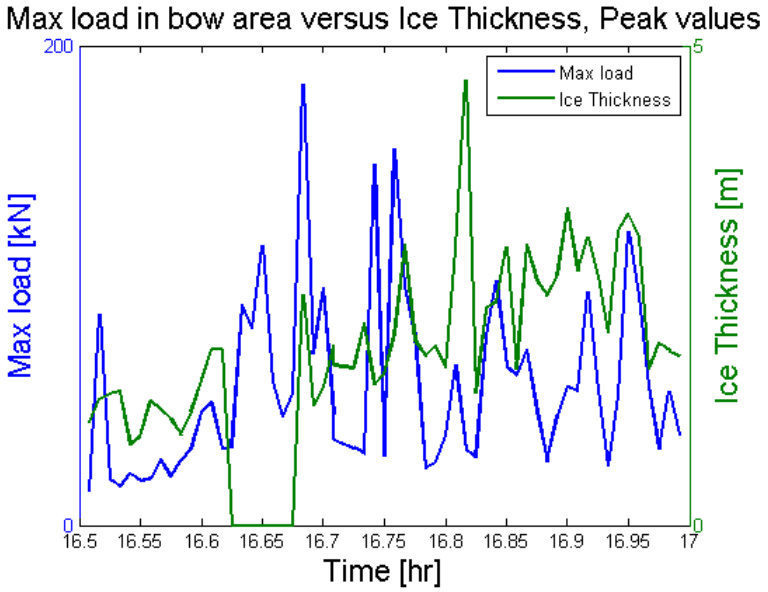

Figure 6.6: Correlation between load and ice thickness frame 4 between 16:30 and 17:00

consistency in the correlation between the ice thickness and the resulting load in this time interval. One of the error sources is that the ice thickness is measured at the bow, and frame 4 does not necessarily rammed by these ice thicknesses. The ice breaking pattern of the ship is not very predictable, and the features of the ice could affect this in many ways (see chapter 3). The vessel speed and heading would also affect the results.

11 different peak loads with a total load on the frame above 50 kN have been chosen and presented in appendix B. 2 figures are presented for each peak load. The first showing the force on the frame, with 3 lines that represent: the total load, load on the 2 upper sensors (F_top) and the last showing the loading on the 3 lower sensor. With this figure, it is possible to see if the acting load on the frame is positioning above or below the stringer at 5900 mm ABL. This is a part of DNVs load decision scheme. The second figure shows the calculated shear force at each sensor based on the procedure presented in A.2. For the peak load of total force in each load peak, the total force on the frame is presented. Also, the measured/calculated shear stress, von Mises stress and shear force for each of the sensors is presented. Some of these values will be used in the finite element analysis.

6.5 Determine load area and pressure based on measured load and DNV rules

In the following section the method for calculating the load area or patch pressure based on the measured force on frame 4 and DNV rules for calculating the load area and patch pressure.

We need to review the DNV rules from Chapter 4. The basic ice pressure is given in equation 4.24 :

$$p_0 = 1000 F_A \sigma_{ice} \qquad (\frac{kN}{m^2})$$

Equation (4.26) gives the design ice pressure:

$$p = F_B p_0 \qquad (\frac{kN}{m^2})$$

And equation (4.25) gives the factor of F_B:

$$F_B = \begin{cases} \frac{0.58}{A_C^{0.5}} & \text{if } A_C \leq 1.0m^2 \\ \frac{0.58}{A_C^{0.15}} & \text{if } A_C > 1.0m^2 \end{cases}$$

When combing these equations, we could calculate the contact area A_C based on the

patch pressure p and design pressure p_0.

$$p = p_0 F_B = p_0 \frac{0.58}{(A_C)^e} \tag{6.1a}$$

$$(A_C)^e = 0.58 \frac{p_0}{p} \tag{6.1b}$$

$$A_C = (0.58 \frac{p_0}{p})^{\frac{1}{e}} \tag{6.1c}$$

Where e is 0.5 if $A_C \leq 1.0m^2$ and 0.15 when $A_C > 1.0m^2$

To able to estimate either the contact area A_C or the patch pressure p, we need formulas that are just dependent of one of these factors. One way is to use the definition of force and combine with the other equations in this section.

Force F is defined as:

$$F = pA \tag{6.2}$$

The first alternative is to replace the area A in equation (6.2) with A_C from equation 6.1c:

$$F = pA_C = (0.58 \frac{p_0}{p})^{\frac{1}{e}} = p^{1-\frac{1}{e}} (0.58 p_0)^{\frac{1}{e}} \tag{6.3a}$$

$$p^{1-\frac{1}{e}} = \frac{F}{(0.58 p_0)^{\frac{1}{e}}} \tag{6.3b}$$

$$p = \left(\frac{F}{(0.58 p_0)^{\frac{1}{e}}} \right)^{1-\frac{1}{e}} \tag{6.3c}$$

The second alternative is to replace the pressure in equation (6.2) with p from equation (4.26) :

$$F = pA_C = F_B p_0 A_C = A_C p_0 \frac{0.58}{A_C^e} = p_0 0.58 A_C^{1-e} \tag{6.4a}$$

$$A_C^{1-e} = \frac{F}{0.58 p_0} \tag{6.4b}$$

$$A_C = \left(\frac{F}{0.58 p_0} \right)^{\frac{1}{1-e}} \tag{6.4c}$$

6.5.1 Area and pressure from loadpeak 35

When we derived equation 6.3c and 6.4c we assumed the force F was from measured results. In this section we will use the results from load peak 35 in appendix B. The applied force on the frame at the load peak is 173.9609 kN. σ_{ice} in equation 4.24 is given in table 4.3. KV Svalbard is classed as Polar-10 which gives σ_{ice} as 7 MPa.

The first alternative gives (equation 6.3c) :

$$p = \left(\frac{173.9609}{(0.587000)^{\frac{1}{e}}} \right)^{1-\frac{1}{e}}$$

$$e = 0.5 \Rightarrow p = 94754.6259kPa = 94.7546259MPa$$

$$e = 0.15 \Rightarrow p = 7078.657923kPa = 7.078657923MPa$$

When using equation 6.1c we could find the resulting area

$$e = 0.5 \Rightarrow A_C = 0.0018359m^2$$

$$e = 0.15 \Rightarrow A_C = 0.0245754m^2$$

Since both areas are below 1 m^2, the resulting area $A_C = 0.0018359m^2$ and the patch pressure $p = 94.7546259MPa$

The second alternative yields (equation 6.4c)

$$A_C = \left(\frac{173.9609}{0.587000} \right)^{\frac{1}{1-e}}$$

$$e = 0.5 \Rightarrow A_C = 0.0018359m^2$$

$$e = 0.15 \Rightarrow A_C = 0.0245754m^2$$

Both of the areas are below 1 m^2 and this yields that $A_C = 0.0018359m^2$ and the patch pressure from equation (4.26) and (4.25) yields $p = 94.7546259MPa$

The area predicted here using measured results and DNV rules is too low to be realistic. The pressure on this small area would probably be too high to withstand local yielding. If we take a closer look on the formulas, we see that the local ice pressure σ_{ice} is the factor that regulates the correlation between the contact area and the patch pressure (equation 6.3c and 6.4c). If we constrain this value to a lower value, we might get an area that is more realistic to use. This would be done in the next chapter when applying loads to the finite element model.

Chapter 7

Finite Element Analysis

7.1 Introduction

The following chapter contains an analysis of the bow part of KV Svalbard when it is subjected to loads along the ship side. We will use the submodel of the bow made by Erland (2006), and apply a patch load to different locations along the hull and measure stress at the sensor location at frame 4 (see figure 6.3).

The stress factors measured are shear stress τ_{xy}, axial stress σ_x, transverse stress σ_y and the von Mises stress. This could tell us how far from the frame a patch load would affect the sensors, how the different stress factors changes along the hull and which stress factors are the most dominating at the different load cases.

The model was made by modelling software *MSc. Patran-Pre*. After the model have been applied for definition of load cases and boundary conditions, the model is exported from Patran-Pre as an input-file (.inp). This .inp is imported into the FEM software *Abaqus/CAE*. *Abaqus/CAE* is used for the linear static analysis (linear perturbation) and post-processing of the results. In the post-processing of the results, the values for τ_{xy}, σ_x, σ_y and von Mises at the sensor location (see section 6.3) was extracted. At the shell elements, the value of the mid integration point is extracted. These values have then been imported to Microsoft Excel, systematized and used to produce graphs shown in this chapter.

7.2 Load applied to model

The patch load used in this analysis will have dimension of 400 mm * 400 mm. The assumed local ice pressure σ_{ice} is 3 MPa. By using equation (4.25) and (4.26), the local patch pressure will be:

$$p = p_0 F_B = p_0 \frac{0.58}{(A_C)^{0.5}} = 3000 \frac{0.58}{(0.4^2)^{0.5}} = 4350kPa$$

The load area is marked inside as the red lines in figure 7.1. The model shows the starboard side of KV Svalbard. When we apply the load from the bow and backwards, this will mean the applied loads will start from left to right in figure 7.1. The total length of the loaded area is 3600 mm and the height is 1400 mm. The load patches do not start side-by-side, but will overlap the previous load patch by 200 mm (both vertical and horizontally). In total there will be 17 load patches for each level of load along the hull and 6 levels to cover the whole load area. In total this will give 102 load cases for this analysis.

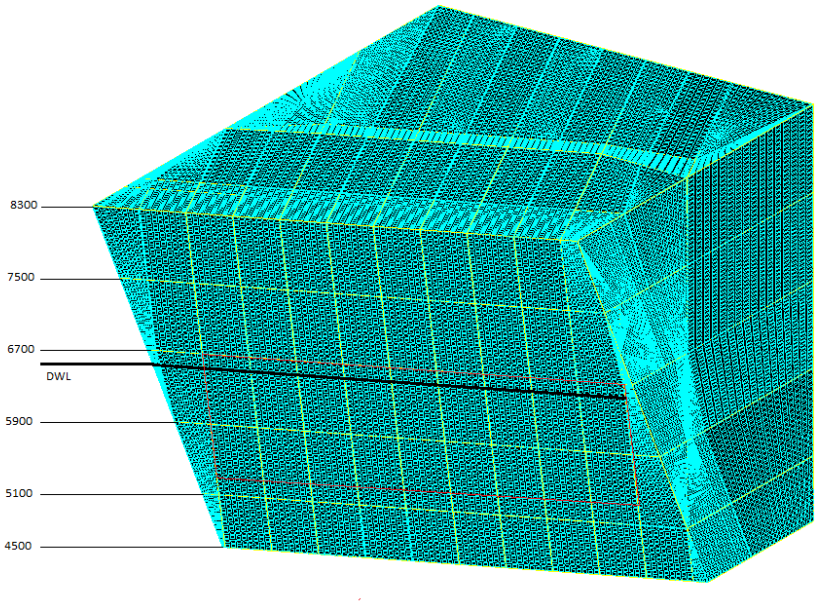

Figure 7.1: Part of FEM model subjected to load

7.3 Level 1

Level 1 upper constraint is at the stringer 200 mm above the waterline, 6700 mm ABL. In figure 7.2 the area between the black line is the area for 17 load patches that is included for level 1. The area within the red lines is the total load area. The elements marked with orange are elements used in the 2^{nd} load case. The white area shows elements used in the 1^{st} load case that is not shared with the 2^{nd}.

7.3.1 Load case 8

In figure 7.3 the model is subjected to the patch load in load case 8 for level 1. This is the load case when the patch load is symmetrically loaded on each of frame L4 where the sensor are located. The red elements indicates where the different sensor are located when we look at the from the side of the ship. The contour plot shows the von Mises stress at this load case. As the figure also shows the deformed shape of the model, it

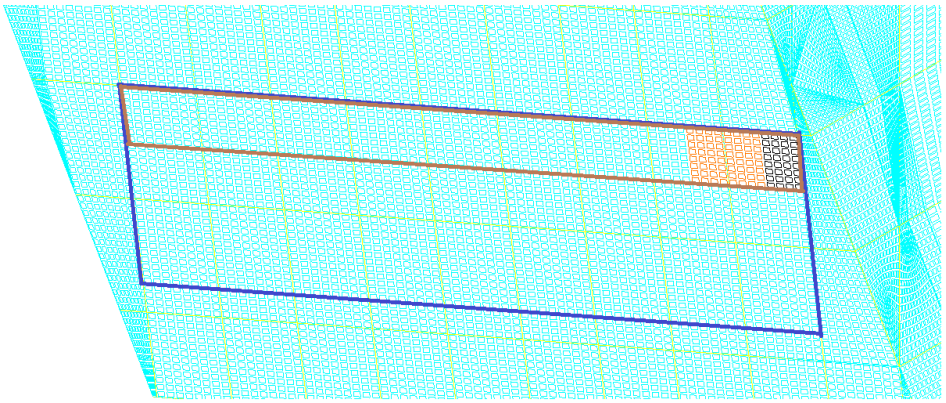

Figure 7.2: Level 1 load area. Blue lines indicates the total load area, brown lines the load area for level 1, orange area are element used for the 2^{nd} load case and black area are elements used for the 1^{st} that is not included in the 2^{nd} load case

is possible to detect where the plate deflects without having stiffeners to supporting it, and where the frame and stringers supports the plate to not deflects as much.

Figure 7.4 shows the inside of the bow region at the location of the sensors in load case 8, level 1. The 5 figures are the contour plots of the deformed shape 7.4(a) and the 4 stress states von Mises 7.4(b), τ_{xy} 7.4(c), σ_x 7.4(d), and σ_y 7.4(e).

As we could observe in figure 7.3, we could see in figure 7.4(a) that the deflections are largest where the plate is unsupported by the frame and the stringer. The intermediate frame also gets high deflections in the area of loading and the stringers get smaller deflections. The magnitude of the largest deflection is 0.77 mm.

The von Mises criterion is a common used scantling requirements. If we use coordinate stress instead of principle stress and assuming plane stress condition the von Mises equation from equation (4.1) will be:

$$\sigma_j = \sqrt{\sigma_x^2 + \sigma_y^2 - \sigma_x\sigma_y + 3 \cdot \tau_{xy}} \tag{7.1}$$

In figure 7.4(b) we could see which part of the hull that is subjected to stress. The highest consecration of stress is found at the intermediate frame at the end facing towards centerline of the ship and close to the stringer at 6700 mm above baseline. This stringer is also subjected to high von Mises stress for the part extending from the intersection with the fram and towards the centerline of the ship.

The contour plot for von Mises stress will in a way sum up the total stress applied to the model. To be able to see which stress factors that influences which parts, we have to look on the contour plots for τ_{xy}, σ_x and σ_y.

Figure 7.4(c) shows the contour plot of the shear stress τ_{xy}. The plate is not influenced by much shear stress. This seams reasonably since a plate with an applied patch load would not generate hear stress in the plate. The stringer at 6700 mm ABL has shear

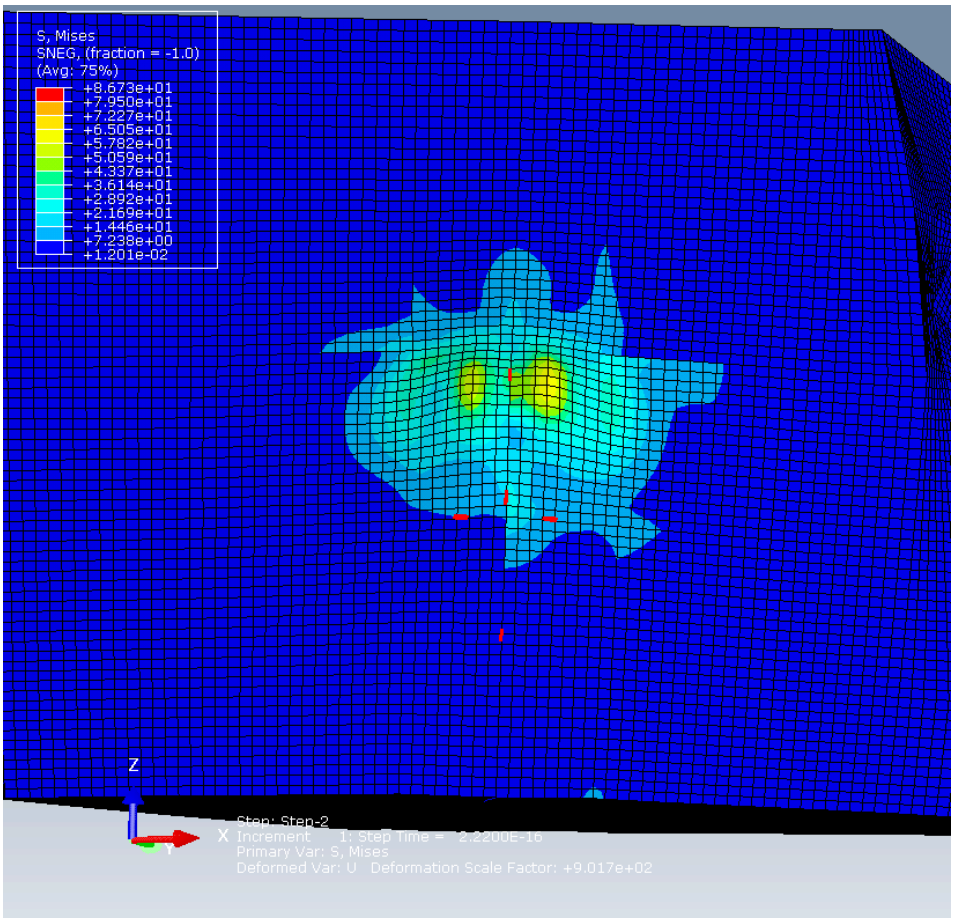

Figure 7.3: Load case 8 on level 1; red elements indicates where the sensors are located and the contour plot shows the von Mises stress in this load case

stress at both side of the intermediate frame, but with opposite values. The left side of the stringer has an larger area that is subjected to shear stress. The largest stress concentration of shear stress is found at the intermediate frame, in a small area right below the stringer. This is in the same area where the load is applied to the plate. At the bottom of the intermediate frame towards the stringer at level 5900 mm ABL there is an larger area of shear stress with the opposite sign compared to the small area at the top. This has also an absolute value of stress that is half compared to the small area.

Next it is time take a look on the axial stress σ_x in figure 7.4(d). Where the plate has it highest deflection, we also find axial stress. Both side of the intermediate frame has almost the same absolute value of the axial stress. The intermediate frame has an small area where it is subjected to high axial stress, and this relates to the area where the frame has the largest deflection. At the stringer 6800 ABL there is large axial stress along the edge of the stringer, in the approximate area where the load is subjected to the plate. The same effect could also be seen in the stringer below, but here with smaller values.

In figure 7.4(e) the transverse stress is in focus. For the plate there are transverse stress in the area where the plate has large deflection, but the peak area here is smaller than

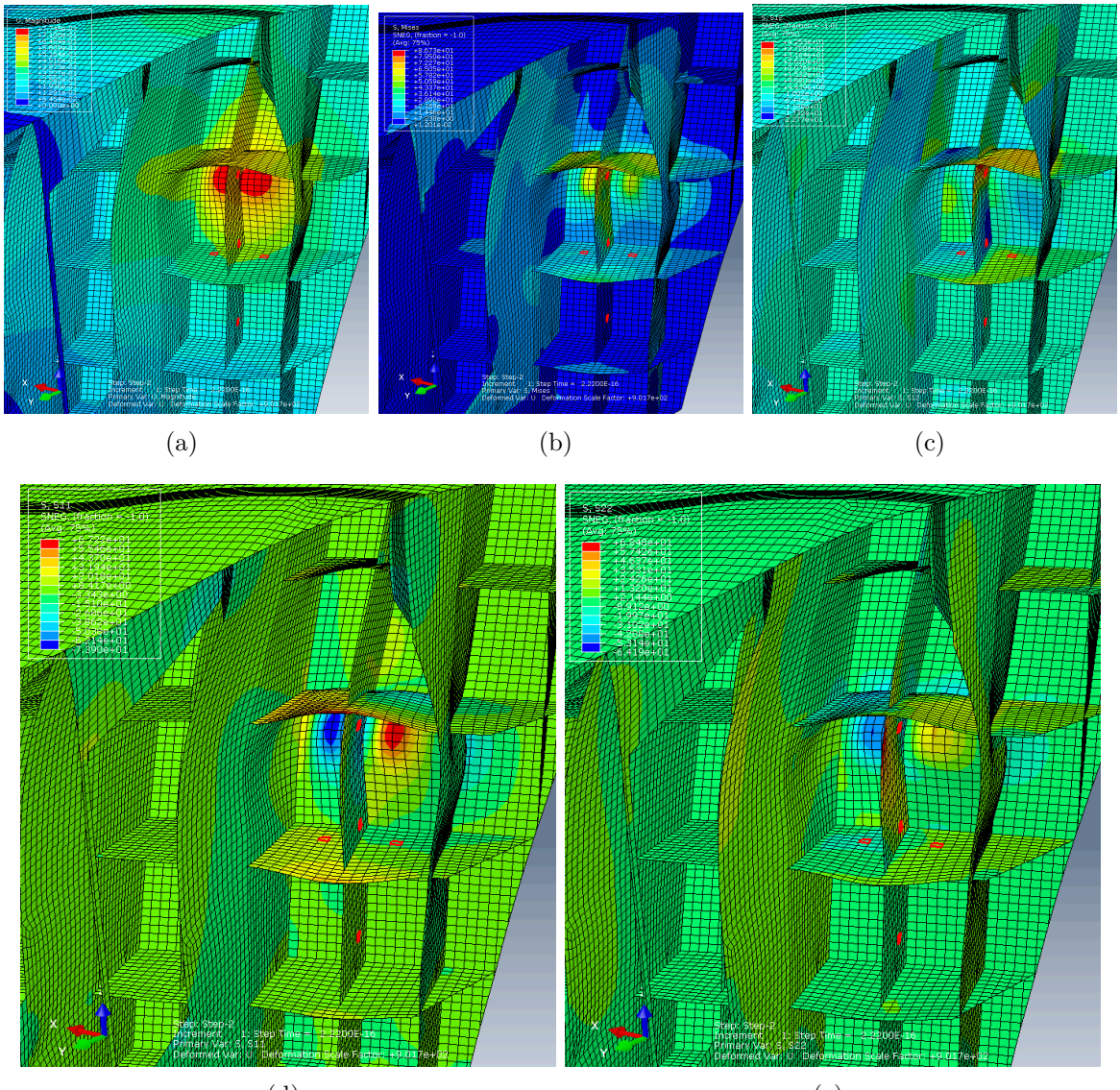

(a) (b) (c)

(d) (e)

Figure 7.4: Contour plots from inside of the bow area at load case 8, level 1; 7.4(a) shows the deformation magnitude U, 7.4(b) showing the von Mises stress, 7.4(c) showing τ_{xy}, 7.4(d) showing σ_x, and 7.4(e) showing σ_y. Red elements shows where the different sensors are located

	von Mises	τ_{xy}	σ_x	σ_y
Sensor 1	55.9044	28.0498	-31.0508	-9.0586
Sensor 2	38.6081	-17.8287	-9.45415	16.9516
Sensor 3	1.5154	-0.695017	-0.360848	-1.04623
Sensor 4	22.6707	-5.3893	11.6286	-12.2247
Sensor 5	22.6363	11.5221	-6.48051	5.84985

Table 7.1: Values for the stress factors in load case 8 at level 1

for the axial stress. There is also a difference between the two side of the frame, the left side has an large peak area and larger absolute value of the transverse stress. In the stringer there is an area at the left side of the intermediate frame, towards the plate, of transverse stress. This area is of same extent as transverse stress area at the plate on the left side of the intermediate frame. The highest values of transverse stress is found at the edge of the intermediate frame, from the stringer at 6700 mm and 1/3 down the frame towards next stringer.

By systematically inspect the contour plot for τ_{xy}, σ_x and σ_y we could detect where these stress factors contributes to the von Mises contour plot. The stress at the plate in the largest deflection areas are dominated by σ_x, but also have contribution from σ_y. The stringer has most of its contribution from τ_{xy}, but towards the plate it has influence from σ_y and is highly dominated by σ_y along the edge towards centerline. The intermediate frame has an mixture of all the stress factor. The dominating are the σ_y at the edge and the area of τ_{xy} close to the stringer at 6700 mm.

In table 7.1 the values for the stress factors at the sensor locations are listed.

If we use equation 7.1 to calculate the von Mises stress based on the 3 components stress given in table 7.1, and then compare it to the von Mises stress Abaqus gives us in the same table, there is a major difference between them. Both the values and their difference are shown in table 7.2. When calculating the value, the absolute values of the different stress components are used to give the largest possible von Mises stress. When comparing the contour plots for the 4 different stress components in figure 7.4, there does not seem to be missing any other major stress component. But when we compare the shear stress τ_{xy} with the axial and and transverse stress, there might be other shear stress components in other directions that could effect the von Mises stress. This might mean that we do not have a plane stress situation. An attempt to find out how Abaqus calculates its von Mises stress in its theory manual was attempted. This problem was discovered late in the completion of the thesis, and due to time limits, not figured out before the completion. This problem does not seem to inflict on the found results.

7.3.2 Stress at sensors with patch load in level 1

In this section we will study the effects of the measured stress at the sensor location when we apply the 17 different load cases along the hull in level 1. The values are extracted from the Abaqus analysis and imported to Microsoft Excel. Then the figures

Sensor	von Mises from Abaqus	von Mises calculated	Difference
1	55.9044	37.5717	32.79 %
2	38.6081	24.2999	37.06 %
3	1.5154	1.9202	-26.72 %
4	22.6707	21.0473	7.16 %
5	22.6363	12.1940	46.13 %

Table 7.2: Comparing values for von Mises with Abaqus results and by using equation for von Mises based on plane stress assumption

in this section is created. The figures for all the different levels are found in appendix C in larger size.

Axial stress

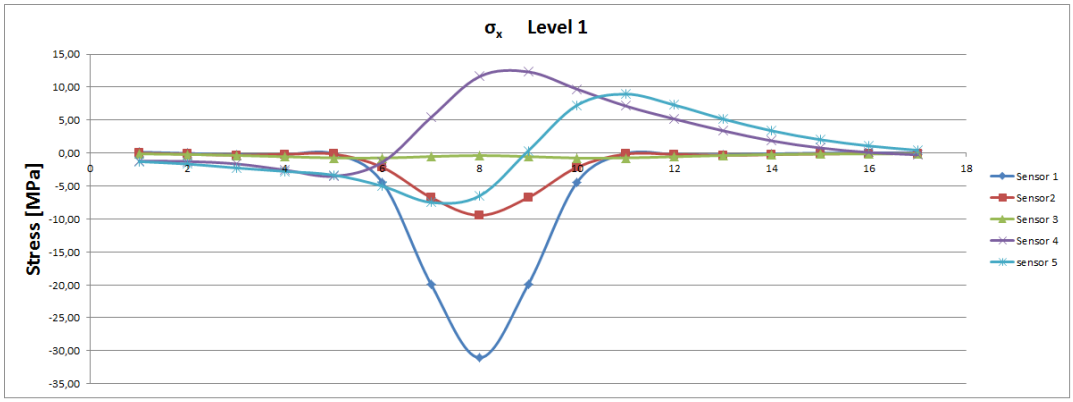

Figure 7.5: Axial stress σ_x at sensors for load cases in level 1. Stress at the y-axis and the load case number along the x-axis. The load cases start at the bow, and backwards along the hull (see fig 7.2)

In figure 7.5 we could see the measured axial stress in each sensor for the different locations of the patch load. Load case 1 is located nearest the bow, load case 8 is symmetrically loaded on each side of the frame where the sensors are located and load case 17 is located aft of the model (see figures 7.2 and 7.3) With this figure it is possible to see the effects of the load "travelling" along the hull, when it is passing area where the sensors are changing sign from positive to negative (or opposite) and the effects of the geometry of the hull makes on the measured stress.

The axial stress on sensor 1 is symmetrical around load case 8, and the stress is taken as compressive stress. This agrees with the evenly distributed patch loading on the plate. For sensor 1 the axial stress does not much effect before load case 6. In this load case the patch load is applied symmetrically on the adjacent frame compared to the intermediate frame the sensor is located on. This is illustrated in figure 7.6. The loading on the sensor increases to load case 8 where the patch load is symmetrically loaded on intermediate frame where the sensor is located (see figure 7.4).

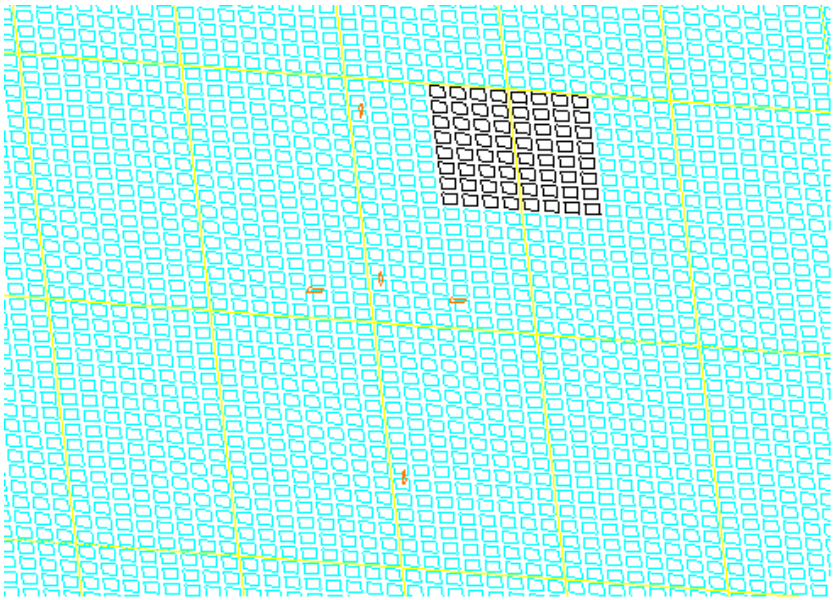

Figure 7.6: Load area for load case 6 at level 1. Black elements are the elements subjected to the patch load and orange elements indicates where the sensors are located.

Sensor 2 experience much of the same stress conditions as sensor 1, since it is located on the same intermediate frame and in between stringer 6700 mm and 5900 mm ABL. The peak load is naturally lower since this sensor is not within the area of the patch load on the plate. This could closely studied on figure 7.4(d)

Sensor 3 is not subjected to much axial load by the load cases in level 1. This sensor is situated far from the load patch area, and from the geometry of model we could see that the axial stress will be taken up by stringers and frames before acting on sensor 3.

Sensor 4 and sensor 5 is located on stringer 5900 mm ABL. Sensor 4 is placed on left side of the intermediate frame (Seen from center line, see figure 7.6), closest to the bow. This causes sensor 4 to experience stress before sensor 5, and when the load has passed both sensors, sensor 5 will have the highest stress due do the fact that it is closer to the load.

Sensor 4 experience compressive stress until between load case 6 and 7. When the load patch is situated on the sensor location or has passed the location, on this position on the stringer will experience tensile stress. This is the same case for sensor 5, the stress will go from compressive to tensile after passing the sensor location. It was not expected that these sensor would measure so much stress outside the load area of the frame. This could indicate that the stringer is transferring loads from other parts of the hull, and these sensor could measure these loads.

The stress peaks for sensor 4 and 5 have different maximum value. This is due to the mesh of the model and the chosen element to represent these sensor. There are in total 8 elements between the frame and intermediate frame, and both sensor 4 and 5 are chosen as the 4^{th} element from the intermediate frame towards the frames on each side.

Both sensors will then not be in the center of the stringer between the frame (but one of the edges of the element is). Since the load patches are placed symmetrically in the load cases, this could make the sensor to measure different stress levels when they actually should have been the same. If the mesh generated 9 elements between the frames and then have chosen the sensors to be the middle element. Or if the load patches was incremented by 1 element by each load case made instead of 4, this should have yielded the same result.

Transverse stress

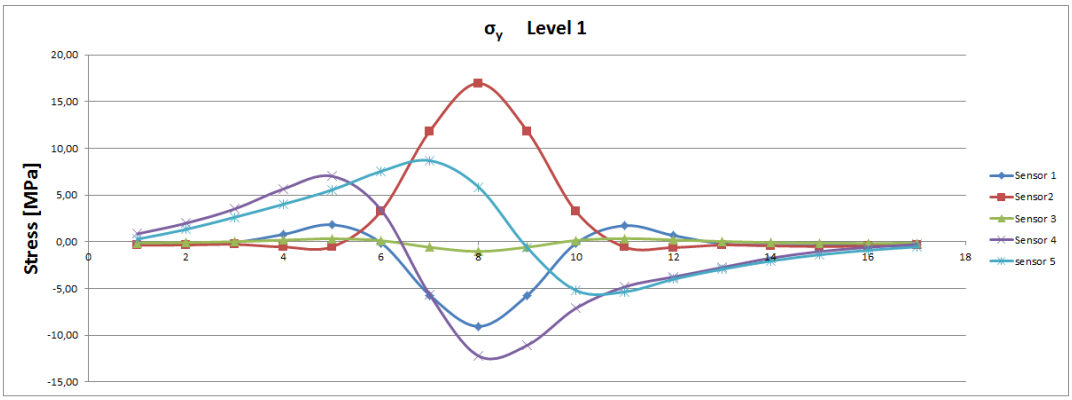

Figure 7.7: Transverse stress σ_y at sensors for load cases in level 1. Stress at the y-axis and the load case number along the x-axis.

The transverse stress for the sensors over level 1 in figure 7.7 is in many ways the opposite stress pattern for the sensors as the axial stress in figure 7.5.

For sensor 1 the transverse stress is experienced as tensile stress until load case 5. As long as the load patch is on the other side of a adjacent frame, the plate will try to "pull out" the intermediate frame. When the load patch is within the load area of the intermediate frame (loadcase 6 to 10), this sensor will experience compressive stress. If we look closer on figure 7.4(e) we could see in the area of this sensor, the intermediate frames takes much compressive stress at the edge due to the location of the patch load.

Sensor 2 has the opposite stress pattern compared to sensor 1. It experience compressive stress until load case 6, where the experienced stress is shifted to tensile stress. Again if we look on figure 7.4(e), sensor 2 is located close to the boundaries of stringer on level 5900 ABL. The boundary conditions of the frame will inflict on the transverse stress at this location.

Sensor 3 is still to far from the load patch area to experienced any significant stress.

Sensor 4 and 5 are experiencing stress for all load cases since the stringer they are located on are carrying the inflicted stress along the hull until the stress is transferred to a bulkhead. Sensor 4 is still experiencing the stress before sensor 5. Both sensor experience tensile transverse stress before the load patch passes the sensor location. After the load patch has passed the sensor location, the stress is taken as compressive.

As in figure 7.5, the peak stress at sensor 4 and 5 does not match. For sensor 4 the highest stress is the compressive stress and for sensor 5 it is the tensile stress that is highest.

Shear stress

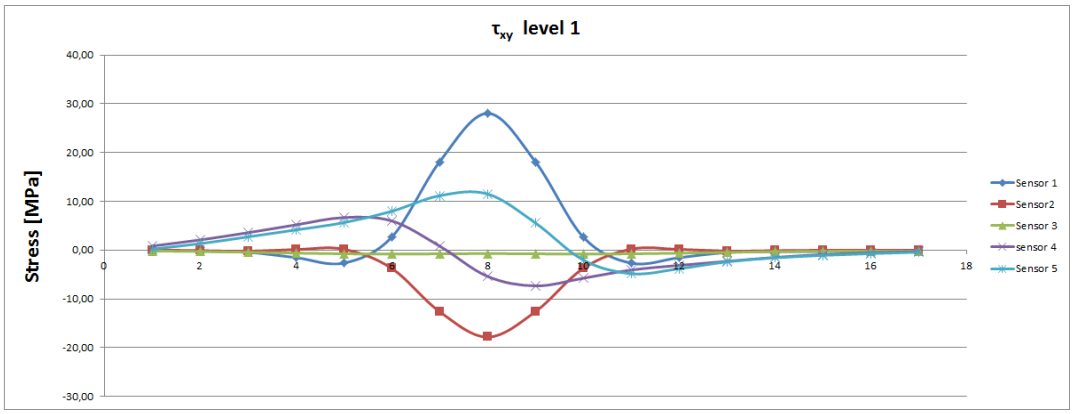

Figure 7.8: Shear stress τ_{xy} at sensors for load cases in level 1. Stress at the y-axis and the load case number along the x-axis.

The shear stress for the sensors over level 1 is shown in figure 7.8. For sensor 1 the shear stress starts around zero for the 4 first load cases and then starts out as a small compressive stress before turning into a tensile stress at load case 6. Around load case 6, the load patch is located on the other side of the adjacent frame to the intermediate frame where the sensors are located. This geometrical condition could make the plate to transfer compressive stress to the sensors. The same could be observed at load case 10. Inside the load patch area of the frame we get an high tensile load peak for sensor 1. The peak at load case 8 is illustrated in figure 7.4(c). We could see that the frame in the area of sensor 1 has a very local high tensile area due to the frame is close to the stringer at this point.

For sensor 2 we get an compressive stress peak within the load area of the frame. If we refer again to figure 7.4(c) we could see that also sensor 2 is close to a stringer, and this conditions makes the area of sensor 2 to take high compressive shear stress. Sensor 3 is still to far away to experience any shear stress.

As for the axial and transverse stress, sensor 4 and 5 experiences shear stress for all of the load cases. Both starts out as tensile stress, before they change to compressive stress when they pass their sensor location. They are also not symmetrical on their load peaks due to my placements of the sensor and the mesh on this location.

von Mises stress

The von Mises stress criterion for plane stress will include the effects from τ_{xy}, σ_x and σ_y (see equation (7.1)). By comparing figure 7.9 with figure 7.5, 7.7 and 7.8, we could

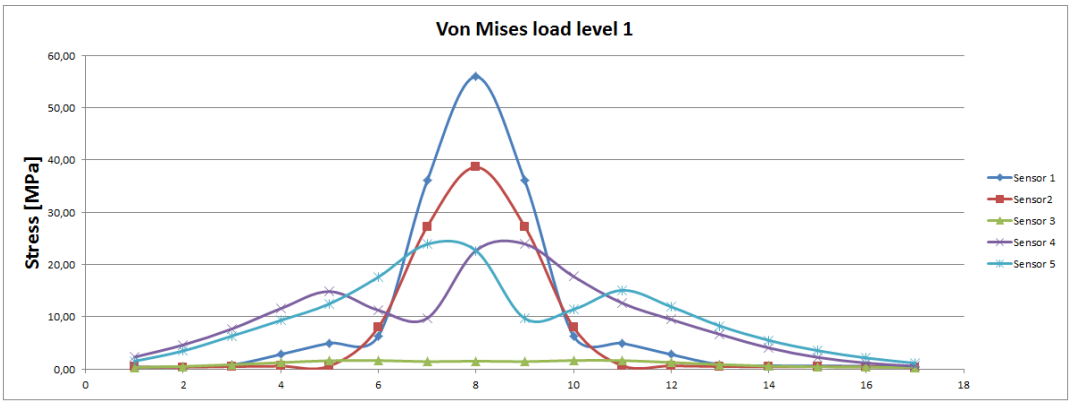

Figure 7.9: von Mises stress at sensors for load cases in level 1. Stress at the y-axis and the load case number along the x-axis.

see which of the stress factors that is dominating the von Mises plot. We should keep in mind how von Mises is calculated (see equation (7.1)) since the different factors have different influence. Both σ_x and σ_y are squared terms, so τ_{xy} need to be large value to have an influence.

For sensor 1 the dominating factor is the axial stress σ_x. This is not surprising since this sensor is close to the load patch area. Even though τ_{xy} has almost the same absolute value as σ_x at load case 8 (see table 7.1), this does not effect the total von Mises stress by much.

For sensor 2 the dominating factor is the transverse stress σ_y.

Sensor 3 is too far from the load area to experience any significant stress.

Sensor 4 and 5 has an interesting von Mises stress pattern. Both sensors has symmetric stress around load case 8, so here the error of not placing the sensor exactly on the midpoint between the frame and intermediate frame cancel out. Both the sensors are affected by the 3 different stress factors, but σ_x and σ_y are still dominating. And compared to the other sensors that are located on the frame, these sensor are definitely experiencing loads outside the frame loading area. The stringer will carry stresses from loads from other parts of the hull along the hull through this frame location.

7.4 Level 2 to 6

The levels 2 to 6 with corresponding load cases will not be analysed as level 1 was in the previous section. The graphs over the stress components for each sensor and level could also be found in appendix C.

Level 2

The load area of level 2 overlap level 1 with 200 mm in vertical direction. Figure 7.10 shows how load case 2 at level 2 overlap load case 1 at level 1.

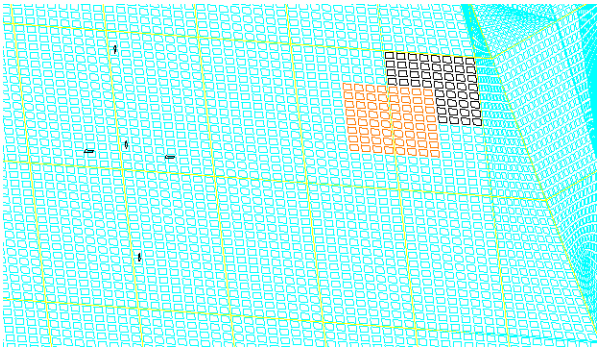

Figure 7.10: Load case 2 on level 2; Black elements are the elements subjected to the patch load at load case 1 level 1 and orange elements indicates Load case 2 on level 2. The sensor locations are also shown as black elements

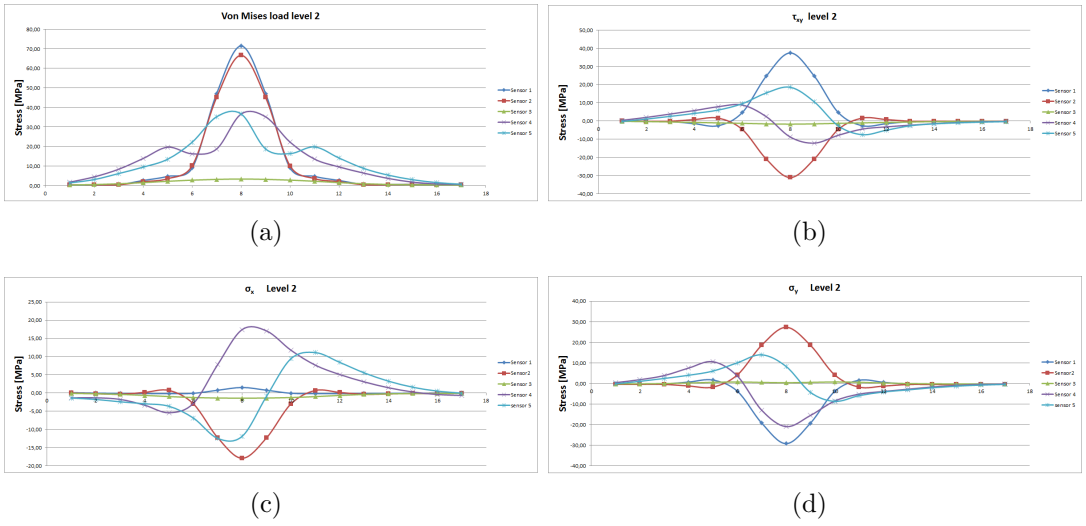

Figure 7.11: The 4 different stress factor at Load level 2

The effect of the load area is shifted vertically by 200 mm is clearly present in the graph over von Mises stress in figure 7.11(a). Sensor 1 and Sensor 2 are at an higher stress level than in figure 7.9. They are also much closer in value. Sensor 4 and 5 have still their same stress pattern and they have an higher stress level. Sensor 3 is still not effected much by the load patch. If we look closer on to sub figures 7.11(b) to 7.11(d), the difference from level 1 is mostly increased stress levels for all the sensor. The only exception is the axial stress for sensor 1, which goes from being a high compressive stress to being a small tensile stress.

Figure 7.12 shows the von Mises contour plot for load case 8 at level 2. The red elements shows the placement of the elements. The area of highest von Mises stress concentration

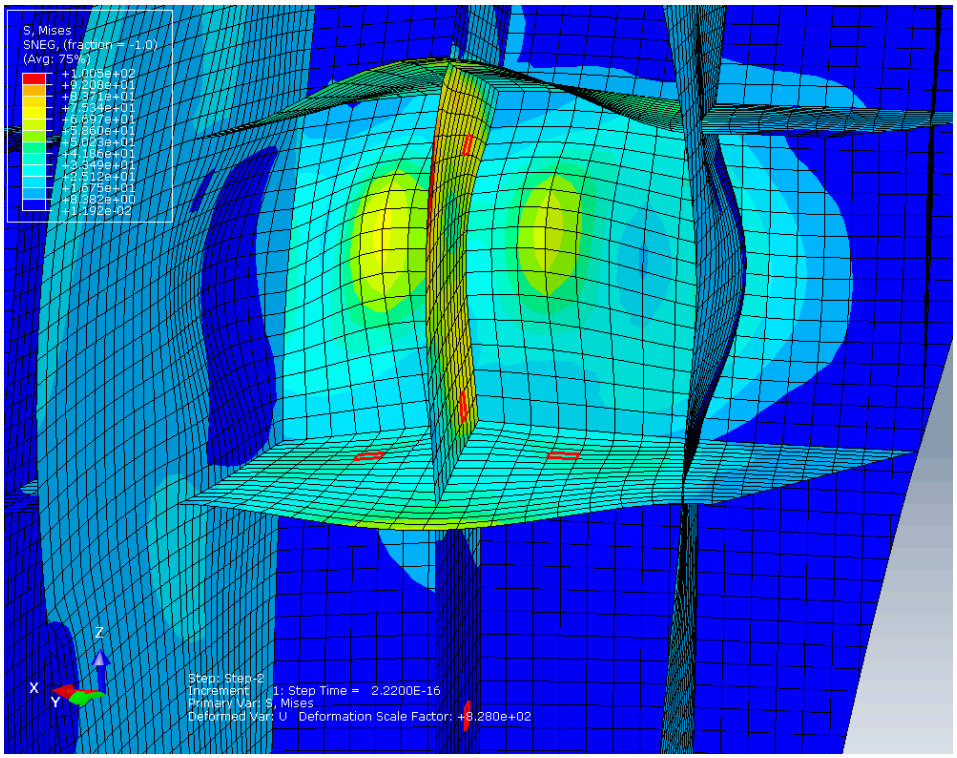

Figure 7.12: Load case 8 on level 2; red elements indicates where the sensors are located and the contour plot shows the von Mises stress in this load case

is as in figure 7.4(b) at the edge of the intermediate frame. Since the load now is lower than i level 1, the peak area is also lowered. σ_y is the dominating factor here, but also τ_{xy} at the frame towards the stringer plays a part.

Level 3

In figure 7.13(a) we could see the von Mises stress pattern changes some from level 2. Sensor 1 decreases, sensor 2 increases some, sensor 3 has influence of the stress factors, and sensor 4 and 5 increases to above sensor 1. τ_{xy} is increased for all stress factors in figure 7.13(b) except sensor 1. In figure 7.13(c) sensor 1 gets a increased tensile stress and sensor 2 gets increased compressive stress for σ_x. The other factors also gets an higher load peak compared to level 2. Sensor 4 and 5 gets most increase in σ_y in figure 7.13(d) compared to the other sensor that are almost at the same level. All of the figures are compared to the corresponding figures for level 2.

Figure 7.14 gives an interesting change of the von Mises contour plot compared to figures 7.12 and 7.4(b). We still get at stress concentration at the edge of the intermediate frame that moves along with the moving load. But we also get an high stress concentration at the lower part of the intermediate frame towards the plate and stringer at 5900 ABL, and at the middle of the edge of the stringer. The stringer also sees more stress than the other load case 8 at the levels above.

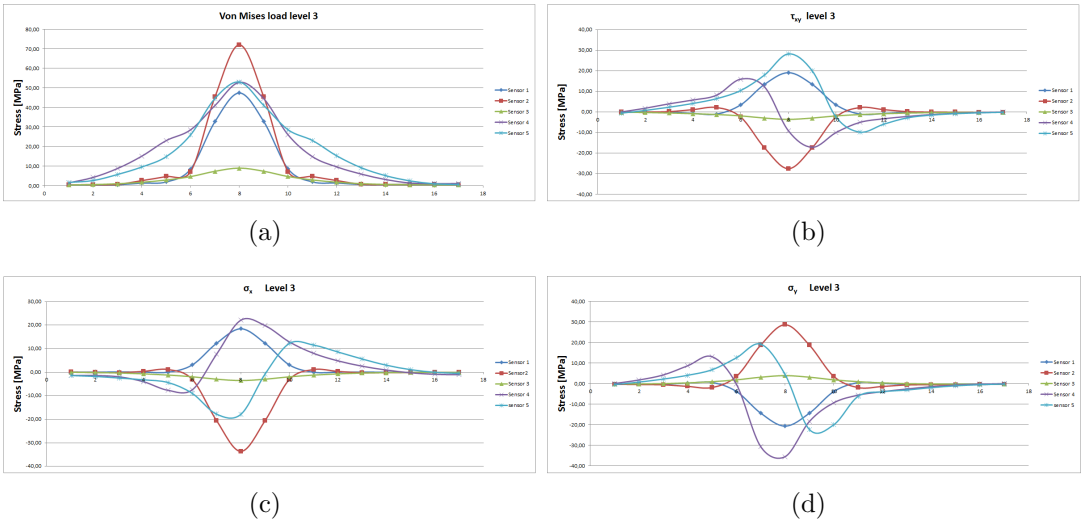

Figure 7.13: The 4 different stress factor at Load level 3

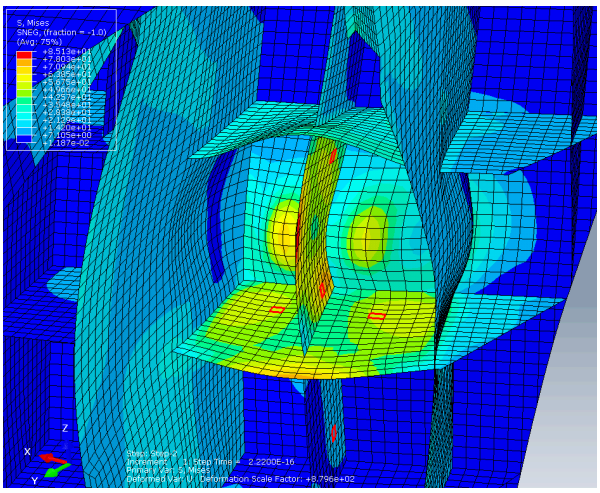

Figure 7.14: Load case 8 on level 3; red elements indicates where the sensors are located and the contour plot shows the von Mises stress in this load case

Level 4

On level 4, the patch load is symmetrically loaded on stringer 5900 ABL. Since sensor 1 and 3 are situated at the same distance from this stringer, both these sensor will have the same von Mises stress for all level load cases as seen in figure 7.15(a). Sensor 4 and 5 will have the largest von Mises stress here, and this will be the highest stress these sensor will have under all the load cases in the different levels. Sensor 2 have the same von Mises peak as sensor 1 and 3 at load case 8, but has an different stress pattern for the other load cases.

In figures 7.15(b) to 7.15(d) we see that sensor 1 and 3 has the same absolute value, but have opposite signs. This seems appropriate due to the symmetrical load area and the sensor are placed symmetrical on each side of the load patch. Sensor 2 is most

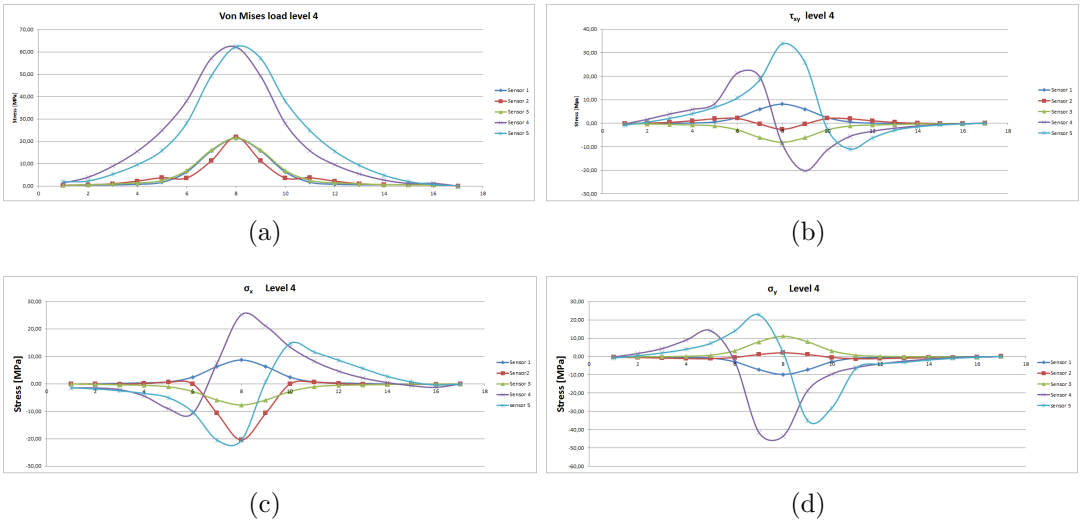

Figure 7.15: The 4 different stress factor at Load level 4

influenced by compressive σ_x since this sensor is situated in the load patch area. Sensor 4 and 5 are influenced by all the 3 stress factors.

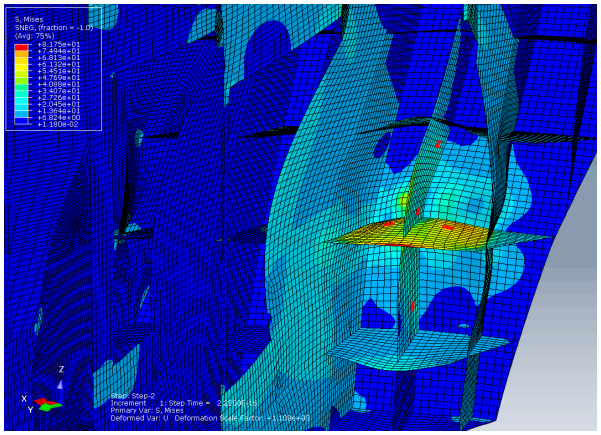

Figure 7.16: Load case 8 on level 4; red elements indicates where the sensors are located and the contour plot shows the von Mises stress in this load case

The contour plot of load case 8 at level 4 in figure 7.16 yields new places for high stress concentration. As in figure 7.16 in middle at the edge of the stringer has high stress, but also at stringer in the middle between the intermediate frame and the frame towards the plate yields 2 new hot spots. The intermediate frame on both side of the stringer is also influenced by quite some stress.

Level 5

For level 5, the patch load area is on the other side of the stringer compared to level 3. If we look closer on figure 7.17(a) and compare it with figure 7.13(a), we could see that sensor 4 and 5 have the same stress peak, but the stress pattern around load case 8 are

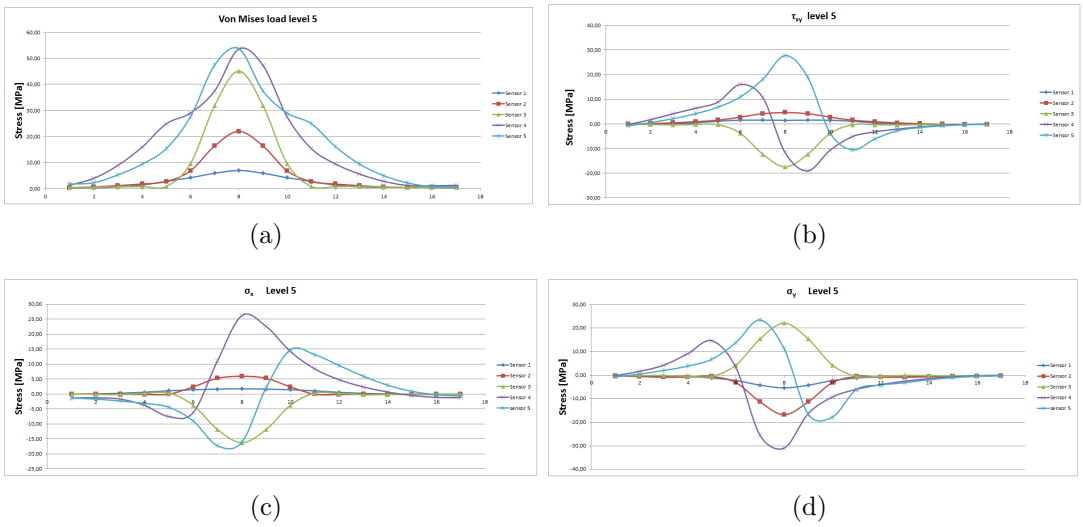

Figure 7.17: The 4 different stress factor at Load level 5

slightly different. Sensor 1 experience an lower stress level than under level 4, sensor 2 has the same peak load as level 3, but with an other stress pattern, and sensor 3 has an higher stress level. This is natural since the load patch area is closer to sensor 3 for each new level of load cases.

If we compare figure 7.17(b) with 7.15(b), we could that all the sensor experience an lower τ_{xy} in level 5 than in level 4, except for sensor 3. For σ_x we could see in figure 7.17(c) that it changes from a compressive stress to a tensile stress. The other sensor experience the same stress level, or lower. In the last stress factor σ_y in figure 7.17(d), all sensor except 2 and 3 are lowered. Sensor 3 increases its tensile stress, and sensor 2 changes from a tensile stress to a larger compressive stress.

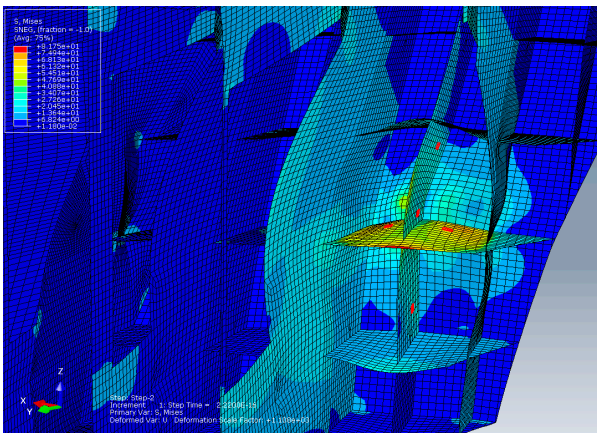

Figure 7.18: Load case 8 on level 5; red elements indicates where the sensors are located and the contour plot shows the von Mises stress in this load case

Figure 7.18 shows the von Mises contour plot of load case 8 at level 5 looks very similar to figure 7.4(b), except that the stress is shifted down one stringer level.

Level 6

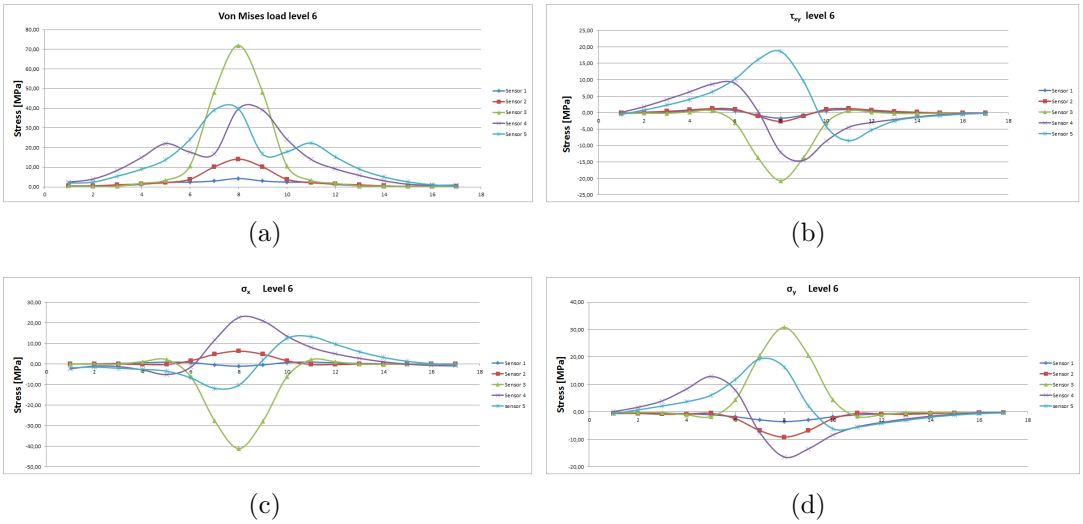

Figure 7.19: The 4 different stress factor at load level 6

On level 6, the patch load area is closest to sensor 3, and this is shown in figure 7.19(a) as this sensor has the largest stress peak. Sensor 4 and 5 has almost the same stress pattern as in level 2, as seen in figure 7.11(a). Sensor 1 and 2 experience an lower stress level than under level 5.

For the other stress factors in figures 7.19(b) to 7.19(d), all sensors except sensor 3 experience lower stress than in level 5.

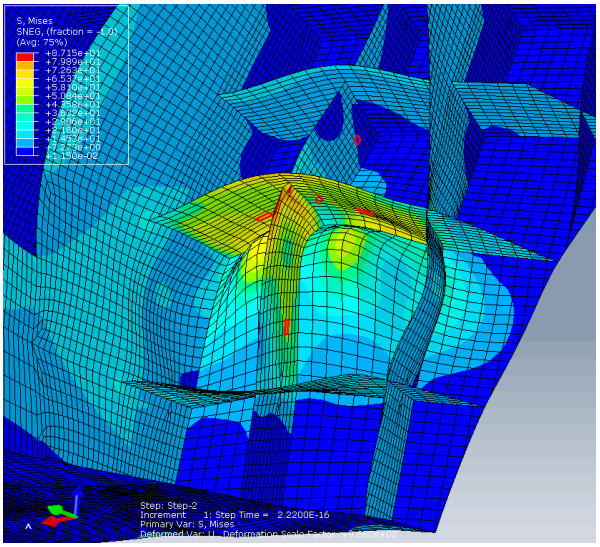

Figure 7.20: Load case 8 on level 6; red elements indicates where the sensors are located and the contour plot shows the von Mises stress in this load case

Figure 7.20 shows the contour plot of load case 8 at level 6 looks also similar to an other contour plot, figure 7.4(b), and here also the stress is shifted down one stringer level.

7.5 Stress at each sensor over the different load case levels

In this section we will compare the stress values of each sensor at different load levels compared to the previous section where all the 5 sensor where compared at each level. All the figures are found in appendix C from figure C.7 to C.11.

Sensor 1

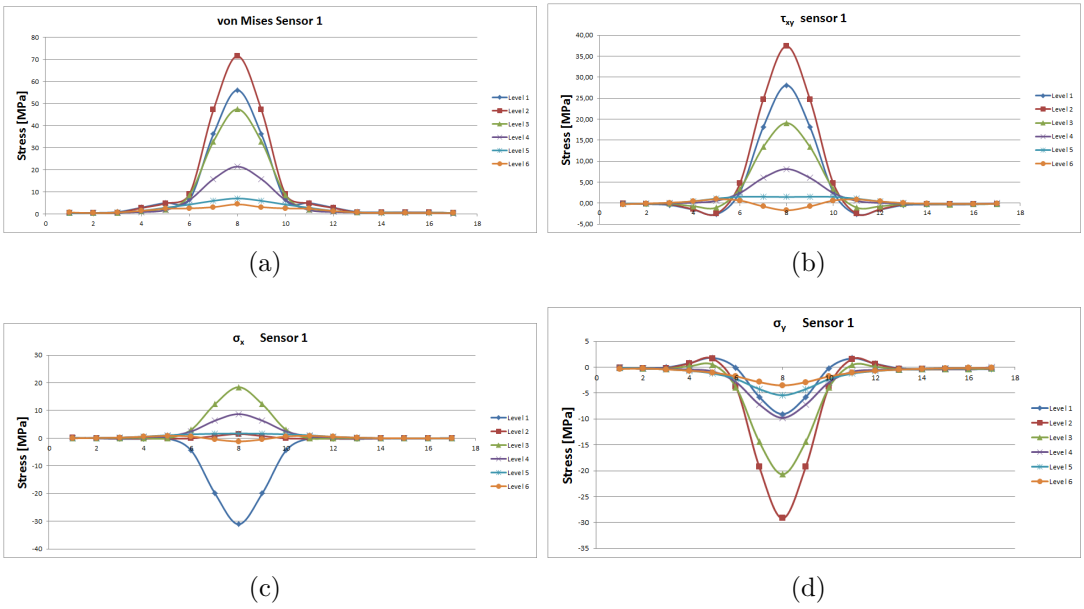

Figure 7.21: The 4 different stress factor for sensor 1 for the 6 different load levels

In figure 7.21(a) we could see that the von Mises stress decreases as the load patch area moves down along the hull with the level. The trend for this sensor is that it only measure patch loads that are within load cases 6 to 10. Load case 6 and 10 extend over the neighbouring frames to the intermediate frame. These load cases are within the area where frame 4 is expected to carry loads exposed to plate.

Figure 7.21(b) shows the change in shear stress over the different levels. Within the frame load area the shear stress is positive and descending for the levels, and for level 6 it has become negative. At this level, the load is below the stringer, this shift could be explained by this geometrical change between the sensor and the load. We could also observe that we have some negative shear strain between load case 3 and 6, and 10 and 13. These cases are located on the other side of a frame from the load area and the sensor. As the example with the stringer, these geometrical changes will give different boundary conditions.

The axial stress illustrated in figure 7.21(c) shows a highly compressive stress over the sensor for level 1. In this case the load patch is situated on top of the sensor, and is

naturally yielding a large compressive stress. In level 2, the axial stress transfers to a become small tensile stress, before it gets its largest tensile stress at level 3 and the descends for the following levels. This change in tensile stress could be tracked when watching the contour plots for von Mises in the previous sections.

Transverse stress in figure 7.21(d) has the same trend as figure 7.21(b) for load cases outside the expected frame loading area. The geometrical layout gives different boundary conditions for the transverse stress. The transverse stress for level 1 is not too high, since we have an high axial stress at this point. The largest compressive stress is found in level 2, and descends as the load patch is placed further down the hull.

Sensor 2

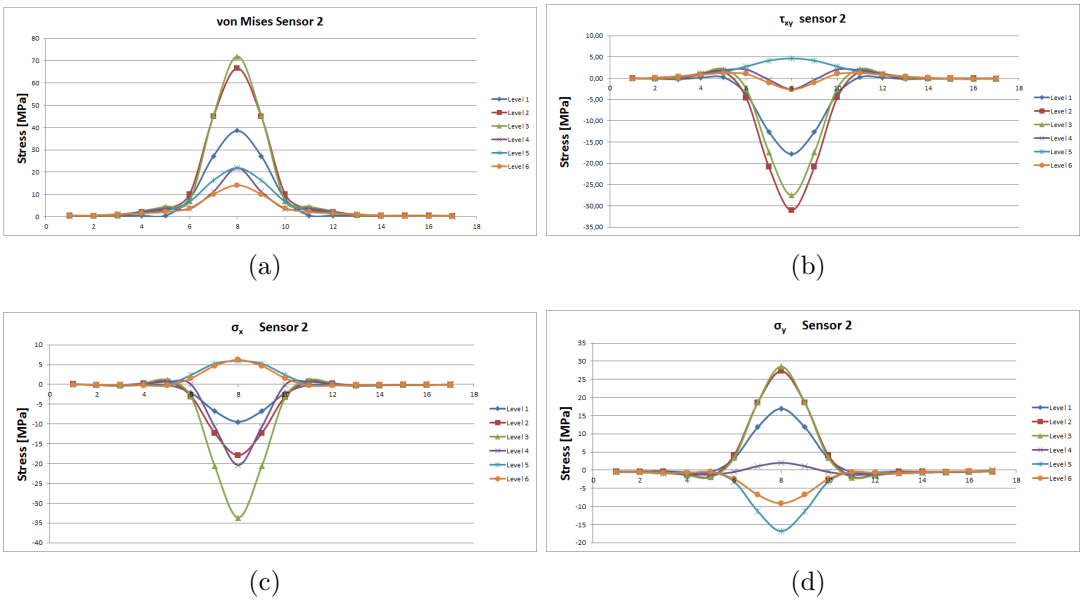

(a) (b)

(c) (d)

Figure 7.22: The 4 different stress factor for sensor 2 for the 6 different load levels

For sensor 2 we could see in figure 7.22(a) that the von Mises stress increases from level 1 to level 2 and then peak at level 3, before it decreases as the load patch area moves down along the hull.

The same trend is evident in figure 7.22(c) for the axial stress. For level it starts as a small compressive stress before it increases to level 2 and peaks at level 3. The axial stress changes to a tensile stress at level 5. This is due to combinations of that sensor 2 is close to the stringer at 5900 mm, with geometrically effects this has on stress. and level 5 the load patch is also lower located than sensor 2.

In figure 7.22(b) that shows the shear stress, at level 1 the shear stress is a tensile stress. This state is shown in contour plot in figure 7.4(c). The patch loads create a compressive stress in the frame up against stringer at 6700 ABL, and this is counteracted by a tensile stress in the lower part of the frame against the stringer at 5900 ABL. The peak for

the shear stress is in level 2 as a compressive stress, and decreases as the load patch is placed further down the hull

The transverse stress in figure 7.22(d) is very different compared to sensor 1. As the axial stress, the transverse stress increases from level to 2 and peaks at 3 before it decreases. But here the peak loads are tensile until level 5. It should be noted that the stress is higher in level 5 than 4 when considering absolute values. Level 4 is symmetrical loaded around the stringer, and level 5 starts at the stringer and extends 400 mm further down. The placement of this load cases should yield more transverse stress.

Sensor 3

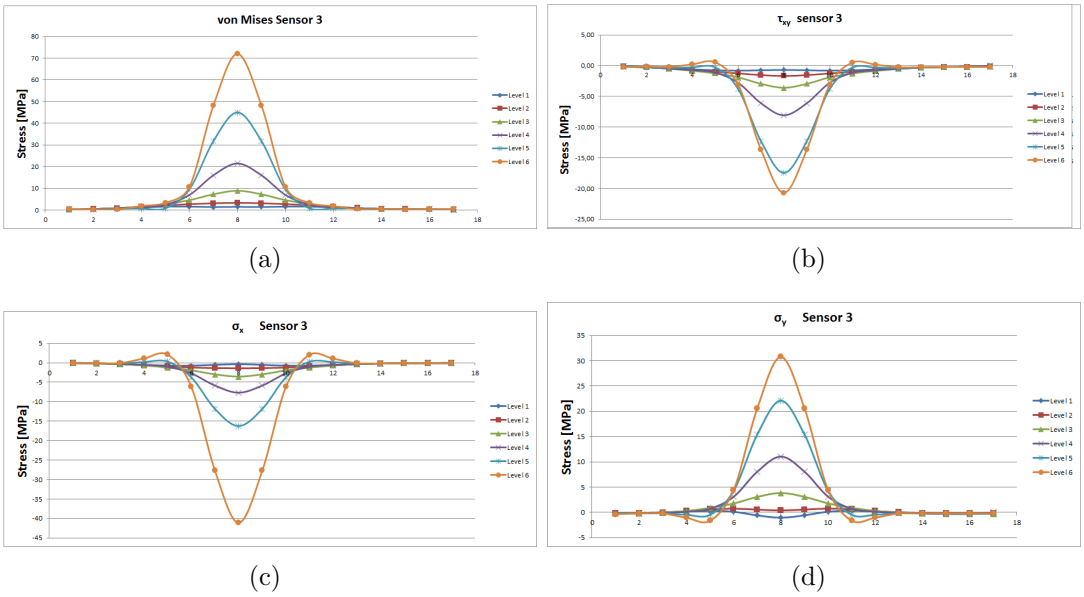

Figure 7.23: The 4 different stress factor for sensor 3 for the 6 different load levels

Since sensor 3 is located close to level 6 load patch area, the von Mises stress in figure 7.23(a) will increase for each level and peak at level 6.

The shear stress in figure 7.23(b) has almost the opposite figure as for sensor 1, expect that all values here is negative. Shear stress increases as the load patch area is closer to the sensor location.

In figure 7.23(c) the axial stress starts almost at zero before it gets more compressive stress for each level down the side of the hull. The peak is at level 6 where the load patch is situated on top of sensor 3. We see the same effect here as for transverse stress with sensor 1 where load cases outside the frame load area give some tensile stress to the sensor.

The tensile stress figure 7.23(d) is almost the opposite figure of the axial stress, except that we have 1 levels with compressive stress, the load peak is not so high and the levels in between are closer to the peak.

Sensor 4

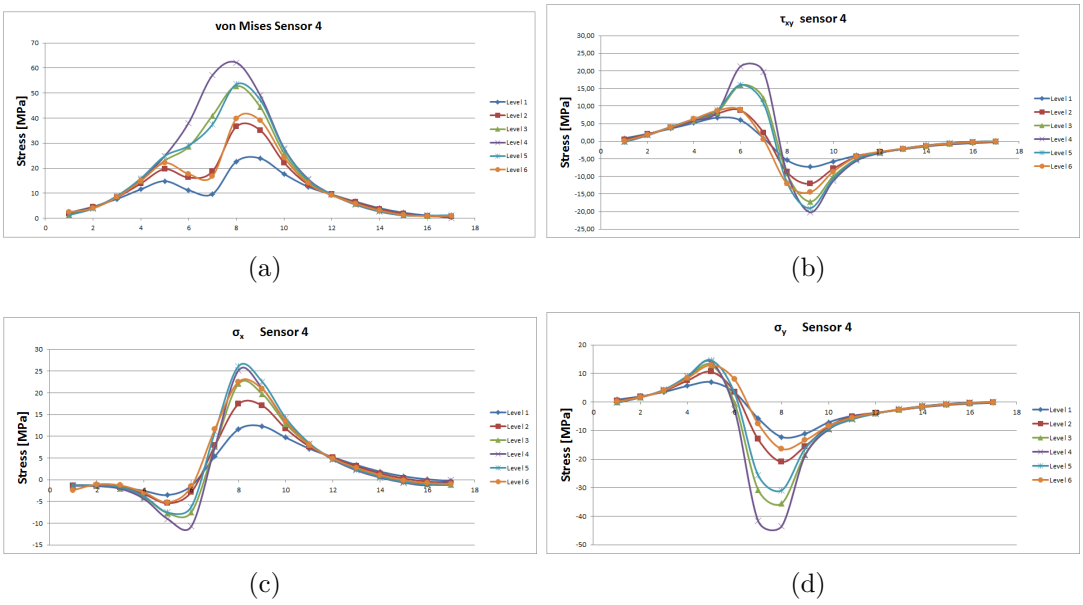

Figure 7.24: The 4 different stress factor for sensor 4 for the 6 different load levels

The von Mises stress for sensor 4 in figure 7.24(a) seems a little odd looking on for the first time. In this case we have the problem with the sensors that are not are placed in the center between the intermediate frame and the frame. If we combine this figure with the von Mises figure for sensor 5, we will get symmetry around the intermediate frame (see the figures for each level). The major difference for this sensor compared to sensor located on the frame, is that load cases outside the frame loading area is measurable in the sensor. This could mean that the stringer could transfer loads from other parts of the ship through it, and this could be picked up by the sensors here. In figure 7.24(a) we could see that the von Mises stress is smallest in level 1 before it increases up to peak at level 4 and then decreases again. Level 4 is when the stringer is symmetrically loaded on each side of it. Level 2 and 6, and level 3 and 4 are very close to each other. These load cases are at the same distance from the stringer on each side.

For the shear stress in figure 7.24(b) the different levels are approximately the same until load case 5 and from load case 11 and outwards. This could support the theory that loads outside the frame area could be carried by the stringer along the hull to sensors on different places than where the load is acting. Inside this area the levels have different steepness of the curves and load peaks. The order of lowest and highest load peak is as in the von Mises stress. The shear force shifts sign from tensile to compressive approximately at the sensor location.

The axial stress in figure 7.24(c) has many of the same trends as the shear stress. The levels have approximately the same value until load case 4, where they separate. But the value is very close to 0, so it might seem that the stringer does not carry axial stress outside the frame loading area for compressive stress. But on the other side of the frame loading area, the levels meet again at load case 11. This time the values are not close to

0, so the stringer might carry tensile stress along the stringer. The axial stress changes sign some before the sensor location. The peak load for the axial tensile stress is not level 4 as expected, but level 5.

The transverse stress shown in figure 7.24(d) is similar to figure 7.24(b). But here the the tensile stress is much lower than the compressive stress, and the stress shifts sign some before the sensor location. The effect of the geometry of the stringer and its boundary conditions to the frames could be the cause of this.

Sensor 5

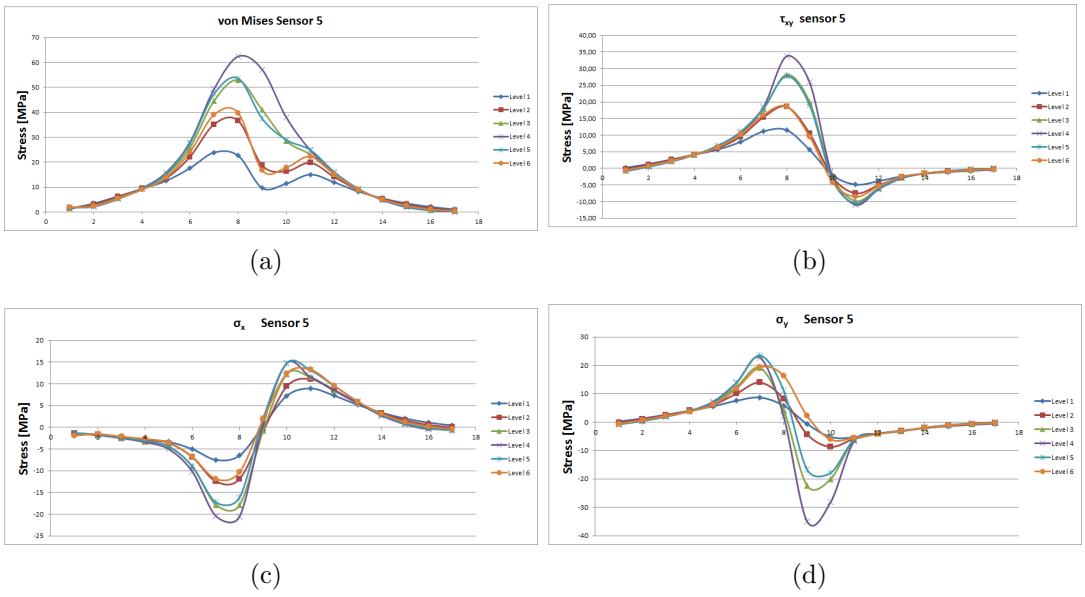

(a) (b)

(c) (d)

Figure 7.25: The 4 different stress factor for sensor 5 for the 6 different load levels

When considering the symmetrical placement of sensor 4 and 5, these sensor yields almost the same results for the von Mises stress (figures 7.24(a) and 7.25(a)). The shear stress shown for sensor 5 in figure 7.25(b) have some differences from sensor 4. The tensile peak is higher and the compressive peak is smaller than for sensor 4. It also changes sign from tensile to compressive some after the sensor.

For the axial stress in figure 7.25(c) we could see that before the frame load area the levels have the same value until load case 5. So the assumption made for sensor 4 that the stringer would not carry compressive stress from outside the load area is clearly wrong. Sensor 4 has also an higher compressive stress peak and lower tensile peak than sensor 4. The axial stress goes from compressive to tensile stress approximately at the sensor location.

Figure 7.25(d) shows the transverse stress at sensor 5, and have many similarities to the same load factor for sensor 4. But here the tensile stress has higher peak and the compressive stress a lower peak when we see on the absolute values. The different levels shifts sign from tensile to compressive stress over many different load cases.

All the figures in this section containing graphs could be found enlarged in appendix C.

7.6 Discussion of FEM results

In this chapter we have studied 102 load cases with the size of 400 x 400 mm subjected to the finite element model made by Erland (2006). These load cases have been subjected in an systematic way with 17 load cases in horizontal direction and these 17 load cases are repeated in 6 levels in vertical direction. Each load case is over leaping the previous load case with 200 mm in both vertical and horizontal direction. Frame 4 where the sensors are mounted is approximately centred in the middle of this patch load area.

We have seen how the different stress factor changes at the sensor location as we moved the patch load along the horizontal and vertical direction. For the sensor located on the frame, these did not experience much stress for load patch outside the loading area of the intermediate frame. The sensors on the stringer did however experience much stress when the load cases was outside the frame loading area. Loads outside the frame area are most likely transferred along the hull through the stringer.

We also saw the effect of the local geometry had on the different stress distributions. We could notice on the graphs when the load patches passed the sensor location, since the stress changes its sign. The mesh size of the model also gave an effect on the sensors on the stringer. They should have been symmetrically placed between the intermediate frame and frames, but since their is only 8 elements in between there is not possible to choose the element in the middle.

In this case study of these 102 load cases we have used patch load of same size and same pressure load. There results could be different if we used different sized patch loads and patch pressure. The total area these load cases extends over could be extended to fully see the effect of stress being transferred through the stringer.

Chapter 8

Estimation of Load Factors

8.1 Introduction

In this section the method of determine location of load based on weighted summation method presented in A.3 will be tried out with an large number of load cases and measured stress.

The principle behind the method is to describe the total load as a weighted sum of several smaller loads. When the stress is known in five different locations it is possible to perform a linear superposition of five different load scenarios. For frame L4 there are 5 sensors, and to be able to solve a system of equation, we need 5 different load cases from the FE analysis to solve 1 specific measured load pattern. It is worth noting that there are several different scenarios that may be able to create the same stress response, depending on the selected loads.

$$\underbrace{\begin{bmatrix}\sigma_1\\ \sigma_2\\ \sigma_3\\ \sigma_4\\ \sigma_5\end{bmatrix}}_{\text{Measured Strain}} = A \cdot \underbrace{\begin{bmatrix}\sigma_1\\ \sigma_2\\ \sigma_3\\ \sigma_4\\ \sigma_5\end{bmatrix}}_{\text{Load i}} + B \cdot \underbrace{\begin{bmatrix}\sigma_1\\ \sigma_2\\ \sigma_3\\ \sigma_4\\ \sigma_5\end{bmatrix}}_{\text{Load j}} + C \cdot \underbrace{\begin{bmatrix}\sigma_1\\ \sigma_2\\ \sigma_3\\ \sigma_4\\ \sigma_5\end{bmatrix}}_{\text{Load k}} + D \cdot \underbrace{\begin{bmatrix}\sigma_1\\ \sigma_2\\ \sigma_3\\ \sigma_4\\ \sigma_5\end{bmatrix}}_{\text{Load l}} + E \cdot \underbrace{\begin{bmatrix}\sigma_1\\ \sigma_2\\ \sigma_3\\ \sigma_4\\ \sigma_5\end{bmatrix}}_{\text{Load m}} \tag{8.1}$$

At each sensor there are several stress components available. Depending on the experienced load it is either shear stress of the transverse stress that will be the governing factor. Therefore the method will be applied using both the shear force and the von Mises stress as the governing factor.

In chapter 7.2 in the master thesis of Boersheim (2007) this method was tried out on an small number of load cases and measured result, without yielding an result that gave positive load factors when using all 5 sensors for both shear and von Mises stress. The only solution that was given was to chose the 3 sensors at the frame, and then only

the vertical determination of patch load was possible to determine. In the preliminary analysis of this Master's thesis, several new load cases was tested. These analysis yielded the same results as Boersheim (2007).

After the systematic analysis of the ship hull was done in section 7, time allowed to use the result from these analysis to see if some of the 102 load cases could yield a result. But it was not possible to manually choose between these load cases, so an more systematic approach was chosen.

8.2 Solution Method

Since the amount of load cases called for an systematic approach to solve for many load cases, a Matlab script was developed. In this script, a matrix with 5 different load cases is made by an iteration process and tested against the measured stress from full scale measurements. If the result yields positive load factors for all of the load cases, these load cases are stored in a file.

When developing the matrix for the different load cases, the order of the load cases in the matrix does not inflict on the result. If the order would have inflict in the result, an total of 9 995 000 400 different matrices had to be developed for the 102 load cases. Instead we have to consider 83 291 670 different cases of matrices. Cases where the matrix would consist of the same load cases would not be considered.

The load cases result from the FE analysis in section 7 are stored in a large matrix, where the number of each line in the matrix indicates the load case number. This is done both for shear stress and von Mises stress. When constructing the 5x5 matrix, a 5xtime for-loop are extracting the load cases from this large matrix. All the full scale measurements in appendix B are considered in this script.

An example of the matlab script could be found in appendix D .

8.3 Results

The matlab script was first tested with one of the layer load cases and one of the measured result. With 17 load cases, there are 6188 possible combinations of the matrix. When using the load cases in layer 1 and the measured load peak $T_0 = 16.955$ (no 35, see equations B.1 and B.2 for used measurements) there are in total 57 combinations that will yield positive load factors for the shear stress in load peak $T_0 = 16.955$. For the von Mises stress, all of the load cases will yield positive load factors. The load cases that yields positive load factors results are load case 1, 2, 3, 6, 7, 8, 9 and 10. This shows that already in the first layer there are several solutions to our load decision scheme for this shear stress measurement. In figure 8.1 the area of the solution load cases are indicated as white elements and orange elements are sensor location.

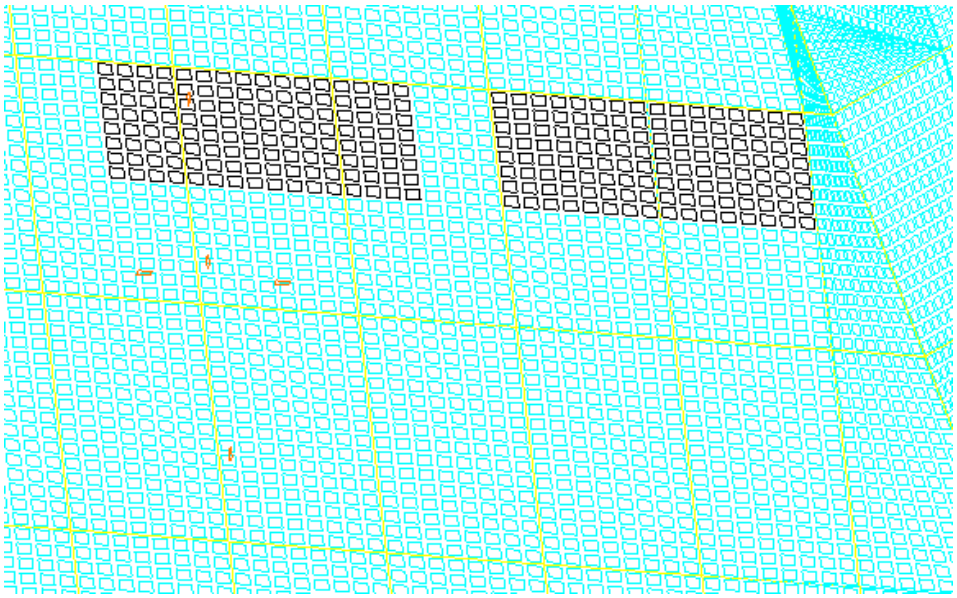

Figure 8.1: Solutions area for measured peak load 35 at case load level 1; black elements shows where the solution load cases are placed and orange elements shows sensor location

In table 8.1 all the measured values in appendix B are tested against the load cases in layer 1. We could see from the table that load peak 9 does not have any load cases for layer 1. This is not necessarily true, since the load decision scheme requires 5 load cases that all yields positive factors to indicate the load case as a possible solution. Load peak 9 could have 1 to 4 load cases that yields positive load factors, so if we combine more layers together we could say if load peak 9 has any possible load cases from layer 1. This will be assessed later on.

If we take away load peak 9, we could see that all the load cases in layer 1 are a possible solution to one or more of the load peaks. Load case 1 is represented in all of the cases, and load case 2 and 3 is present in many cases. It is also evident that the load cases around the frame where there sensor is located (6 to 10) is also represented in many of the cases. The cases where load case 8 is present, this case would dominate the result for the load factors. One of solutions are shown in the following result scheme

8.3.1 Layer 1, Load case 1, 2, 3, 6, 8, $T_0 = 16.955$

$$\underbrace{\begin{bmatrix} \tau_1 \\ \tau_2 \\ \tau_3 \\ \tau_6 \\ \tau_8 \end{bmatrix}}_{\text{Measured Stress}} = \begin{bmatrix} -0.0909532 & 0.0377956 & -0.174301 & 0.838916 & 0.219337 \\ -0.226509 & -0.0979698 & -0.273064 & 2.10031 & 1.33465 \\ -0.450937 & -0.209408 & -0.429619 & 3.58056 & 2.72037 \\ 2.64973 & -3.73825 & -0.81163 & 5.99184 & 7.9635 \\ 28.0498 & -17.8287 & -0.695017 & -5.3893 & 11.5221 \end{bmatrix} \cdot \begin{bmatrix} A \\ B \\ C \\ D \\ E \end{bmatrix} \tag{8.2}$$

The next step is to find the measured shear stress at the different sensor locations.

Load case\Load peak	35	13	11	9	15	38	2	23	19	5	33
1	✓	✓	✓		✓	✓	✓	✓	✓	✓	✓
2	✓	✓	✓		✓	✓	✓	✓	✓		✓
3	✓	✓	✓		✓	✓	✓	✓			
4			✓			✓	✓				
5			✓			✓					
6	✓	✓	✓		✓		✓	✓		✓	✓
7	✓	✓	✓		✓		✓	✓		✓	✓
8	✓	✓	✓		✓		✓	✓		✓	✓
9	✓	✓	✓		✓		✓	✓		✓	✓
10	✓	✓	✓		✓		✓	✓		✓	✓
11						✓			✓		
12					✓	✓			✓		
13					✓				✓	✓	✓
14					✓	✓			✓	✓	✓
15					✓	✓			✓	✓	✓
16						✓	✓		✓	✓	✓
17						✓	✓		✓	✓	✓

Table 8.1: Load cases in layer 1 that yields positive load factors for the measured shear stress load peaks

Based on the measured strain, the shear stresses at the peak are:

$$\begin{bmatrix} \tau_1 \\ \tau_2 \\ \tau_3 \\ \tau_6 \\ \tau_8 \end{bmatrix} = \begin{bmatrix} 9.7743 \\ -13.8824 \\ -1.2717 \\ 5.6296 \\ -3.5788 \end{bmatrix} \tag{8.3}$$

When solving the above system of equations we get the following result:

$$\begin{bmatrix} A \\ B \\ C \\ D \\ E \end{bmatrix} = \begin{bmatrix} 0.0082 \\ 0.0196 \\ 0.0283 \\ 0.2514 \\ 0.9505 \end{bmatrix} \tag{8.4}$$

We could see in equation 8.4 that all of the load factors are positive. We see that load case 8 is the most dominating, and load case 1 has low contribution.

8.3.2 Load cases valid for all measured loads

Since there so many load cases in layer 1 that gave positive load factors for many of the peak load, the script developed in section 8.2 was modified to include all the 102

load cases and the 11 load peaks. Since this gave in total 83 291 670 different cases to test, the script would take some time to run. The requirement was that the load cases should satisfy all the 11 peak loads at the same time.

The result gave 462 different combinations of load cases that gave positive load factors for all off the 11 peak loads in appendix B. There were a total of 11 load cases that gave these combinations. These are given in table 8.2

Level number	Load case number
1	1
2	1
3	1
3	2
3	6
4	1
4	2
4	6
4	7
5	1
5	2

Table 8.2: These are the load cases that satisfy all of the shear stress measurements in appendix B

Its clear that load cases far from the area that is close to the sensor is highly represented in this table. In figure 8.2 these load cases have been illustrated on the model as white area and the sensor location as orange elements. All of the load cases lays to the left of the sensor locations. Since this model shows the starboard part of the vessel, this means that these load cases lays closer to the bow than the sensor. This seams logical since the bow part of the ship will break up the ice first

8.3.3 Load cases for each of the peak loads

In this part it has been investigated how many of the load cases satisfy each of the load peaks. This is done layer by layer, since the computational time when calculating for all of the 102 load cases at the time is very long. In table 8.3 the load peaks with the associated number of load cases are shown.

In table 8.4 the 102 load cases are sorted under each of the level, and shows hos many time each load case satisfy as positive load factor for each of the 11 load peaks. If a load case has 11, it satisfies all of the load peaks. By this it is possible to identify where these load cases are located on the model. In figure 8.3 this is shown as a graph. The colours identify the number of load peaks each of the load cases could solve for; blue indicates 0-5 peaks, red 5-10 and green 10-11. The load cases are situated in the corner of the squares. Load case 1 in level 1 is found in the upper left corner and load case 1 in level 6 is found in the lower left corner. Load case 1 is closest to the bow. The

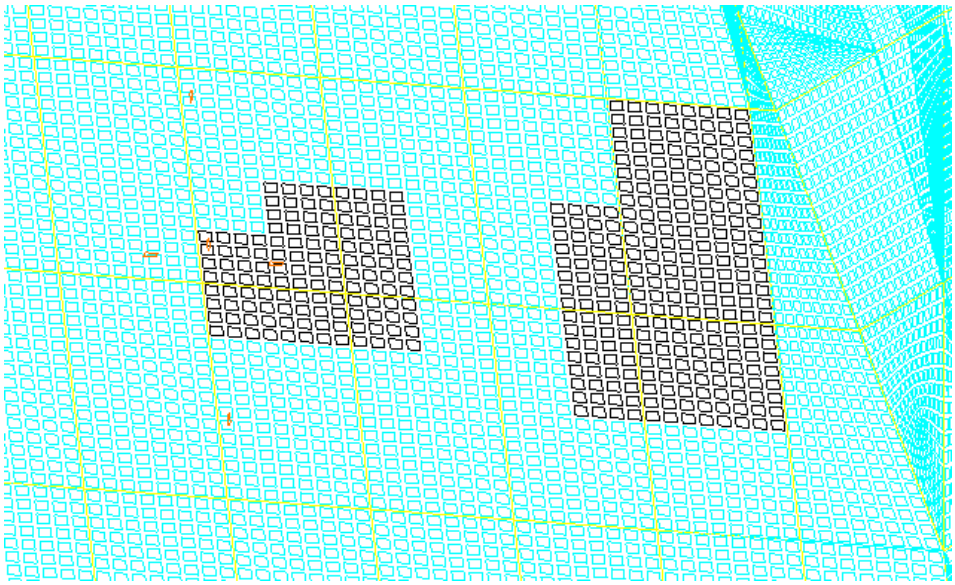

Figure 8.2: Solutions area for all measured peak loads; black elements shows where the solution load cases are placed and orange elements shows sensor location

Load peak	Load case solutions
35	49
13	54
11	54
9	63
15	84
38	77
2	71
23	50
19	75
5	63
33	66

Table 8.3: Shows how many of the 102 load cases that satisfy each of the load peaks

frame that the sensor are located on is at load case 8 over all levels. Sensor 4 and 5 are located on the stringer, and the stringer is loaded symmetrical on each side with level 4. Load case 7 on this is loaded on top of sensor 4 and load case 9 is loaded on top of sensor 5. The load cases that is expected to be take up by frame 4 are load cases from 6 to 10 for all levels.

From figure 8.3 it is possible to detect where the sensors on frame 4 are able to register ice loadings on this part of the hull. In the load area of the frame (load cases from 6-10) we could see that load cases above the stringer at level 4 could represent in many of the measurements. In table 8.4 these load cases ranges for 7 to 11 possible load peaks they could be solved for. For load cases below the stringer, these are seldom used by any of the measurements for the solution. This is also the largest area in the figure where the load cases are rarely a solution for the load peaks.

Load case\Level	Level 1	Level 2	Level 3	Level 4	Level 5	Level 6
1	11	11	11	11	11	10
2	9	10	11	11	11	10
3	7	9	9	9	9	9
4	3	3	5	8	9	9
5	2	2	4	7	9	8
6	8	10	11	11	9	6
7	8	9	8	11	2	0
8	9	9	7	0	0	0
9	8	9	7	0	0	0
10	8	9	7	1	2	2
11	2	3	6	8	9	9
12	3	3	6	7	8	8
13	4	6	7	7	6	6
14	5	6	6	7	6	6
15	5	5	6	6	6	6
16	6	6	7	10	10	10
17	6	9	10	10	10	10

Table 8.4: Shows how many times each of the 102 load cases satisfy as a positive load factor of the 11 peak loads

The areas that gives most load cases valid for all load peaks are the load cases closest to the bow (load case 1 and 2 for all levels), load case 6 for level 3 and 4 and load case 7 for level 4. The area around load case 16 and 17 for level 5 and 6 is also valid for most of the load peaks.

The general trend of this figure is that we need both load cases that are close to the sensor area, but also some cases that are further away from the sensor area.

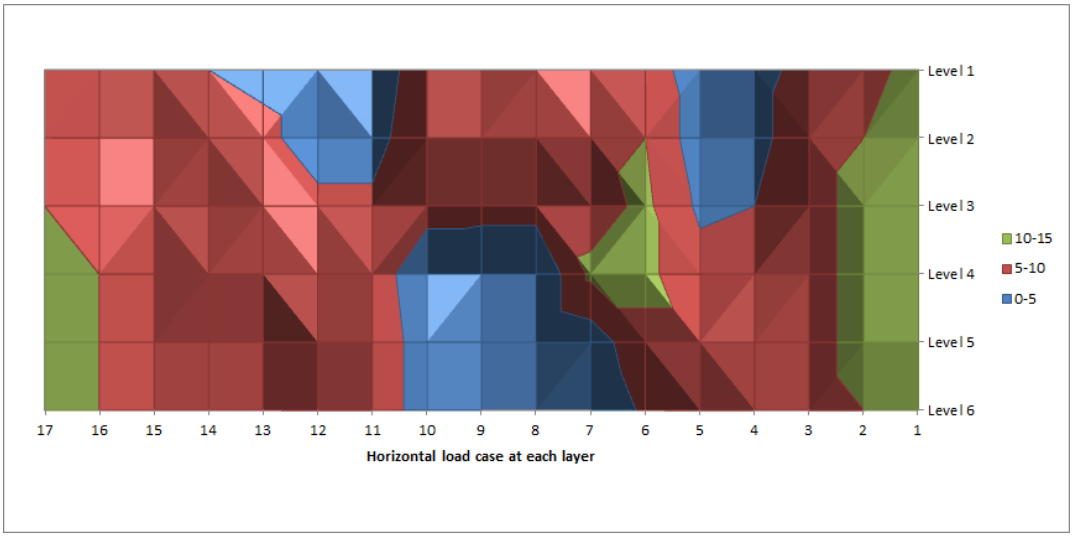

Figure 8.3: Shows how many times each of the horizontal load cases are used in the solution of load peaks. Load case 1 is closest to the bow

In appendix E a table of each load peak with associated load cases that gives positive load factors are given.

8.3.4 Average load factor

In this part we will look closer onto to the load factors and their averaged value over all the 102 load cases and 11 measured load peaks. For each solution of the load cases, the load factors are added together, and then averaged over the number of solutions each load case gives. The values for the average load factors are shown appendix E in table E.12

We could see in table that values at the frame loading area above the stringer is the dominating area. Load case 8 in level 2 is the most dominating. To better visualize where the largest load factors are found, the values from table E.12 are made into graphs.

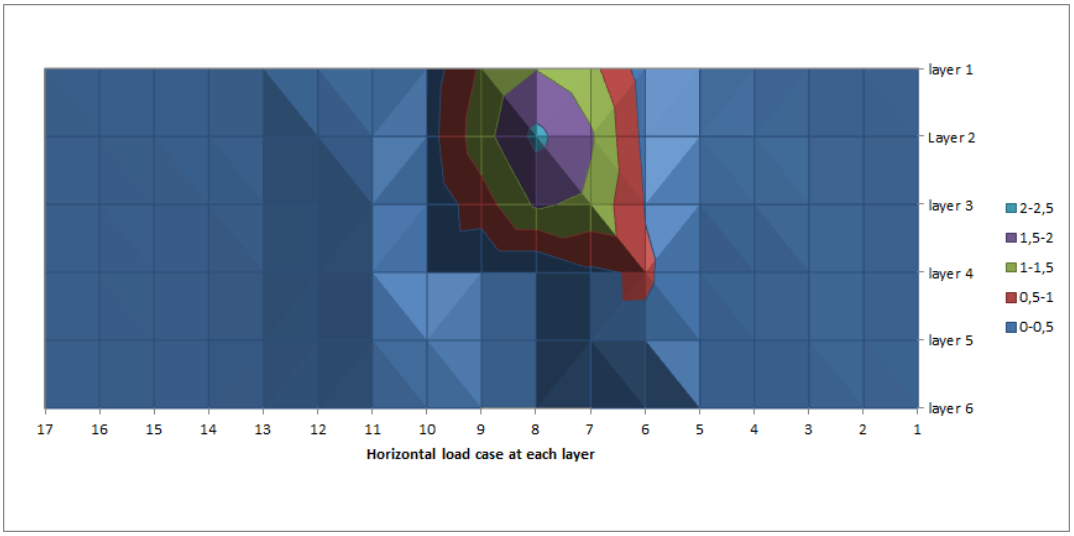

Figure 8.4: Shows the average load factor for each of the load cases. Load case 1 is closest to the bow

Both figure 8.4 and figure 8.5 shows the same, but the last figure is tilted so we easier could identify the highest load factors.

The load factors in the frame loading area above the stringer gives the highest load factors. We could also see that the load factors gets smaller further away from the sensor area.

To see which load factor that gives most solutions for the 11 load peaks, the values for the average load factors and the number of solution to the 11 load peaks are added together. This is as adding figure 8.3 and 8.5. This is shown in figure 8.6

When comparing figure 8.5 and 8.6 there doe not seem to be big difference between them. But we could see that some load cases are lowered and some gets higher contribution. The area above the stringer in the frame loading area is still giving the most contribution

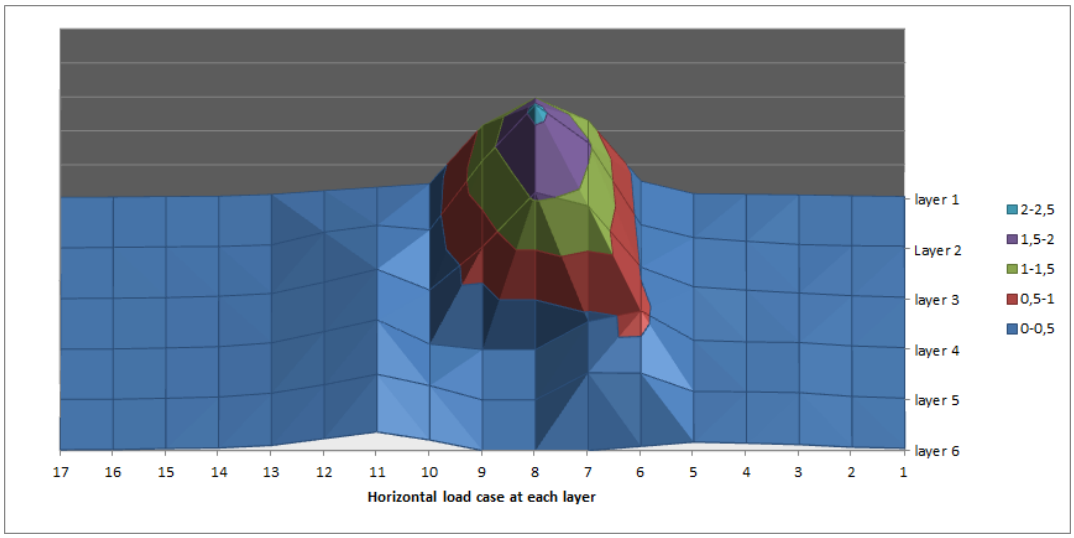

Figure 8.5: Shows the average load factor for each of the load cases. The figure is tilted compared to figure 8.3 to better identify the peak. Load case 1 is closest to the bow

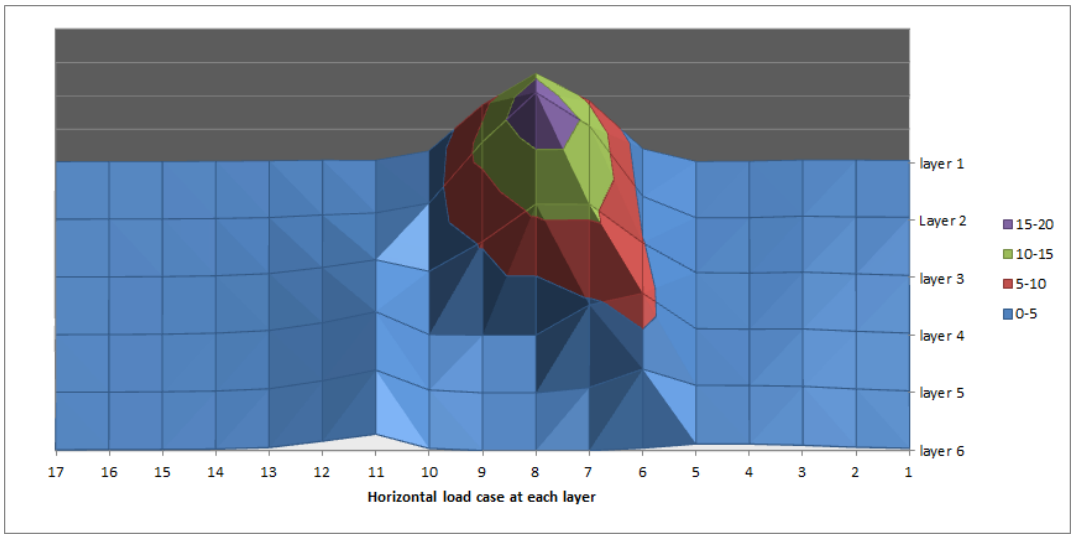

Figure 8.6: Shows the average load factor combined with the number of solutions for the 11 load peaks, for each of the load cases. Load case 1 is closest to the bow

to the load factors. An other general trend is that load cases closer to the bow are more participating in the solution of the load peaks with their load factors.

8.4 Effect of changing boundary conditions in FE model.

Through this thesis the finite element model from Erland (2006), the boundary conditions have been unchanged. In figure 6.2 these boundary conditions is shown. The model is fixed in all degrees of freedom along the frames and bulkheads at the center line. To see if changing the boundary conditions would make an effect on the load factors, we will make the model fixed in all degrees of freedom along the bulkheads in the front and back of the model. This is shown in figure 8.7. This is a more conservative situation than we would expect if we had made an model of the whole ship.

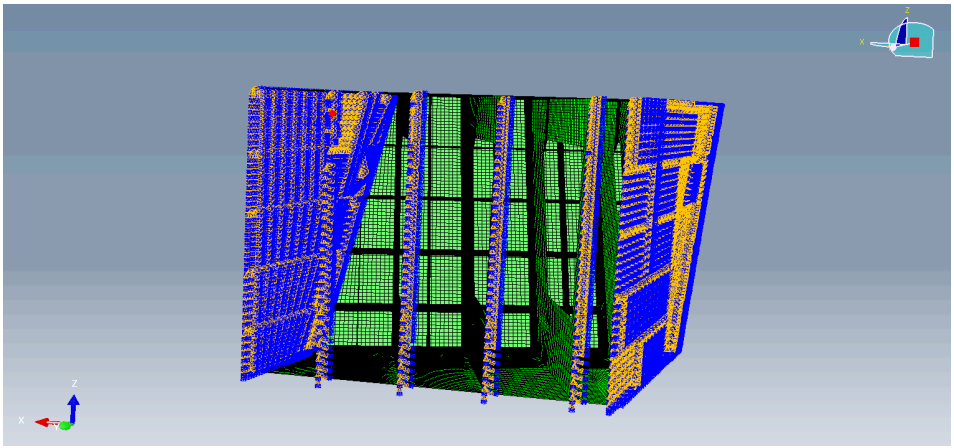

Figure 8.7: The FE model from Erland (2006) with fixed all degrees of freedom boundary conditions along the bulkheads

Due to time considerations, we will only consider 9 different load cases with these boundary conditions. 7 of these are giving positive solution of load factors and 2 that does not do this. When choosing these load cases, we would take a look on figure 8.3. In order to not choose load cases that are certain that would work for any boundary conditions, we will use load cases from both highly used load cases (green in figure 8.3) and load cases that are not so much used (blue area in figure). We also need to choose a set of load cases that already gives us positive load factors, and then we have to see through the tables in appendix E. These tables gives us the load cases that gives positive load factors for each of the load peaks. Load cases in the blue area of figure 8.3 are naturally seldom in the tables, so we have to be careful when choosing a load peak we would use. The load peak we would use when considering the different boundary conditions are load peak 9. This load peak is shown in table E.4. Two load cases that does not give positive load factor with the old boundary conditions are chosen to see if they could give another solution with the new boundary conditions. The load cases we will consider are shown in table 8.5.

With the 7 load cases that gave positive load factors with the old boundary conditions, there where 15 possible combinations of these. With the new boundary conditions, there were just 1 combinations of the total 9 load cases that gave positive load factors. These load cases are shown in table 8.6

Level number	Load case number
1	8
3	1
3	13
4	10
4	14
5	7
6	10
2	5
3	14

Table 8.5: Load cases used for the boundary condition consideration, 2 last cases are not giving positive load factors with the old boundary conditions

Level number	Load case number	Measurement no
1	8	τ_1
3	13	τ_2
4	10	τ_3
5	7	τ_4
6	10	τ_5

Table 8.6: Load cases that gives positive load factors for both boundary conditions

8.4.1 Measured results with old boundary conditions

The measured shear stress for this load peak is given in equation 8.5.

$$\begin{bmatrix} \tau_1 \\ \tau_2 \\ \tau_3 \\ \tau_4 \\ \tau_5 \end{bmatrix} = \begin{bmatrix} 8.5689 \\ 9.5009 \\ -0.6612 \\ 3.2416 \\ -3.7008 \end{bmatrix} \tag{8.5}$$

The shear stress for the load cases chosen is given in equation

$$\underbrace{\begin{bmatrix} \tau_1 \\ \tau_2 \\ \tau_3 \\ \tau_4 \\ \tau_5 \end{bmatrix}}_{\text{Measured Stress}} = \begin{bmatrix} 28.0498 & -17.8287 & -0.695017 & -5.3893 & 11.5221 \\ -0.187929 & 0.154459 & -0.526693 & -2.17027 & -2.83158 \\ 2.41058 & 2.04852 & -2.78813 & -11.2597 & -2.58098 \\ 1.53617 & 4.16255 & -12.2858 & 10.7068 & 18.1477 \\ 0.632847 & 0.996386 & -3.10765 & -8.63685 & -4.1938 \end{bmatrix} \cdot \begin{bmatrix} A \\ B \\ C \\ D \\ E \end{bmatrix} \tag{8.6}$$

When solving the above system of equations we get the following result:

$$\begin{bmatrix} A \\ B \\ C \\ D \\ E \end{bmatrix} = \begin{bmatrix} 0.0601 \\ 0.0194 \\ 0.0797 \\ 0.1507 \\ 0.0237 \end{bmatrix} \tag{8.7}$$

8.4.2 Measured results with new boundary conditions

The measured stress for sensors in the load cases with new boundary conditions are given in equation 8.8.

$$\underbrace{\begin{bmatrix} \tau_1 \\ \tau_2 \\ \tau_3 \\ \tau_4 \\ \tau_5 \end{bmatrix}}_{\text{Measured Stress}} = \begin{bmatrix} 28.1355 & -17.8681 & -0.692458 & -5.9083 & 11.1163 \\ -0.11154 & 0.0844078 & -0.437001 & -1.80012 & -2.33554 \\ 2.46255 & 1.97867 & -2.75216 & -11.5115 & -2.69409 \\ 1.55631 & 4.08988 & -12.2679 & 9.91317 & 17.5555 \\ 0.648038 & 0.909897 & -3.08751 & -8.77995 & -4.21105 \end{bmatrix} \cdot \begin{bmatrix} A \\ B \\ C \\ D \\ E \end{bmatrix} \tag{8.8}$$

We could see that the values of the stress measured in the sensor are some different for equation 8.8 compared with equation 8.7. The largest difference is for sensor 5 in level 4 load case 14 of 0.79 MPa. But none of the values shifts sign from negative to positive or the opposite way. The load factor values could still be positive, but they might be different.

When solving the above system of equations we get the following result:

$$\begin{bmatrix} A \\ B \\ C \\ D \\ E \end{bmatrix} = \begin{bmatrix} 0.0610 \\ 0.0156 \\ 0.0763 \\ 0.1459 \\ 0.0179 \end{bmatrix} \tag{8.9}$$

8.9

We could see here that the load factors have changed some.

Changing the boundary conditions will clearly effect the load factors as well. of the total 15 combinations we had, only 1 combination was valid after we changed the boundary conditions. Since this was done with so few load cases, it it difficult to say if other combinations of load cases will change from positive to negative or vice versa. This has to be further assessed, and this should probably be done with an larger model and larger load area.

8.5 Discussion and conclusions

In this chapter we have taken a closer look on to the determination of the load factors so we could use load cases from FEM analysis to solve for full scale measurements. The problem with this method earlier is that this method is very sensitive to which load cases that are chosen to represent the measurements and has to this point not yielded good results. In stead of manually choose load cases that are close to the sensor area and is close to the measured result, an more systematic approach has been chosen. Based on the 102 load cases from the previous chapter, these load cases have been been combined in pairs of 5 in a total of 83 291 670 combinations. The order of which these cases have been put together has also been disregarded.

The combination of load cases have been tested against are the 11 measurements from appendix B. This gave us many combination of load cases that gave us positive load factors. There are in total 11 load cases that gives positive load factors for all of the 11 measurements, and these load cases are shown in table 8.2. In appendix E there are tables that shows the load cases that gives positive load factors for each of the 11 measurements. In table 8.3 the number of load cases solution per measurement is shown. When adding together the tables in appendix E, there is possible to detect which of load cases that gives the most number of positive load factors and where these are placed in our loading area. The number of each load case used is shown in table 8.4. To easier visualized which of these load cases are most frequently used, an area graph is made of the numbers in the table and this is figure 8.3.

This figure gives us some interesting results. We would expect load cases close to the frame where the sensors are mounted will be highly represented. This is partly true, load cases above the stringer (at level 4) are highly participating. But for the area under the stringer the load cases are seldom used for solving the measurements. 7 of these load cases in this area are zero. These results could be connected to the result of the analysis of the load cases in chapter 7. Here we saw that patch loads outside the frame loading area was carried as stress through the stringer. This could also be seen in figure 8.3 where many of the load cases outside the loading area gives positive results for the measurements. In fact the 11 load cases found in table 8.2 are almost all outside the frame loading area, except for the 3 cases located around level 4 just inside of this area. The majority of these cases are located at load case 1 and 2. We also have another area of highly used load cases at the other side of the loading area at load cases 16 and 17. The other areas of load cases that are not used so often is found just in front and behind of the frame load area above the stringer.

The different load cases gives different load factors for the measurements. In figure 8.5 the average load factor for each load case is shown. Load cases far away from the frame area are not contributing too much, but they are essential to be able to solve the load factors. In figure 8.6 the average load factor is combined with the number of solutions each load case gives for the 11 load peaks. The load cases in the sensor area above the stringer is the most dominant. But we could also observe that the load cases towards the bow are contributing.

Changing the boundary conditions of the model had also an effect on the load factors. 9 load cases had their changed boundary conditions, and 2 among them did not give positive load factors before this change. The 7 load cases with positive load factors gave 15 combinations to solve for, but after the change, only 1 combination gave positive load factors. This method is very sensitive to the selection of the load cases, so to be able to tell how the boundary conditions would change the load factors for the loading area, all of the 102 load cases should be retested with the new constraints and then tried to solve for the measurements again. The remaining time of this Master thesis did not allow for this, but this only shows how sensitive this method is to the chosen load cases.

In retrospect, the load area chosen was to small since so many of the load cases that gave positive load factors was placed at the edge of the area. However, the FEM model used from Erland (2006) did not have to much area in the horizontal direction that not already was inside the loading area. The FEM model made by Boersheim (2007) was not possible use since this was made in an older version of Patran, and not possible to convert to the version used in this thesis. A model made of the whole bow area would have given us some more conclusive results regarding stress that is transferred through the stringer. The patch size and pressure has also been constant through this assessment, and the effects of changing these values should also be addressed. The mesh size of the model could also yield an effect of the results.

Chapter 9

Conclusion

The present master thesis consists of four parts. The following conclusion is a summary of the most important aspects within each chapter.

The first part is a literature review of the mechanical and physical properties of sea ice and contains models for calculating ice contact pressure.

The second part is a review of the rule sets developed by DNV and the IACS regarding vessels operating in ice infested waters. Both design principles and numerical values have been evaluated. The main difference between the designs principles used, is that IACS base their rules on a plastic a method of approach, while DNV uses an elastic method. Despite the difference in the design principles, when comparing their numerical values turned out to be quite similar. The DNV rules are in general most conservative for the smaller vessels and the IACS rules the most conservative for large vessels. In the IACS rules there is a strong correlation between the vessels displacement and scantling requirements. The scantling requirements in the DNV rules are only determined by the ice class.

The third part consists of finite study of a part of the bow on KV Svalbard. The patch load is obtained from DNV rules with a restriction on the local ice σ_{ice} to 3 MPa. A systematic load scheme is used, consisting of 17 load cases in the horizontal direction these are repeated in 6 levels in the vertical direction. This will give 102 load cases.

The output from these load cases are the 4 stress components τ_{xy} , σ_x, σ_y and von Mises, and these are taken at 5 different location on frame 4. These positions corresponds to the sensor location L4 where full scale measurements where done with KV Svalbard in DNVs *ice load monitoring* project. For each of the stress factors there where made graphs showing the measured stress at the given sensor location when the load was moved in the horizontal direction. This was done for each of the 6 levels. These graphs showed where the different sensor locations where able to detect patch loads subjected to the FE model. For the sensor mounted on the frame, they could measure load that was within the frame loading area, i.e. from the intermediate frame to the adjacent frames. For the sensor mounted on the stringer, there was another story. These could measure stress for all of the load cases. One of the explanations for this is that the stringer

transfers stress from the load patch area that could be measured by the sensors. The local geometry gave also an effect on the different stress distributions, and it was also possible to detect when the load patch passed the sensor locations. The mesh size made it not possible to select elements that where in the middle between the intermediate frame and frame, and this made an effect of the stress distribution of sensor location 4 and 5.

The last part consists of a comparison between measurements from full scale trials and the results from the 102 load cases. This comparison is done through a weighted summation method where 5 different load cases are combined to represent the measured result, and a load factor is calculated for each load case for its contribution of the measured results. The stress component used in this comparison is the shear stress τ_{xy}.

The 102 different load cases could be combined in 83 291 670 different combination when we disregarded the order the load cases could be combined. These load cases was tested against the 11 measurements from the full scale trials. From this comparison we got many combinations of load cases that gave positive load factors for all of the 5 cases. There were in total 11 load cases that gave positive factors for all of the 11 measurements at the same time. A table was made for each of the measurements showing the load cases that gave positive factor. These tables are shown in appendix E. When adding these tables together it is possible to detect which of the load cases that are most represented in solutions of the load factors. Figure 8.3 is representing this.

This figure shows that for load cases inside the frame loading area, only those above the stringer level are used for many of the solutions. Load cases in both ends of the total loading area are most represented as solutions to the load. Comparing it with the analysis of the load cases, it is evident that the stringer is transferring stress from other part of the hull. In figure 8.5 the average load factor for each load case is shown. Load cases within the frame loading area have the largest load factors, but also load cases outside this area contribute and are essential to the solutions.

This load decision scheme is very sensitive to the selection of load cases and boundary conditions. A change of the boundary conditions for the model was tried out for a set of 9 load cases, where 7 gave positive load factors. When constraining the model at the bulkheads, the measured value at the sensor location did not change by much. The 7 load cases with positive load factor could give 15 combinations, but after the constraint we got only 1 combinations of 5 load cases that gave positive load factors.

The results of this thesis shows that is possible to find many solution to the measured result by combining many load case, but is it not possible to decide *the* solution. To be able to say in more general terms which areas of the hull that would contribute to loads measured at the sensor location we should test against a larger load area and more measured results. If we had more sensors at the frame we might also be able to reduce the number of load cases that gave positive load factors.

Chapter 10

Recommendation Of Further Work

The load decision scheme used in this thesis gave satisfying results with the set of load cases that was made. But we saw that many of the load cases were at the boundaries of the load area. In a further development of the scheme, a larger finite element model is needed that should cover the whole bow area. Then we have to systematically apply load cases to cover a large area and test this against measured results. This could also verify if, and for how long the stringer transfers stress for other parts of the hull. There should also be used more measurements to verify which area within the loading area that could be used to represent the measurements.

With a lager model of the bow, the boundary conditions of the model would probably not affect the load factors too much. Also the load cases used in this thesis should be retested with new boundary conditions to see the total effect.

This thesis has only used load patches with the same size and patch pressure. It would be interesting to see if a change of these parameters would affect the load factors and areas of load cases used for the solution of measurements.

The process of collecting the stress data from Abaqus, transferring to excel or Matlab, and then to be systematized is very time consuming. If a new model is to be tested with an increased number of load cases and more measurements to test against, a more systematic method has to be developed. A script that could collect the different stress values at the sensor locations for many load cases from a report file in Abaqus, and then could systematized these values would be very beneficial. The process of making load cases in Patran is time consuming, but at this point there does not seem to be another way to do this.

Nomenclature

ABL	Above Base Line
DNV	Det Norske Veritas
FE	Finite Element
FSICR	Finnish-Swedish Ica Class Rules
IACS	International Association ofClassification Societies
KV	Kystvakt
NTNU	Norges Teknisk-Naturvitenskaplige Universitet
RS	Russian Maritime Register of Shipping

References

Bernt Leira, Lars Boersheim, O. E. and Amdahl, J. (2009). Ice-load estimation for a ship hull based on continuous response monitoring. *Journal of Engineering for the Maritime Environment, Part M*, 223:529-540.

Boersheim, L. (2007). Ship hull monitoring of ice-induced stresses. Master thesis, NTNU.

DNV (2011). Rules for classification of ships, part 5, ch 1 ships for navigation in ice, july 2011.

Erland, R. A. (2006). Ice action and - response monitoring of ships. Project thesis, NTNU.

Erland, R. A. (2007). Ice load monitoring. Master's thesis, Norwegian University of Science and Technology.

Furnes, G. (2011). Lecture notes in ice 1.

Irgens, F. (1979). *Fasthetslaere*. Tapir forlag, sixth edition.

Nyseth, H. (2006). Strain measurements on board kv svalbard with respect to ice loading. Technical report, Det Norske Veritas.

Riska, K. (2011). Lecture notes in ice 2.

Weeks, G. T. W. (2009). A review of the engineering properties of sea ice.

Appendix A

Included chapters from Boersheim (2007)

This chapter is from the Master thesis of Boersheim (2007), and is included to show how different calculations are done for the used measurements in this thesis

A.1 Axial contribution to the different stress components

A.1.1 Introduction

The stress over a cross section of the stiffener is divided into axial, transverse and shear stress. To be able to calculate the three components three strain filaments are needed. To make the instrumentation system cheaper, most stiffeners are only mounted with two sensors. Thus it is not possible to calculate all stress components. Frame 4 was only instrumented with two filaments, but Frame 2 was mounted with three filaments at each sensor.

$$\epsilon(\phi) = \frac{\epsilon_x + \epsilon_y}{2} + \frac{\epsilon_x - \epsilon_y}{2} \cdot \cos(2\phi) + \frac{1}{2} \cdot \gamma_{xy} \sin(2\phi) \tag{A.1}$$

Equation (A.1) is the general expression for the principal strain directions. When using a strain gauge rosette, the different filaments are mounted with the angles 45 degrees with respect to each other. For frame 2 the 3 filaments was mounted with 0, 45 and 135 degrees, where 0 degrees is defined as axial direction.

Equation (A.2) is the matrix form of equation (A.1) when the different values of ϕ are inserted.

$$\begin{bmatrix} \epsilon(0) \\ \epsilon(45) \\ \epsilon(135) \end{bmatrix} = \begin{bmatrix} 1 & 0 & 0 \\ \frac{1}{2} & \frac{1}{2} & \frac{1}{2} \\ \frac{1}{2} & \frac{1}{2} & -\frac{1}{2} \end{bmatrix} \cdot \begin{bmatrix} \epsilon_x \\ \epsilon_y \\ \gamma_x y \end{bmatrix} \tag{A.2}$$

By solving equation (A.2) with respect to ϵ_x, ϵ_y and γ_{xy}, we get the matrix equation for the coordinate strain (Irgens, 1979)

$$\begin{bmatrix} \epsilon_x \\ \epsilon_y \\ \gamma_{xy} \end{bmatrix} = \begin{bmatrix} 1 & 0 & 0 \\ -1 & 1 & 1 \\ 0 & 1 & -1 \end{bmatrix} \cdot \begin{bmatrix} \epsilon_1 \\ \epsilon_2 \\ \epsilon_3 \end{bmatrix} \tag{A.3}$$

ϵ_1, ϵ_2 and ϵ_3 are the principle strain. The directions 1, 2 and 3 are defined as the directions of the filaments. ϵ_x, ϵ_y and τ_{xy} are the coordinate strain, where the subscript indicates the direction according to the local axes. The relation between the coordinate strain and stress is according to plane stress theory defined as:

$$\sigma_x = \frac{E}{1-\nu^2} \cdot (\epsilon_x + \nu\epsilon_y) \tag{A.4}$$

$$\sigma_y = \frac{E}{1-\nu^2} \cdot (\epsilon_y + \nu\epsilon_x) \tag{A.5}$$

$$\tau_{xy} = G \cdot \gamma_{xy} \tag{A.6}$$

For location such as Frame 4, the filament measuring ϵ_1 is missing. As one can see from equation (A.3), ϵ_1 is the same as ϵ_x, and this will mean that ϵ_x is unknown. From equation (A.3) we can also see that ϵ_y is depending on ϵ_1. If the sensor was located at the neutral axis, we know from basic mechanics (Irgens, 1979) that the axial stress is equal to zero, and can therefore state that $\epsilon_x = \nu \cdot \epsilon_y$. This will give the transverse stress without the axial contribution as:

$$\sigma_y = \frac{E}{1-\nu^2} \cdot \epsilon_y \tag{A.7}$$

In chapter 6 in the Master thesis of (Boersheim, 2007) the error of using just 2 filaments instead of 3 is quantified. If the locations of the filaments are placed on the neutral axis of the stringer, this error is relatively small in most cases. But we can't apply this as a general rule since there are errors and due to the fact that the neutral axis of the stringer could change during loading.

A.1.2 von Mises stress

The von Mises criterion is a common used scantling requirement. if we use coordinate stress instead of principle stress and assuming plane stress condition the von Mises equation from equation (4.1) will be:

$$\sigma_j = \sqrt{\sigma_x^2 + \sigma_y^2 - \sigma_x \sigma_y + 3 \cdot \tau_{xy}} \tag{A.8}$$

The advantage is that it includes the effect of stress in all three directions. However, to be able to use the von Mises criterion, one needs the stresses in all three directions, and therefore also the strain in all three directions. As shown in chapter 6 in the Master thesis of (Boersheim, 2007) the axial stress is considerably smaller than the transverse stress.

The von Mises stress without the axial contribution is defined as:

$$\sigma_j = \sqrt{\sigma_y^2 + 3 \cdot \tau_{xy}} \tag{A.9}$$

A.2 FE analysis performed by DNV

In the following section the general procedure, developed by DNV, for converting the measured strain into an estimate of the actual force applied is presented. The complete development of the procedure and all factors included can be found in reference Erland (2007) and Nyseth (2006). This section is only a short summary of the principles behind the procedure.

A.2.1 Estimating Shear Distribution and shear forces

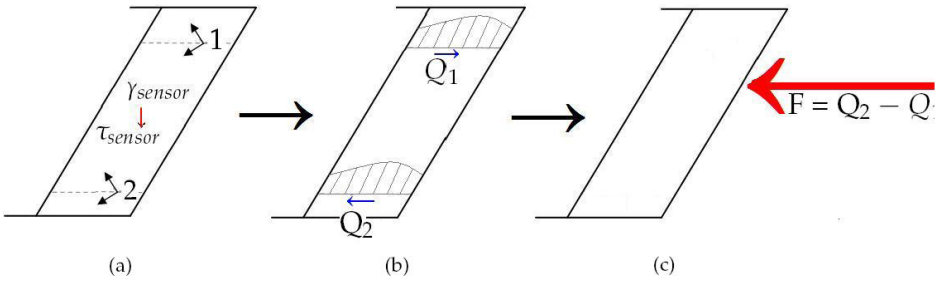

Figure A.1: The main steps of the procedure for converting the measured strains into forces

Figure A.1 show the main steps of the procedure on how to convert the measured strains into actual forces. First the strain is extruded and converted into corresponding shear stress τ_{sensor}. The shear force is found by integrating the assumed shear stress

distribution along the cross section. According to (Nyseth, 2006);depending on the frame geometry and load pattern, the actual neutral axis will be biased relative to the calculated profile neutral axis. Thus, the measured strain will generally not be able to capture the maximum shear stress in the cross section. Therefore a factor describing the relation between the relation between the amount of measured stress and maximum stress for a given load pattern has to be established. This factor is defined as f_a and is used as following:

$$\tau_{max,i} = f_{a,i} * \tau_{sensor,i} \tag{A.10}$$

where i relates to the specific load combination. A more specific description and numerical values of f_a can be found in reference (Erland, 2007).

In order to have a more correct value of the total shear force in the cross section, a factor describing the shear distribution is needed. f_b is the shear force factor and is defined as:

$$f_{b,i} = \frac{Q_i}{\tau_{max,i} \cdot A_w} = \frac{Q_i}{f_{a,i} \cdot \tau_{sensor,i} \cdot A_w} \tag{A.11}$$

where Q_i is the integrated shear force based on a FE analysis for the load combination i and A_w is the cross sectional area at the sensor.

The total shear force in a cross section is then defined as:

$$Q_{calc}^{tot} = f_a \cdot f_b \cdot \tau_{sensor} \cdot A_w \tag{A.12}$$

A.2.2 Calculation of the total forces

Assuming that the load is applied between the two sensor locations, the total applied force is the difference between the shear forces. The difference in the shear forces can be found by:

$$Q_{i,diff} = Q_{i,1} - Q_{i,2} \tag{A.13}$$

where 1 and 2 represent the upper and lower sensor location and i represent the load combination. A part of the applied load is not detected by the sensors, thus it is necessary to have a factor describing how much of the load that is taken as shear. f_c define the portion of the load taken as shear, and we can therefore express the total load as:

$$F_i = f_{c,i} \cdot Q_{i,diff} \tag{A.14}$$

When the total force on the frame is known it is possible to calculate the utilization factor of the frame:

$$\eta_i = \frac{F_i}{C_i} \tag{A.15}$$

where F is the total load on a frame and C is the predefined capacity.

A.3 Load decision scheme, theory

As mentioned earlier in this chapter, one purpose of this analysis is to create a load identification scheme. The goal is to be able to determine the location and the magnitude of the load acting on the ship hull based on the information we get from the strain measurements. The method presented in this section is only developed for frame 4. The principle behind the method is to describe the total load as a weighted sum of several smaller loads.

When the stress is known in five different locations it is possible to perform a linear superposition of five different load scenarios. For each load scenario applied in the FE analysis, the stresses are extracted at the sensor locations. The calculated stresses are inserted in the five columns on the right side of equation (A.16). The measured stresses from KV Svalbard are represented on the left side of the equation.

$$\underbrace{\begin{bmatrix}\sigma_1\\ \sigma_2\\ \sigma_3\\ \sigma_4\\ \sigma_5\end{bmatrix}}_{\text{Measured Strain}} = A \cdot \underbrace{\begin{bmatrix}\sigma_1\\ \sigma_2\\ \sigma_3\\ \sigma_4\\ \sigma_5\end{bmatrix}}_{\text{Load XX}} + B \cdot \underbrace{\begin{bmatrix}\sigma_1\\ \sigma_2\\ \sigma_3\\ \sigma_4\\ \sigma_5\end{bmatrix}}_{\text{Load XX}} + C \cdot \underbrace{\begin{bmatrix}\sigma_1\\ \sigma_2\\ \sigma_3\\ \sigma_4\\ \sigma_5\end{bmatrix}}_{\text{Load XX}} + D \cdot \underbrace{\begin{bmatrix}\sigma_1\\ \sigma_2\\ \sigma_3\\ \sigma_4\\ \sigma_5\end{bmatrix}}_{\text{Load XX}} + E \cdot \underbrace{\begin{bmatrix}\sigma_1\\ \sigma_2\\ \sigma_3\\ \sigma_4\\ \sigma_5\end{bmatrix}}_{\text{Load XX}} \tag{A.16}$$

By solving the system of equations (equation (A.16)), we get a possible solution for the loads applied that can give this specific response pattern. The different arrays represent the stress measured when the structure is subjected to a unit load of 1 MPa, while the constant in front of the array determine the magnitude of the load. However, it is worth noting that there are several different scenarios that may be able to create the same stress response, depending on the selected loads.

At each sensor there are several stress components available. Depending on the experienced load it is either shear stress of the transverse stress that will be the governing factor. Therefore the method will be applied using both the shear force and the von Mises stress as the governing factor.

An efficient way to use the load decision scheme developed in the present thesis has not yet been developed. The calculated stresses from the FE analysis has to be extracted

manually. However, if one has decided what load cases to use and the calculated stresses at the different sensors based on FE analysis are extracted, it is possible to determine the location of a large number of loads relatively fast. The only values that are changing in the equation are the measured stresses from the actual testing. These values are easy to extract and to handle using any programming tool.

Appendix B

Location of load

The following section shows a selection of the peak loads and where the loads are acting on frame L4. Based on the following figures it is possible to determine how much of the load is acting above the stringer and how much below the stringer. The values of shear strain, shear stress and von Mises stress is included for the peak load.

When the load is applied to the plate field at frame 4 the force can be transferred up and down in the stiffener and sideways in the stringer. Thus the total force on the plate field can be calculated by summing the shear forces at the upper sensor, the bottom sensor and in the two sensors at the stringer. The blue line represents the total force.

The amount of the total load that is located above the stringer can be found by summing the shear force at the top two sensors on the stiffener. The load above the stringer is represented by the red line.

The load below the stringer is found by summing the shear force at the lowest sensor and the two sensors on the stringer and also subtract the shear force at the lower sensor above the stringer. The load below the stringer is represented by the green line.

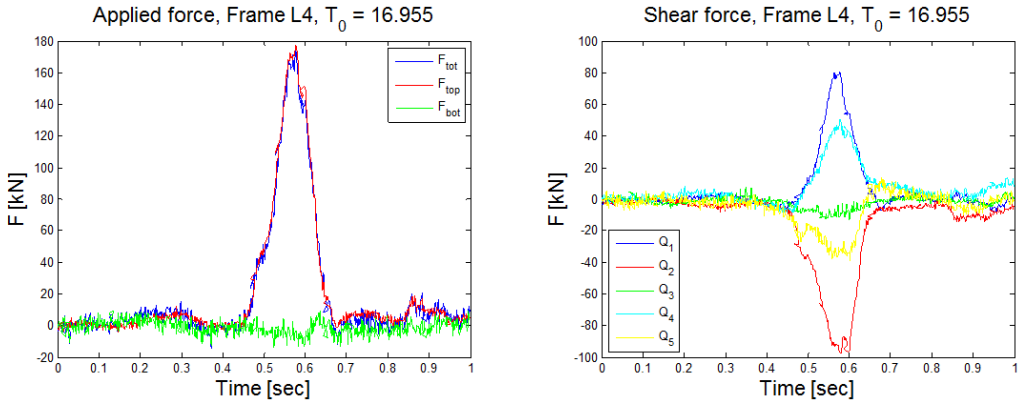

(a) (b)

Figure B.1: Estimated load, peak 35

Total force on frame at peak load: 176.9609 kN

$$\underbrace{\begin{bmatrix} \tau_1 \\ \tau_2 \\ \tau_3 \\ \tau_4 \\ \tau_5 \end{bmatrix}}_{\text{Measured Stress}} = \begin{bmatrix} 9.7743 \\ -13.8824 \\ -1.2717 \\ 5.6296 \\ -3.5788 \end{bmatrix} \tag{B.1}$$

$$\underbrace{\begin{bmatrix} \sigma_1 \\ \sigma_2 \\ \sigma_3 \\ \sigma_4 \\ \sigma_5 \end{bmatrix}}_{\text{Measured Stress}} = \begin{bmatrix} 17.5473 \\ 56.8717 \\ 2.6428 \\ 11.0952 \\ 7.2524 \end{bmatrix} \tag{B.2}$$

$$\underbrace{\begin{bmatrix} Q_1 \\ Q_2 \\ Q_3 \\ Q_4 \\ Q_5 \end{bmatrix}}_{\text{Measured force}} = \begin{bmatrix} 80.5173 \\ -96.5672 \\ -10.5686 \\ 50.6662 \\ -32.2088 \end{bmatrix} \tag{B.3}$$

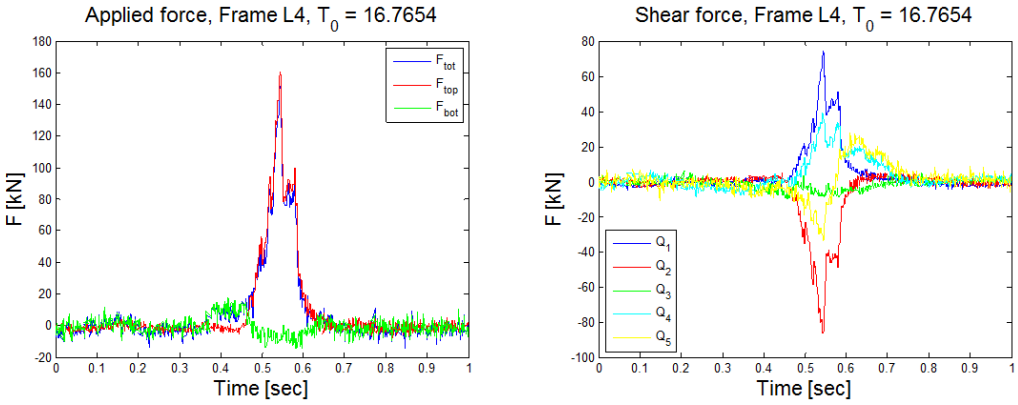

(a) (b)

Figure B.2: Estimated load, peak 13

Total force on frame at peak load : 151.2998 kN

$$\underbrace{\begin{bmatrix} \tau_1 \\ \tau_2 \\ \tau_3 \\ \tau_4 \\ \tau_5 \end{bmatrix}}_{\text{Measured Stress}} = \begin{bmatrix} 9.0291 \\ -12.401 \\ -0.861 \\ 4.0133 \\ -3.7384 \end{bmatrix} \tag{B.4}$$

$$\underbrace{\begin{bmatrix} \sigma_1 \\ \sigma_2 \\ \sigma_3 \\ \sigma_4 \\ \sigma_5 \end{bmatrix}}_{\text{Measured Stress}} = \begin{bmatrix} 16.2892 \\ 22.2957 \\ 1.7863 \\ 7.6517 \\ 9.4726 \end{bmatrix} \tag{B.5}$$

$$\underbrace{\begin{bmatrix} Q_1 \\ Q_2 \\ Q_3 \\ Q_4 \\ Q_5 \end{bmatrix}}_{\text{Measured force}} = \begin{bmatrix} 74.3789 \\ -86.2629 \\ -7.1555 \\ 36.1198 \\ -33.6456 \end{bmatrix} \tag{B.6}$$

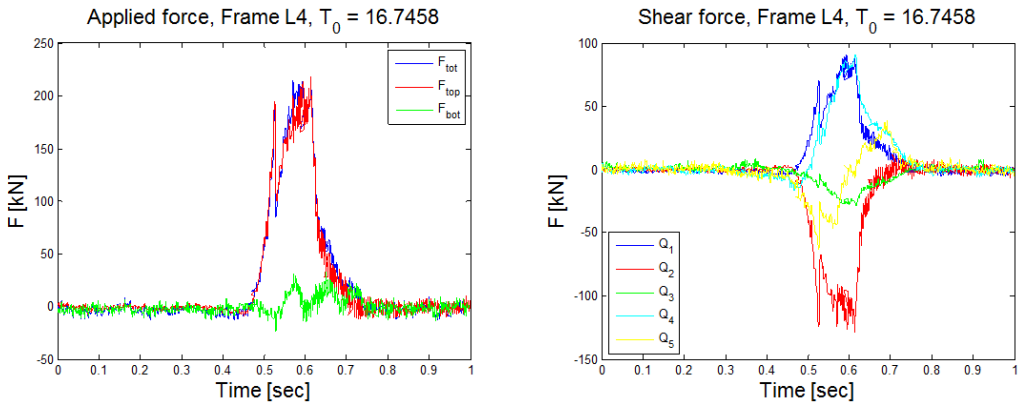

(a) (b)

Figure B.3: Estimated load, peak 11

Total force on frame at peak load : 214.582 kN

$$\underbrace{\begin{bmatrix} \tau_1 \\ \tau_2 \\ \tau_3 \\ \tau_4 \\ \tau_5 \end{bmatrix}}_{\text{Measured Stress}} = \begin{bmatrix} 9.1808 \\ -17.8833 \\ -2.75 \\ 8.0078 \\ -4.8922 \end{bmatrix} \tag{B.7}$$

$$\underbrace{\begin{bmatrix} \sigma_1 \\ \sigma_2 \\ \sigma_3 \\ \sigma_4 \\ \sigma_5 \end{bmatrix}}_{\text{Measured Stress}} = \begin{bmatrix} 15.6717 \\ 29.5784 \\ 4.5344 \\ 15.8043 \\ 17.4294 \end{bmatrix} \tag{B.8}$$

$$\underbrace{\begin{bmatrix} Q_1 \\ Q_2 \\ Q_3 \\ Q_4 \\ Q_5 \end{bmatrix}}_{\text{Measured force}} = \begin{bmatrix} 75.6284 \\ -124.3979 \\ -22.8538 \\ 72.0699 \\ -44.0299 \end{bmatrix} \tag{B.9}$$

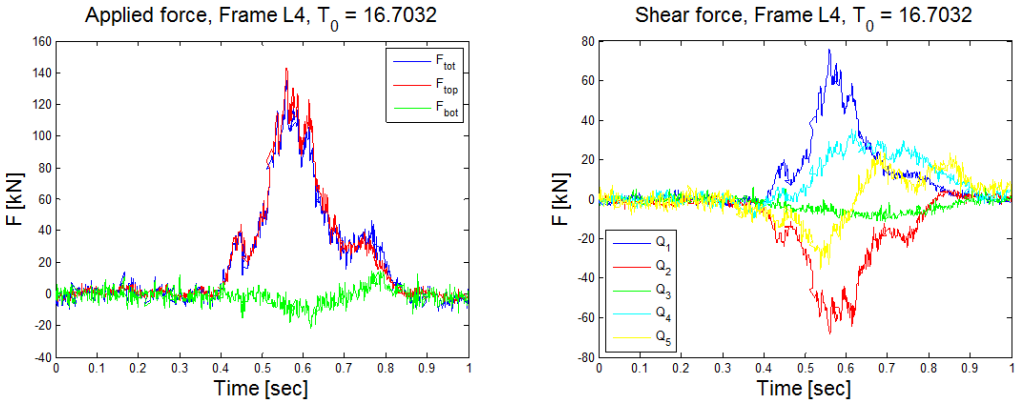

(a) (b)

Figure B.4: Estimated load, peak 9

Total force on frame at peak load : 138.565 kN

$$\underbrace{\begin{bmatrix} \tau_1 \\ \tau_2 \\ \tau_3 \\ \tau_4 \\ \tau_5 \end{bmatrix}}_{\text{Measured Stress}} = \begin{bmatrix} 8.5689 \\ 9.5009 \\ -0.6612 \\ 3.2416 \\ -3.7008 \end{bmatrix} \tag{B.10}$$

$$\underbrace{\begin{bmatrix} \sigma_1 \\ \sigma_2 \\ \sigma_3 \\ \sigma_4 \\ \sigma_5 \end{bmatrix}}_{\text{Measured Stress}} = \begin{bmatrix} 15.6821 \\ 16.5497 \\ 1.6673 \\ 5.2539 \\ 7.0487 \end{bmatrix} \tag{B.11}$$

$$\underbrace{\begin{bmatrix} Q_1 \\ Q_2 \\ Q_3 \\ Q_4 \\ Q_5 \end{bmatrix}}_{\text{Measured force}} = \begin{bmatrix} 70.5884 \\ -66.0893 \\ -5.4949 \\ 29.1745 \\ -33.3072 \end{bmatrix} \tag{B.12}$$

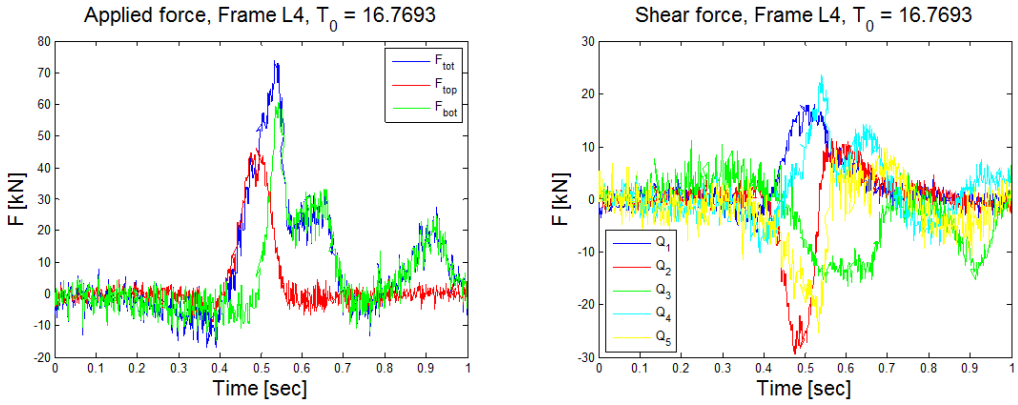

(a) (b)

Figure B.5: Estimated load, peak 15

Total force on frame at peak load : 79.7993 kN

$$\underbrace{\begin{bmatrix} \tau_1 \\ \tau_2 \\ \tau_3 \\ \tau_4 \\ \tau_5 \end{bmatrix}}_{\text{Measured Stress}} = \begin{bmatrix} 1.9353 \\ -0.463 \\ -1.6662 \\ 2.3069 \\ -2.583 \end{bmatrix} \tag{B.13}$$

$$\underbrace{\begin{bmatrix} \sigma_1 \\ \sigma_2 \\ \sigma_3 \\ \sigma_4 \\ \sigma_5 \end{bmatrix}}_{\text{Measured Stress}} = \begin{bmatrix} 3.6766 \\ 4.8413 \\ 3.038 \\ 7.0341 \\ 7.3236 \end{bmatrix} \tag{B.14}$$

$$\underbrace{\begin{bmatrix} Q_1 \\ Q_2 \\ Q_3 \\ Q_4 \\ Q_5 \end{bmatrix}}_{\text{Measured force}} = \begin{bmatrix} 15.9427 \\ -3.2205 \\ -13.847 \\ 20.7623 \\ -23.2473 \end{bmatrix} \tag{B.15}$$

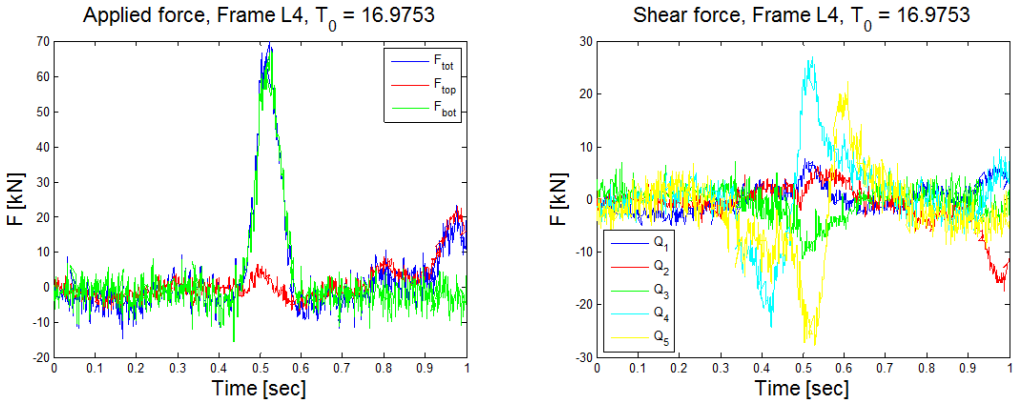

(a) (b)

Figure B.6: Estimated load, peak 38

Total force on frame at peak load : 69.7561 kN

$$\underbrace{\begin{bmatrix} \tau_1 \\ \tau_2 \\ \tau_3 \\ \tau_4 \\ \tau_5 \end{bmatrix}}_{\text{Measured Stress}} = \begin{bmatrix} 0.8642 \\ 0.5786 \\ -1.1927 \\ 3.0124 \\ -2.8459 \end{bmatrix} \tag{B.16}$$

$$\underbrace{\begin{bmatrix} \sigma_1 \\ \sigma_2 \\ \sigma_3 \\ \sigma_4 \\ \sigma_5 \end{bmatrix}}_{\text{Measured Stress}} = \begin{bmatrix} 1.7463 \\ 3.6752 \\ 1.9002 \\ 5.0997 \\ 6.0279 \end{bmatrix} \tag{B.17}$$

$$\underbrace{\begin{bmatrix} Q_1 \\ Q_2 \\ Q_3 \\ Q_4 \\ Q_5 \end{bmatrix}}_{\text{Measured force}} = \begin{bmatrix} 7.119 \\ 4.0246 \\ -9.9117 \\ 27.112 \\ -25.6134 \end{bmatrix} \tag{B.18}$$

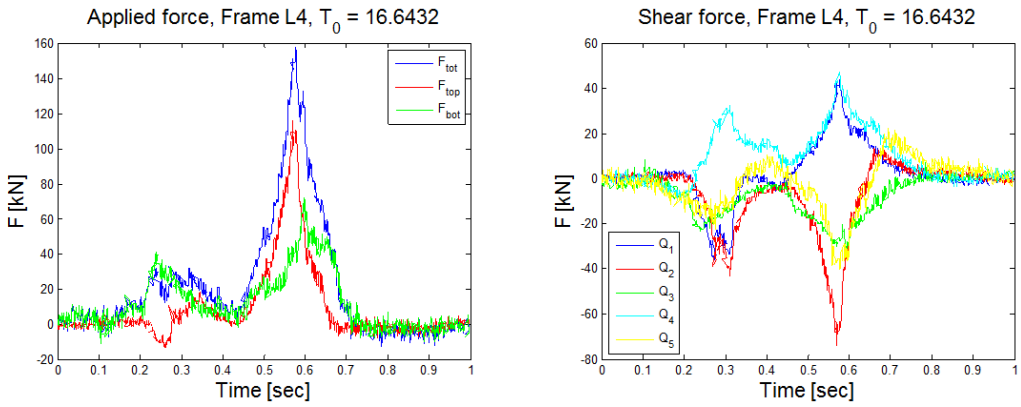

(a) (b)

Figure B.7: Estimated load, peak 2

Total force on frame at peak load : 157.5861 kN

$$\underbrace{\begin{bmatrix} \tau_1 \\ \tau_2 \\ \tau_3 \\ \tau_4 \\ \tau_5 \end{bmatrix}}_{\text{Measured Stress}} = \begin{bmatrix} 5.3365 \\ -9.5385 \\ -3.3159 \\ 5.0868 \\ -4.4764 \end{bmatrix} \tag{B.19}$$

$$\underbrace{\begin{bmatrix} \sigma_1 \\ \sigma_2 \\ \sigma_3 \\ \sigma_4 \\ \sigma_5 \end{bmatrix}}_{\text{Measured Stress}} = \begin{bmatrix} 5.4528 \\ 15.8045 \\ 5.4657 \\ 9.7403 \\ 8.686 \end{bmatrix} \tag{B.20}$$

$$\underbrace{\begin{bmatrix} Q_1 \\ Q_2 \\ Q_3 \\ Q_4 \\ Q_5 \end{bmatrix}}_{\text{Measured force}} = \begin{bmatrix} 43.9604 \\ -66.3508 \\ -27.5573 \\ 45.7811 \\ -40.2873 \end{bmatrix} \tag{B.21}$$

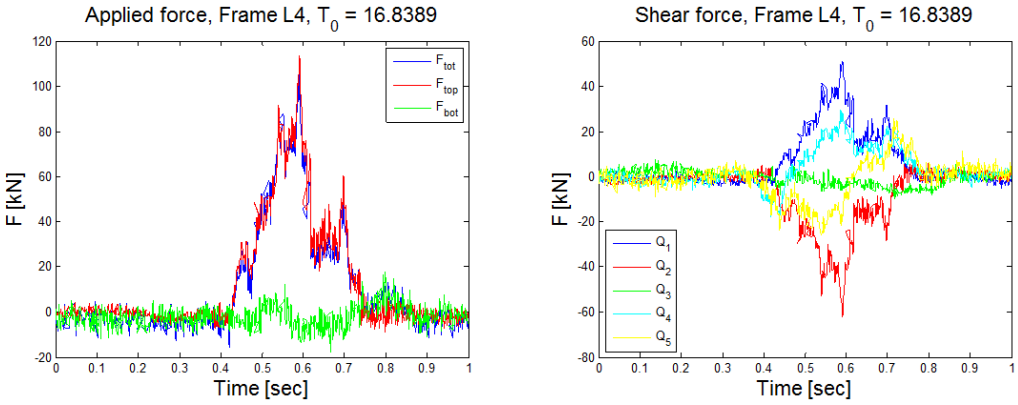

(a) (b)

Figure B.8: Estimated load, peak 23

Total force on frame at peak load : 104.9893 kN

$$\underbrace{\begin{bmatrix} \tau_1 \\ \tau_2 \\ \tau_3 \\ \tau_4 \\ \tau_5 \end{bmatrix}}_{\text{Measured Stress}} = \begin{bmatrix} 6.2086 \\ -8.1223 \\ -0.7454 \\ 3.0598 \\ -2.2346 \end{bmatrix} \tag{B.22}$$

$$\underbrace{\begin{bmatrix} \sigma_1 \\ \sigma_2 \\ \sigma_3 \\ \sigma_4 \\ \sigma_5 \end{bmatrix}}_{\text{Measured Stress}} = \begin{bmatrix} 12.0469 \\ 14.6945 \\ 0.9082 \\ 4.9519 \\ 4.8006 \end{bmatrix} \tag{B.23}$$

$$\underbrace{\begin{bmatrix} Q_1 \\ Q_2 \\ Q_3 \\ Q_4 \\ Q_5 \end{bmatrix}}_{\text{Measured force}} = \begin{bmatrix} 51.1444 \\ -56.4996 \\ -6.1947 \\ 27.5384 \\ -20.1118 \end{bmatrix} \tag{B.24}$$

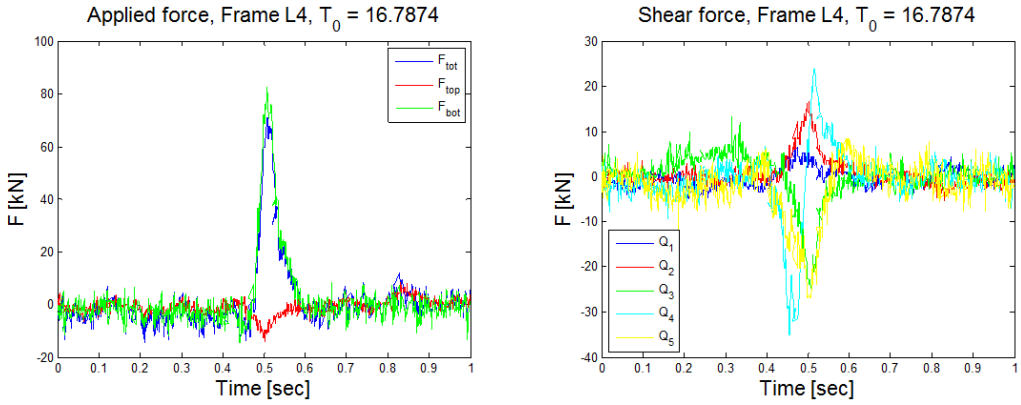

(a) (b)

Figure B.9: Estimated load, peak 19

Total force on frame at peak load : 71.1378 kN

$$\underbrace{\begin{bmatrix} \tau_1 \\ \tau_2 \\ \tau_3 \\ \tau_4 \\ \tau_5 \end{bmatrix}}_{\text{Measured Stress}} = \begin{bmatrix} 0.3878 \\ 2.0733 \\ -2.9691 \\ 1.9019 \\ -2.9057 \end{bmatrix} \tag{B.25}$$

$$\underbrace{\begin{bmatrix} \sigma_1 \\ \sigma_2 \\ \sigma_3 \\ \sigma_4 \\ \sigma_5 \end{bmatrix}}_{\text{Measured Stress}} = \begin{bmatrix} 1.2377 \\ 3.3048 \\ 5.0405 \\ 2.7968 \\ 5.2971 \end{bmatrix} \tag{B.26}$$

$$\underbrace{\begin{bmatrix} Q_1 \\ Q_2 \\ Q_3 \\ Q_4 \\ Q_5 \end{bmatrix}}_{\text{Measured force}} = \begin{bmatrix} 3.1949 \\ 14.4221 \\ -24.6749 \\ 17.117 \\ -26.151 \end{bmatrix} \tag{B.27}$$

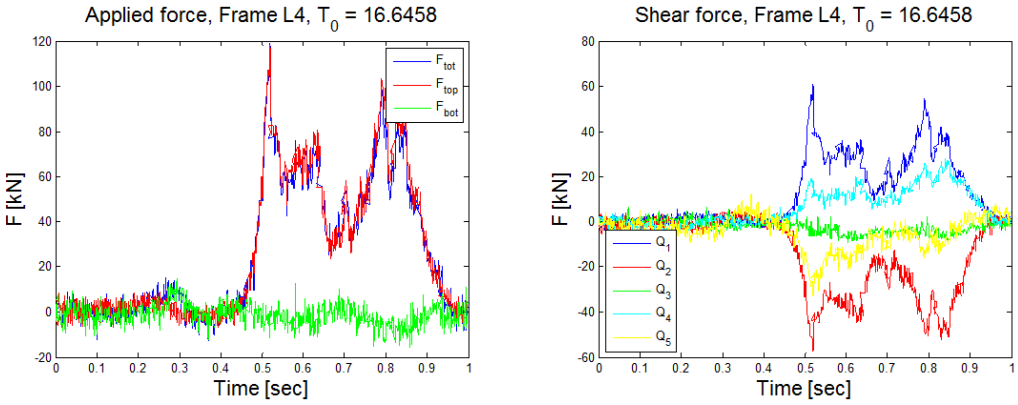

(a) (b)

Figure B.10: Estimated load, peak 5

Total force on frame at peak load : 118.8182 kN

$$\underbrace{\begin{bmatrix} \tau_1 \\ \tau_2 \\ \tau_3 \\ \tau_4 \\ \tau_5 \end{bmatrix}}_{\text{Measured Stress}} = \begin{bmatrix} 60.7994 \\ -57.2483 \\ -6.4985 \\ 18.6024 \\ -32.9179 \end{bmatrix} \tag{B.28}$$

$$\underbrace{\begin{bmatrix} \sigma_1 \\ \sigma_2 \\ \sigma_3 \\ \sigma_4 \\ \sigma_5 \end{bmatrix}}_{\text{Measured Stress}} = \begin{bmatrix} 16.8417 \\ 14.5436 \\ 1.311 \\ 3.677 \\ 5.7225 \end{bmatrix} \tag{B.29}$$

$$\underbrace{\begin{bmatrix} Q_1 \\ Q_2 \\ Q_3 \\ Q_4 \\ Q_5 \end{bmatrix}}_{\text{Measured force}} = \begin{bmatrix} 60.7994 \\ -57.2483 \\ -6.4985 \\ 18.6024 \\ -32.9179 \end{bmatrix} \tag{B.30}$$

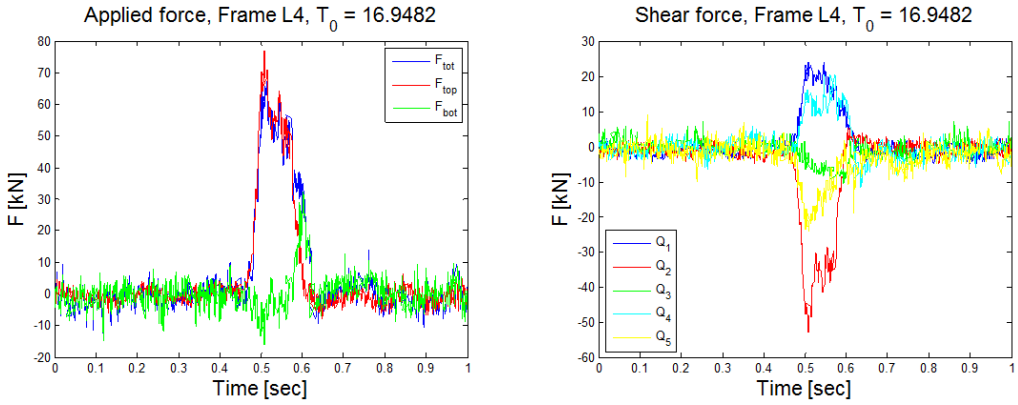

(a) (b)

Figure B.11: Estimated load, peak 33

Total force on frame at peak load : 67.2092 kN

$$\underbrace{\begin{bmatrix} \tau_1 \\ \tau_2 \\ \tau_3 \\ \tau_4 \\ \tau_5 \end{bmatrix}}_{\text{Measured Stress}} = \begin{bmatrix} 2.6768 \\ -6.8699 \\ -0.7977 \\ 1.6943 \\ -2.6142 \end{bmatrix} \tag{B.31}$$

$$\underbrace{\begin{bmatrix} \sigma_1 \\ \sigma_2 \\ \sigma_3 \\ \sigma_4 \\ \sigma_5 \end{bmatrix}}_{\text{Measured Stress}} = \begin{bmatrix} 3.8757 \\ 10.9453 \\ 3.5847 \\ 4.5352 \\ 4.3288 \end{bmatrix} \tag{B.32}$$

$$\underbrace{\begin{bmatrix} Q_1 \\ Q_2 \\ Q_3 \\ Q_4 \\ Q_5 \end{bmatrix}}_{\text{Measured force}} = \begin{bmatrix} 21.8033 \\ -47.7875 \\ -6.6291 \\ 15.2491 \\ -23.5277 \end{bmatrix} \tag{B.33}$$

Appendix C

Results from analysis

The following section contains different graphs from the analysis in chapter 7. The graphs are made for each of the 6 load levels, for the 4 different stress factors τ_{xy}, σ_x, σ_y and von Mises. The section also contains graphs for the 4 different stress factors at each of the sensor for the 6 load levels.

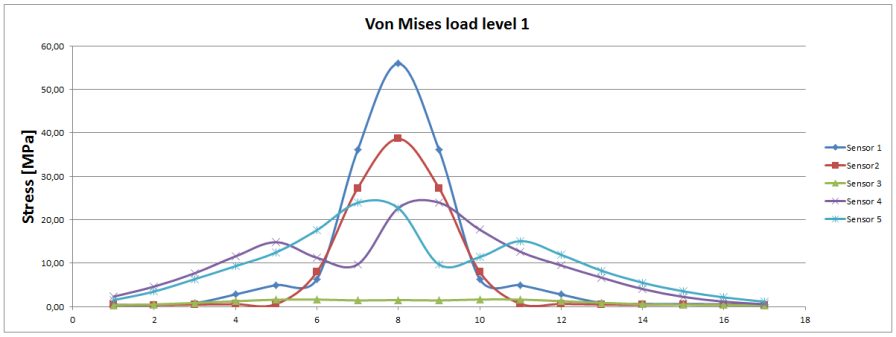

(a)

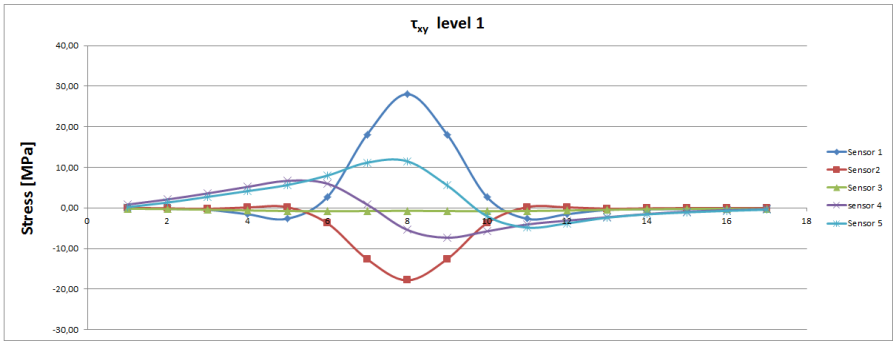

(b)

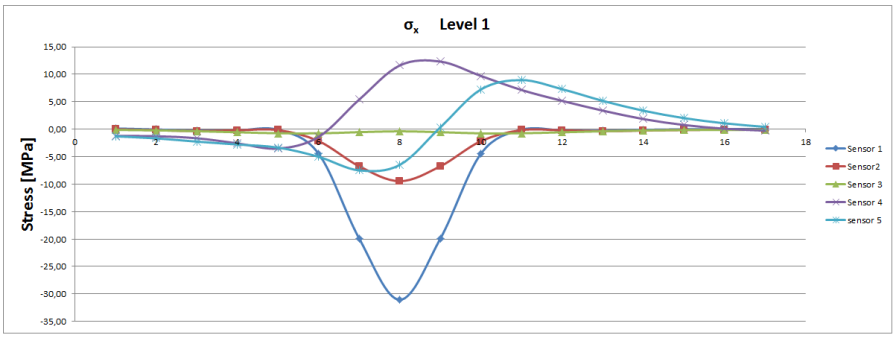

(c)

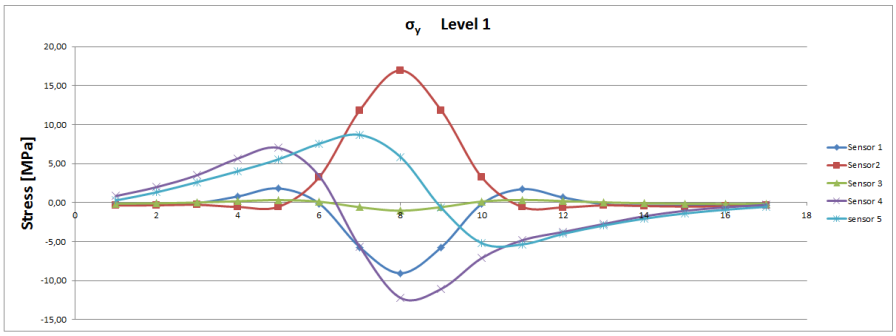

(d)

Figure C.1: The 4 different stress factor at Load level 1

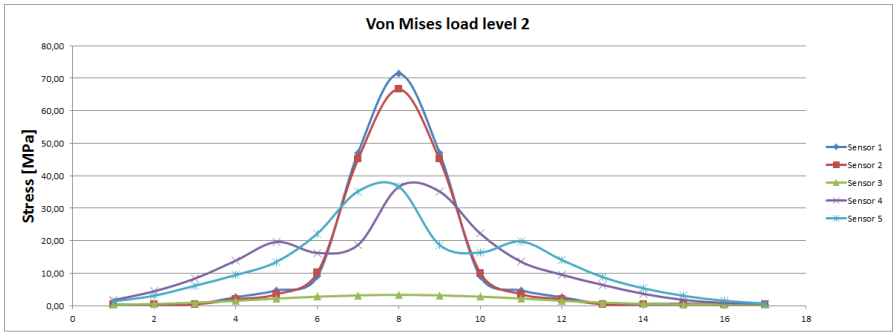

(a)

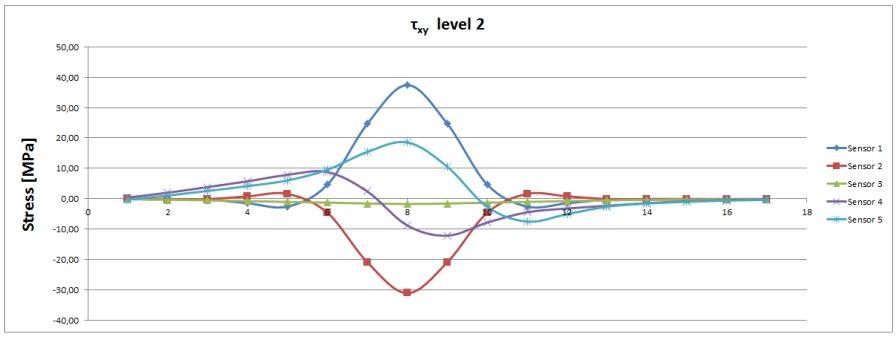

(b)

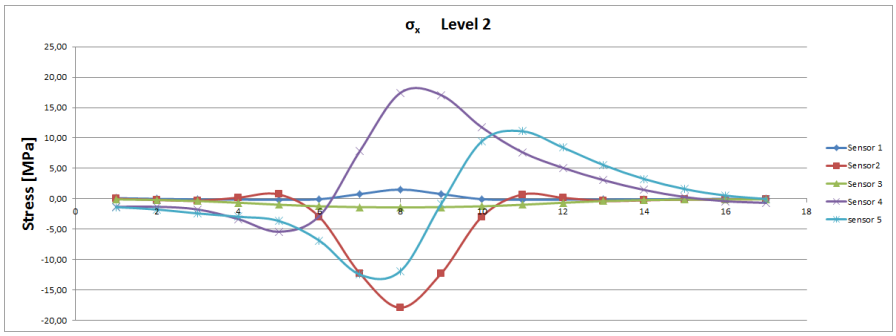

(c)

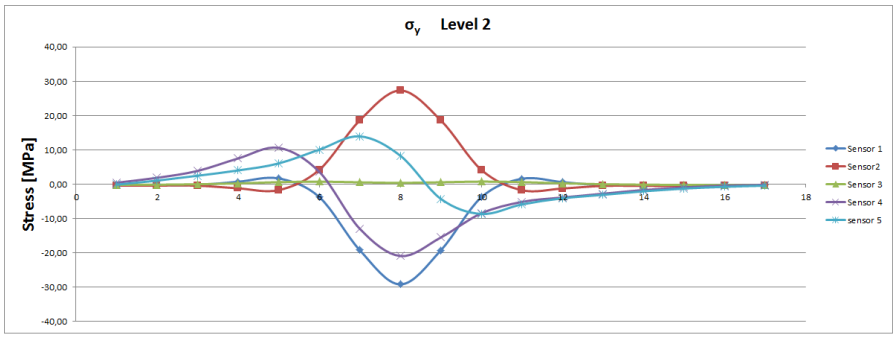

(d)

Figure C.2: The 4 different stress factor at Load level 2

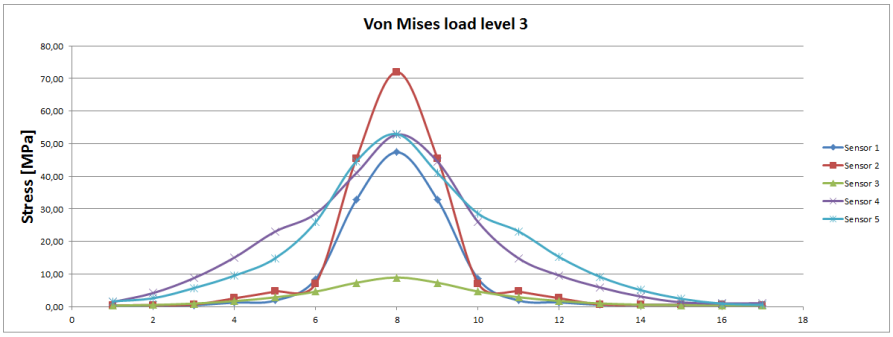

(a)

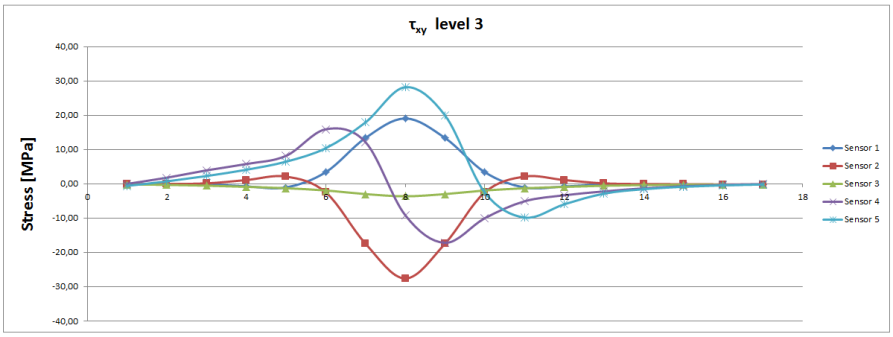

(b)

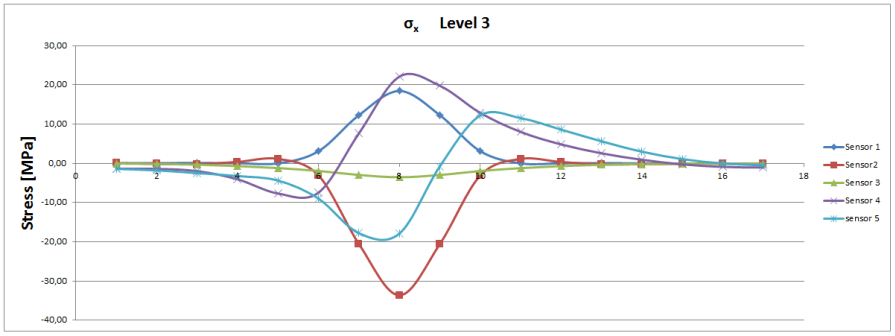

(c)

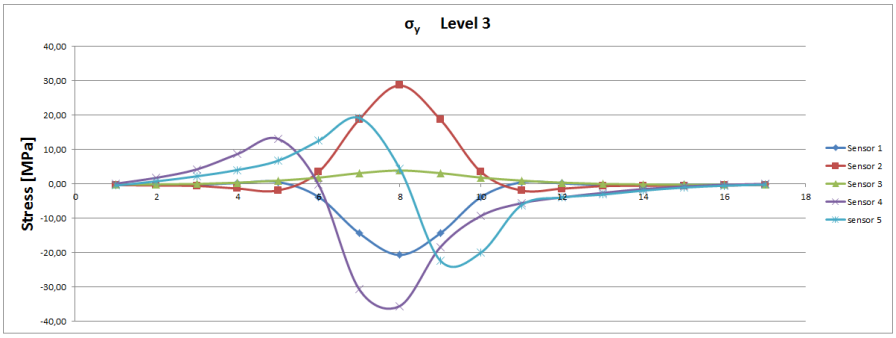

(d)

Figure C.3: The 4 different stress factor at Load level 3

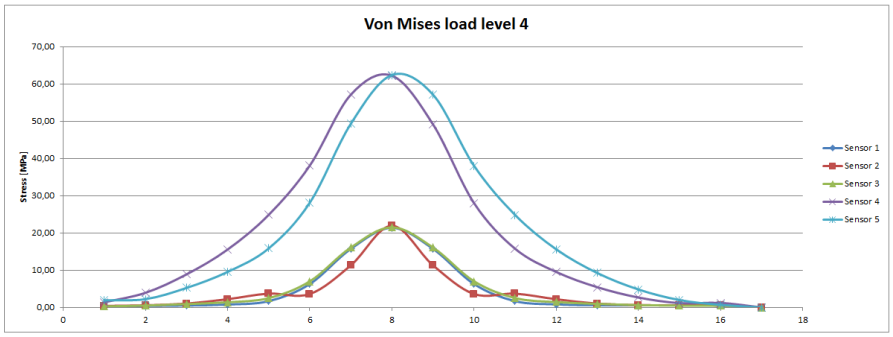

(a)

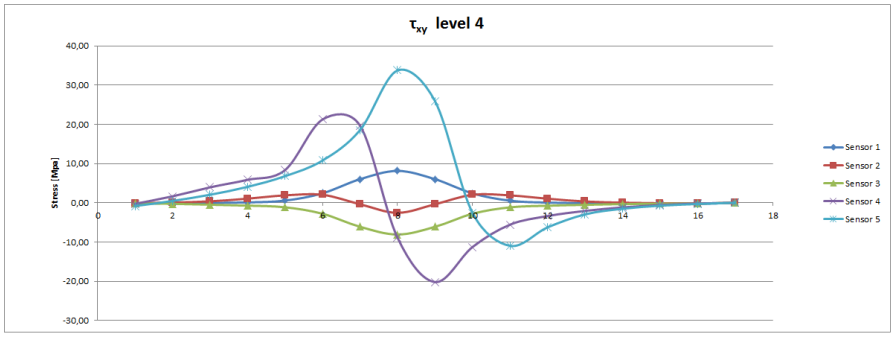

(b)

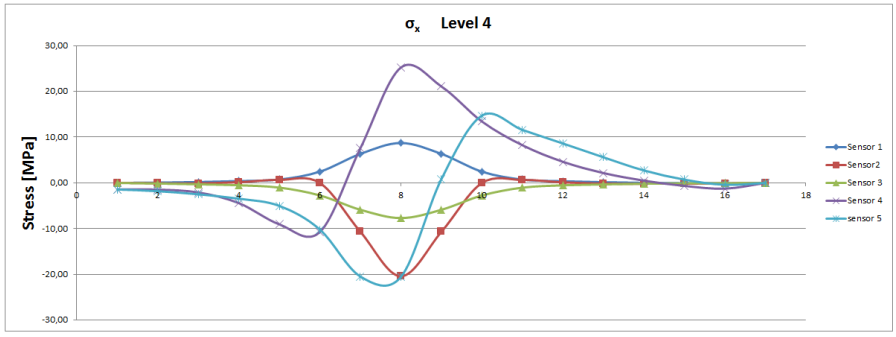

(c)

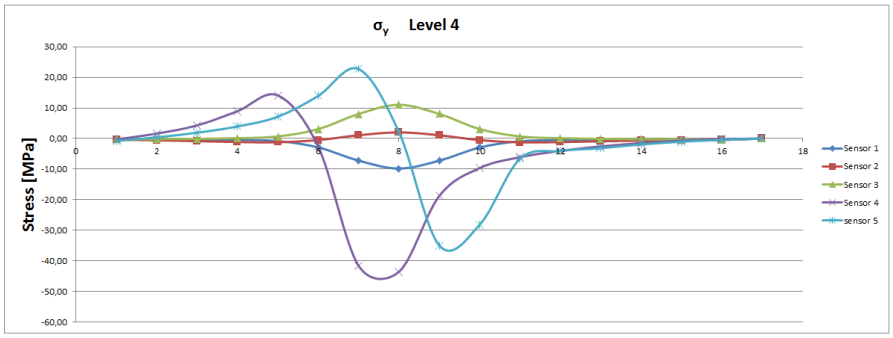

(d)

Figure C.4: The 4 different stress factor at Load level 4

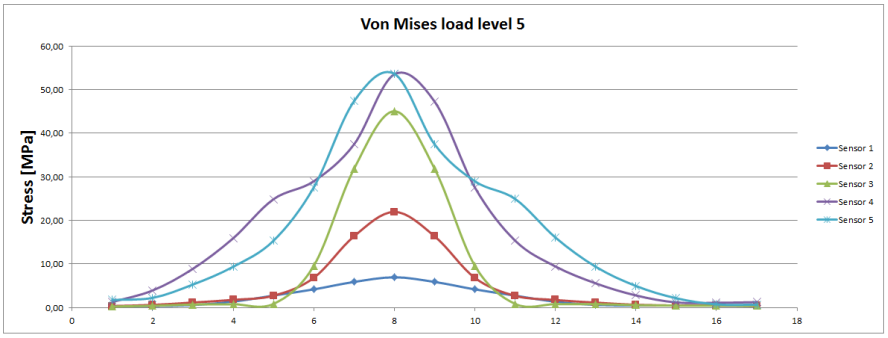

(a)

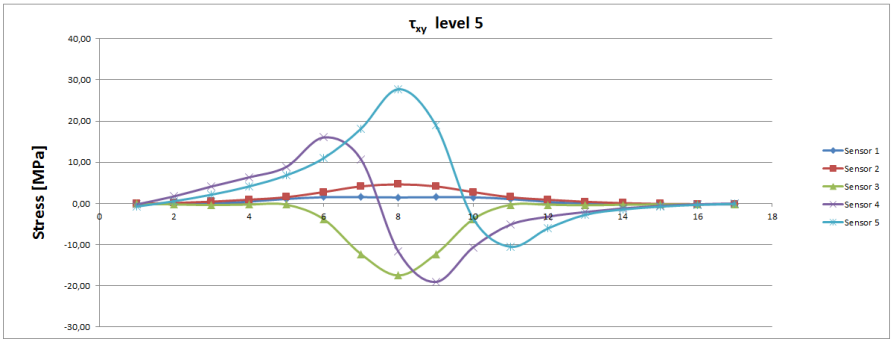

(b)

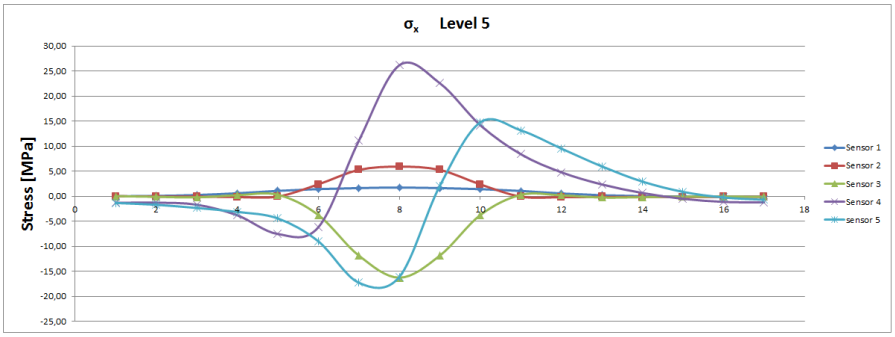

(c)

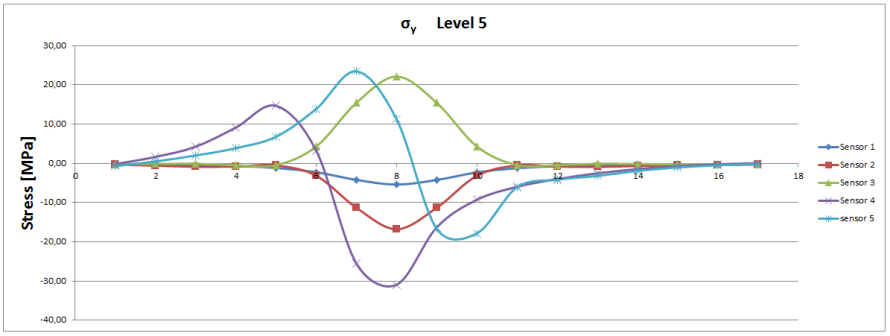

(d)

Figure C.5: The 4 different stress factor at Load level 5

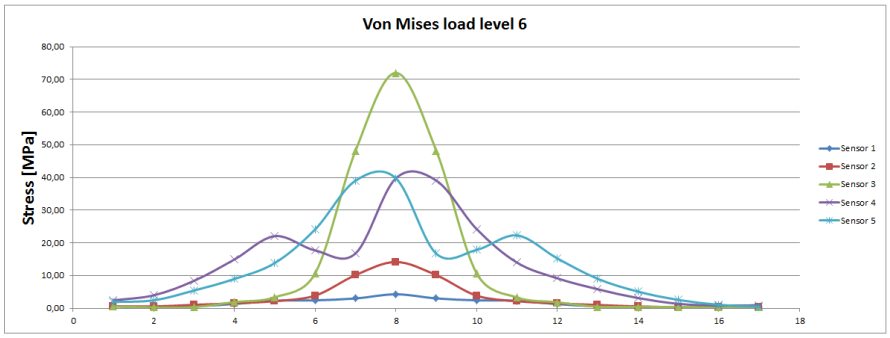

(a)

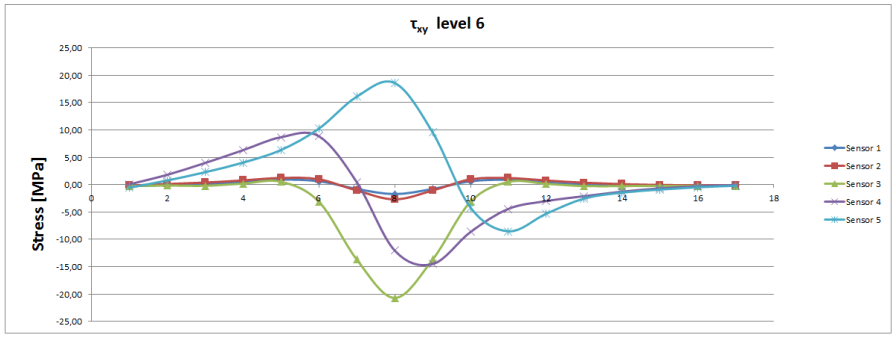

(b)

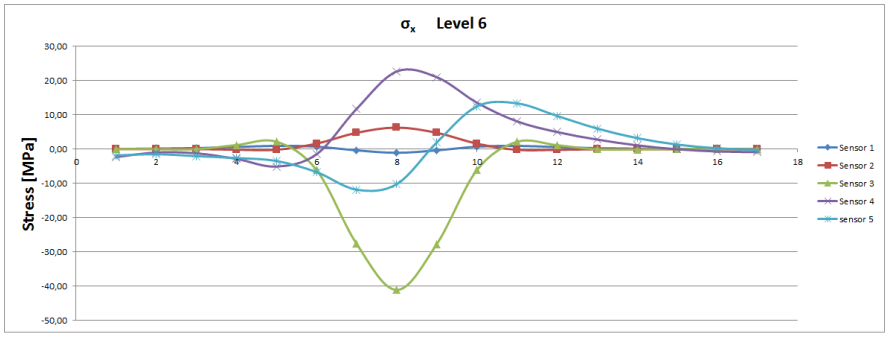

(c)

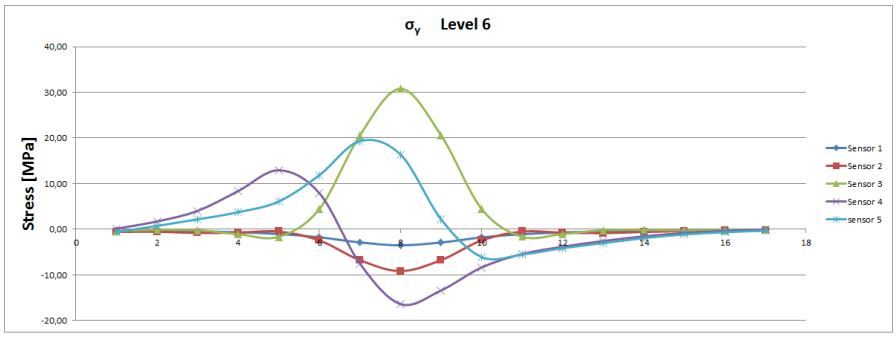

(d)

Figure C.6: The 4 different stress factor at Load level 6

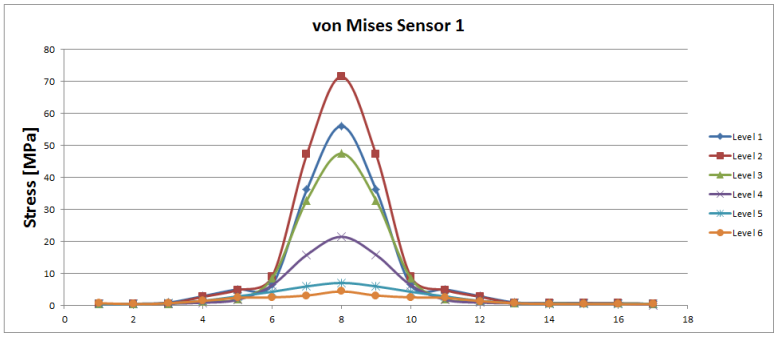

(a)

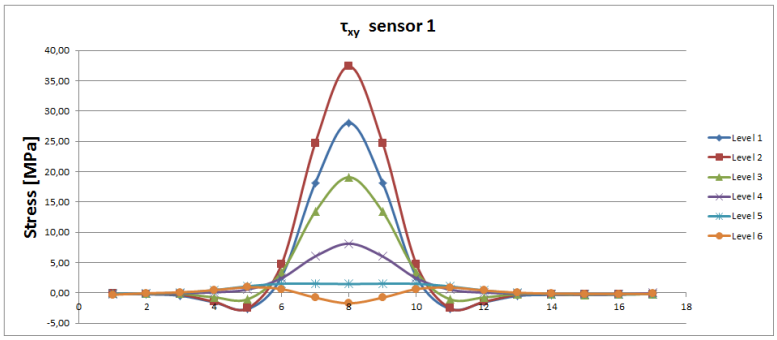

(b)

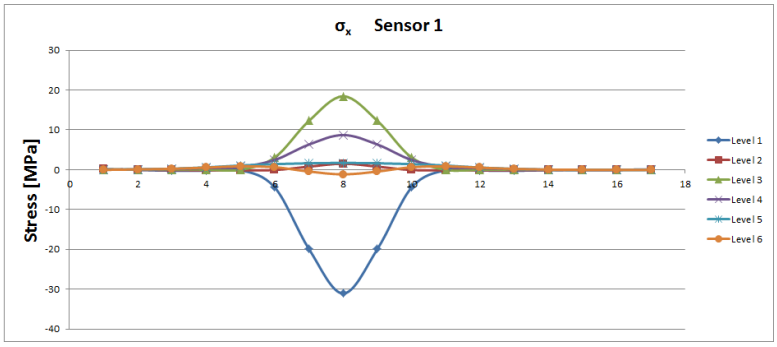

(c)

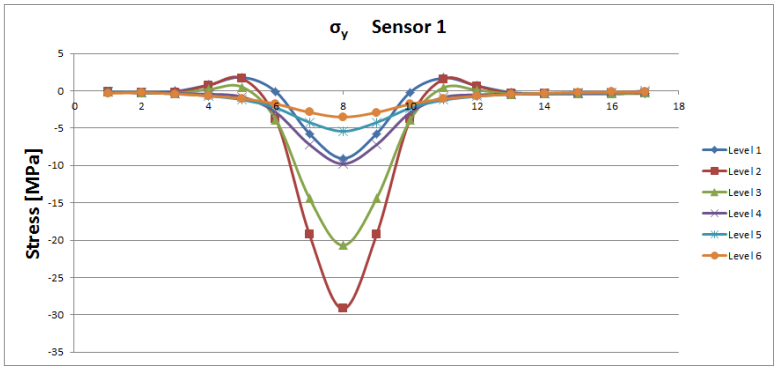

(d)

Figure C.7: The 4 different stress factor for sensor 1 at different load levels

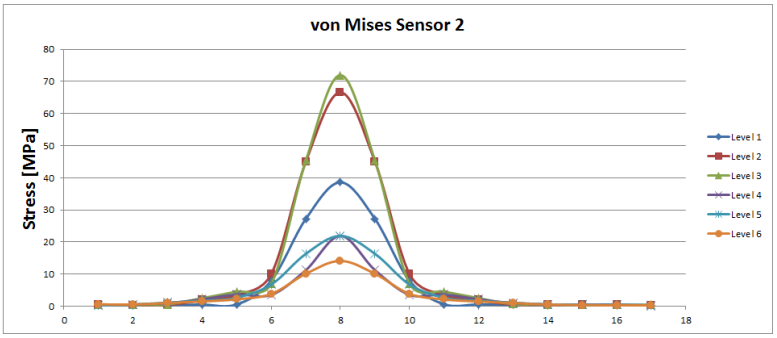

(a)

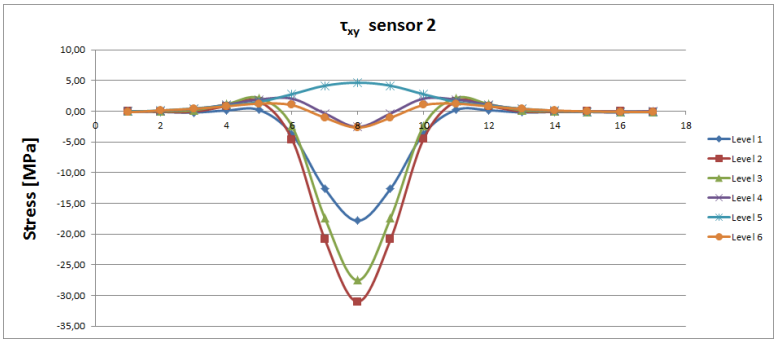

(b)

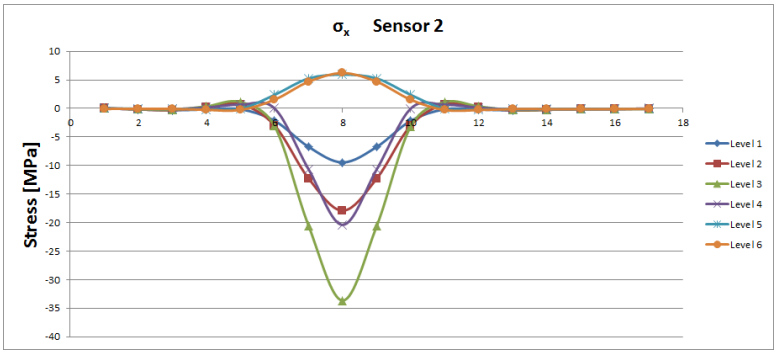

(c)

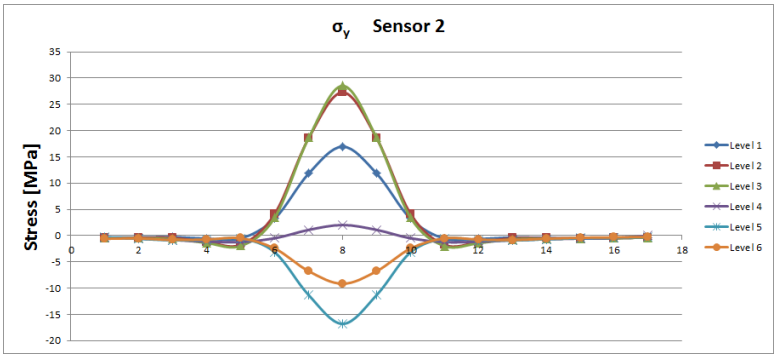

(d)

Figure C.8: The 4 different stress factor for sensor 2 at different load levels

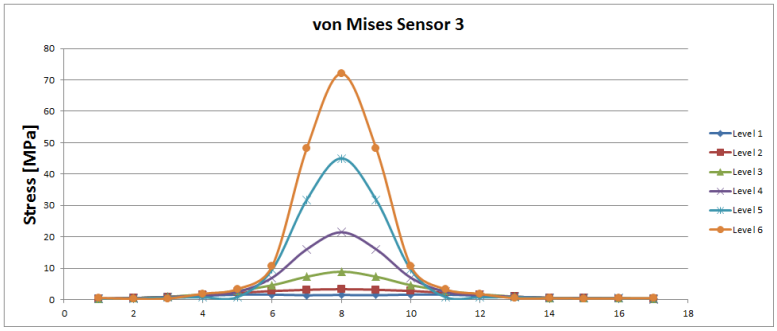

(a)

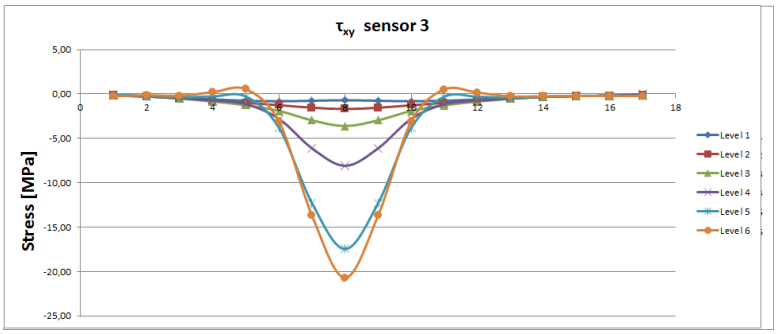

(b)

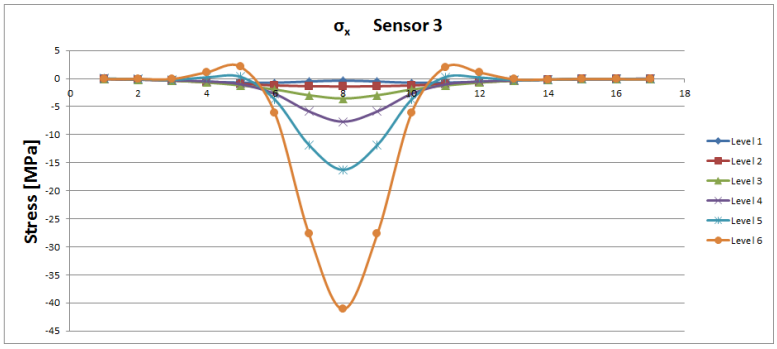

(c)

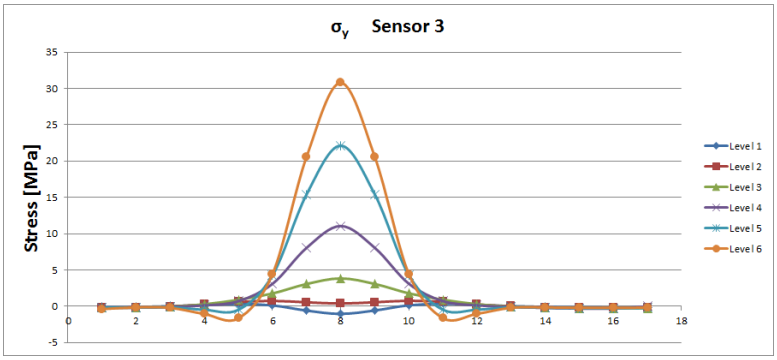

(d)

Figure C.9: The 4 different stress factor for sensor 3 at different load levels

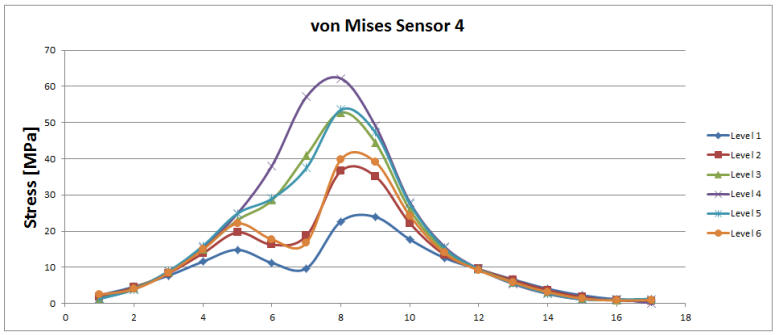

(a)

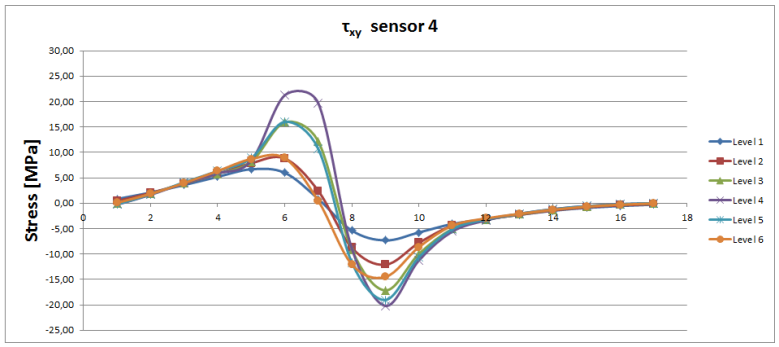

(b)

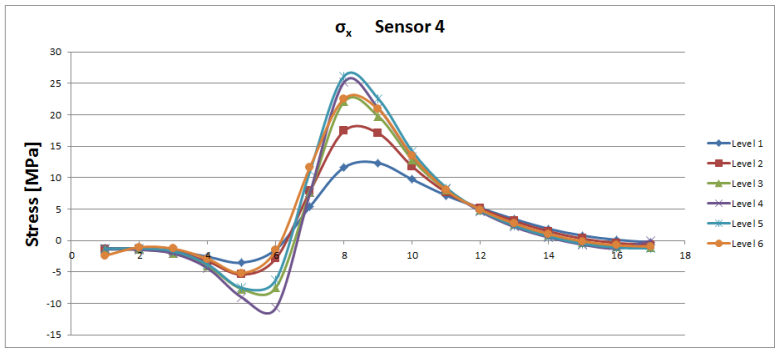

(c)

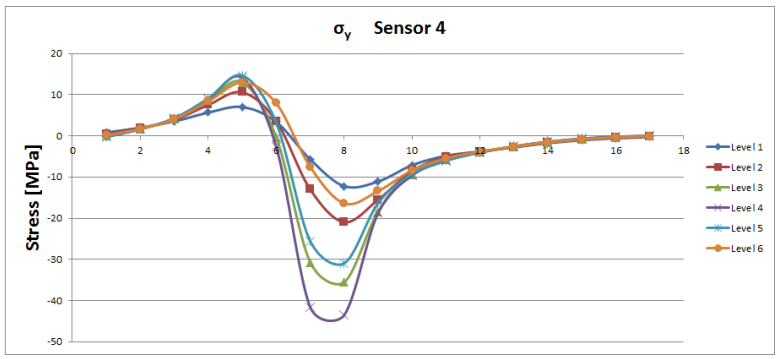

(d)

Figure C.10: The 4 different stress factor for sensor 4 at different load levels

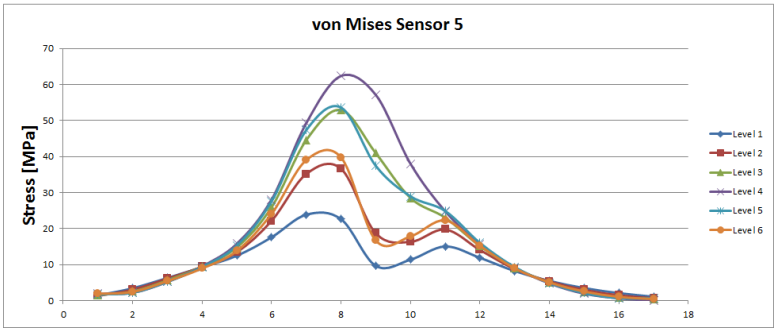

(a)

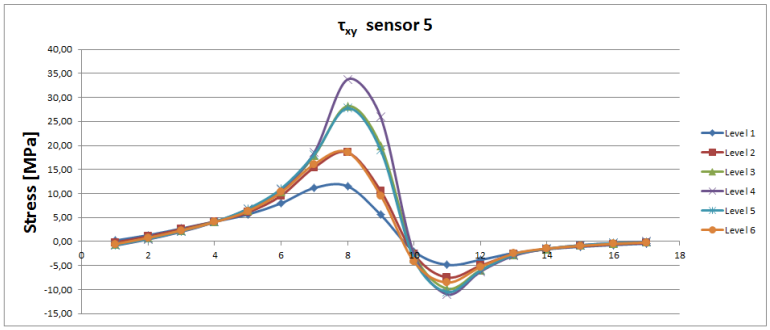

(b)

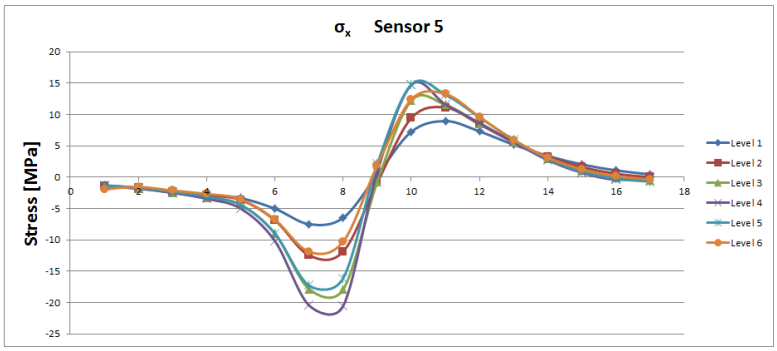

(c)

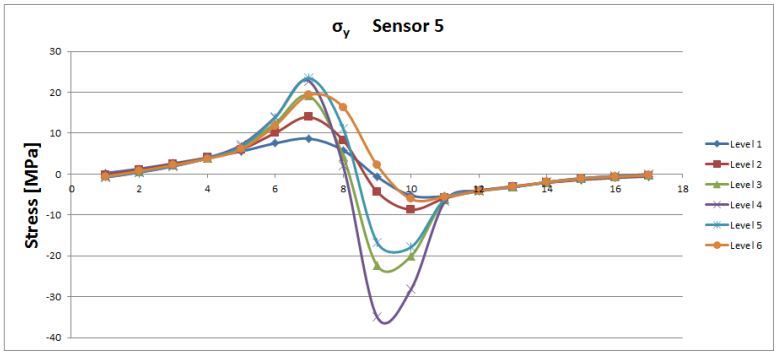

(d)

Figure C.11: The 4 different stress factor for sensor 5 at different load levels

Appendix D

Matlab code for load decision scheme

In this chapter, an example of matlabscript for the load decision scheme is presented. Here the load cases used is from Level one, and all the load peaks for shear stress and von Mises measured result from appendix B is used.

```
%% Equation Solver
clear all
%
%Loadcases on level 1

%shear stress input matrix for load cases in layer 1
m1= [-0.0909532 0.0377956   -0.174301   0.838916    0.219337;
-0.226509   -0.0979698  -0.273064   2.10031     1.33465;
-0.450937   -0.209408   -0.429619   3.58056     2.72037;
-1.53554    0.124399    -0.606704   5.19117     4.15186;
-2.65393    0.199129    -0.752979   6.68209     5.6429;
2.64973     -3.73825    -0.81163    5.99184     7.9635;
18.1099     -12.6154    -0.751501   0.83092     11.1608;
28.0498     -17.8287    -0.695017   -5.3893     11.5221;
18.1115     -12.6067    -0.754069   -7.33173    5.56596;
2.65148     -3.72135    -0.81048    -5.74972    -2.03374;
-2.655      0.224053    -0.758174   -4.07349    -4.84253;
-1.54521    0.15417     -0.613661   -3.11921    -3.80143;
-0.48102    -0.183573   -0.442541   -2.2821     -2.393;
-0.307742   -0.0961168  -0.29968    -1.48015    -1.5783;
-0.269165   -0.0150222  -0.223598   -0.911706   -1.08037;
-0.194186   -0.0158145  -0.1904     -0.542735   -0.708539;
-0.126093   -0.02288    -0.168291   -0.277996   -0.419845
    ]';

%von Mises input matrix for load cases in layer 1
m2= [0.318926   0.381613    0.326917    2.29819     1.49594;
0.432486    0.348629    0.503414    4.61483     3.46758;
0.812382    0.474381    0.824571    7.69532     6.32973;
2.80962     0.543126    1.23463     11.5749     9.31061;
4.96147     0.589743    1.5998      14.8322     12.4938;
6.35113     8.0128      1.62399     11.2257     17.6083;
36.0421     27.2535     1.41726     9.71823     23.8801;
55.9044     38.6081     1.5154      22.6707     22.6363;
36.0396     27.2375     1.41962     23.9335     9.68091;
6.32833     7.97896     1.63855     17.7014     11.4052;
4.92652     0.644453    1.61832     12.6058     15.0758;
2.78628     0.612599    1.25445     9.47        11.9137;
0.866228    0.475233    0.852491    6.63587     8.2383;
0.632436    0.416665    0.552141    4.04671     5.49299;
0.617359    0.460766    0.413981    2.24111     3.52738;
0.541026    0.430673    0.363277    1.14881     2.1247;
0.431512    0.340414    0.324214    0.555315    1.12448
    ]';

%Load peak 35
tau35 = [9.7743;    -13.8824;   -1.2717;    5.6296; -3.5788];
vm35 =  [17.5473; 23.8717; 2.6428; 11.0952; 7.2524];

%Loadpeak 13
tau13 = [9.0291; -12.401; -0.861; 4.0133; -3.7384];
vm13 =  [16.2892; 22.2957; 1.7863; 7.6517; 9.4726];

%Loadpeak 11
```

```
tau11 = [9.1808; -17.8833; -2.75; 8.0078; -4.8922];
vm11 =  [15.6717; 29.5784; 4.5344; 15.8043; 17.4294];

%Loadpeak 9

tau9 = [8.5689; 9.5009; -0.6612; 3.2416; -3.7008];
vm9 =  [15.6821; 16.5497; 1.6673; 5.2539; 7.0487];

%Loadpeak 15

tau15 = [1.9353; -0.463; -1.6662; 2.3069; -2.583];
vm15 =  [3.6766; 4.8413; 3.038; 7.0341; 7.3236];

%Loadpeak 38

tau38 = [0.8642; 0.5786; -1.1927; 3.0124; -2.8459];
vm38 = [1.7463; 3.6752; 1.9002; 5.0997; 6.0279];

%Load peak 2

tau2 = [5.3365; -9.5385; -3.3159; 5.0868; -4.4764];
vm2 =  [5.4528; 15.8045; 5.4657; 9.7403; 8.686];


%Load peak 23

tau23 = [6.2086; -8.1223; -0.7454; 3.0598; -2.2346];
vm23 =  [12.0469; 14.6945; 0.9082; 4.9519; 4.8006];

%Load peak 19

tau19 = [0.3878; 2.0733; -2.9691; 1.9019; -2.9057 ];
vm19 =  [1.2377; 3.3048; 5.0405; 2.7968; 5.2971 ];

%Load peak 5

tau5 = [7.3806; -8.2299; -0.782; 2.0669; -3.6575 ];
vm5 =  [16.8417; 14.5436; 1.311; 3.677; 5.7225 ];

%Load peak 33

tau33 = [2.6768; -6.8699; -0.7977; 1.6943; -2.6142 ];
vm33 =  [3.8757; 10.9453; 3.5847; 4.5352; 4.3288 ];

s = fopen('layer1.txt', 'w'); % open the txt file

t1 = zeros(5:5);
t2 = zeros(5:5);
h = waitbar(0,'please wait');

c=length(m1);
counter =zeros(c,1);

for i=1:c
    waitbar(i/c);
```

```
    for j=i:c
        for k=j:c
            for l=k:c
                for m=l:c

                    %Only one of the load case in each matrix
                    if i==j || i==k || i==l || i==m || j==k || j==l || j==m || k==l ||↙
k==m || l==m

                    else
                        %Shear stress matrices
                        t1(:,1)= m1(:,i);
                        t1(:,2)= m1(:,j);
                        t1(:,3)= m1(:,k);
                        t1(:,4)= m1(:,l);
                        t1(:,5)= m1(:,m);

                        %von Mises matrices
                        t2(:,1)= m2(:,i);
                        t2(:,2)= m2(:,j);
                        t2(:,3)= m2(:,k);
                        t2(:,4)= m2(:,l);
                        t2(:,5)= m2(:,m);

                        %Calculates the load factors for all shear stress peaks
                        TAU35 =tau35\t1;
                        TAU13 =tau13\t1;
                        TAU11 =tau11\t1;
                        TAU9 =tau9\t1;
                        TAU15 =tau15\t1;
                        TAU38 =tau38\t1;
                        TAU2 =tau2\t1;
                        TAU23 =tau23\t1;
                        TAU19 =tau19\t1;
                        TAU5 =tau5\t1;
                        TAU33=tau33\t1;

                         %Calculates the load factors for all von mises stress peaks
                        VM35 =vm35\t2;
                        VM13 =vm13\t2;
                        VM11 =vm11\t2;
                        VM9 =vm9\t2;
                        VM15 =vm15\t2;
                        VM38 =vm38\t2;
                        VM2 =vm2\t2;
                        VM23 =vm23\t2;
                        VM19 =vm19\t2;
                        VM5 =vm5\t2;
                        VM33 =vm33\t2;

                        %Check if the load factors are positive for shear stress
                        TAU35(TAU35<0)=[];
                        TAU13(TAU13<0)=[];
                        TAU11(TAU11<0)=[];
                        TAU9(TAU9<0)=[];
```

```
                        TAU15(TAU15<0)=[];
                        TAU38(TAU38<0)=[];
                        TAU2(TAU2<0)=[];
                        TAU23(TAU23<0)=[];
                        TAU19(TAU19<0)=[];
                        TAU5(TAU5<0)=[];
                        TAU33(TAU33<0)=[];

                        %Check if the load factors are positive for von Mises stress
                        VM35(VM35<0)=[];
                        VM13(VM13<0)=[];
                        VM11(VM11<0)=[];
                        VM9(VM9<0)=[];
                        VM15(VM15<0)=[];
                        VM38(VM38<0)=[];
                        VM2(VM2<0)=[];
                        VM23(VM23<0)=[];
                        VM19(VM19<0)=[];
                        VM5(VM5<0)=[];
                        VM33(TAU33<0)=[];

                    % Requires that load peak 35, 13, 11, 15, 2, 23, 5, 33
                        if  length(TAU35)==5 && length(TAU13)==5  && length(TAU11)==5↙
&& length(TAU15)==5 && length(TAU2)==5 && length(TAU23)==5 && length(TAU5)==5 && length↙
(TAU33)==5 ...
                            length(VM35)==5 && length(VM13)==5  && length(VM11)==5 &&↙
length(VM15)==5 && length(VM2)==5 && length(VM23)==5 && length(VM5)==5 && length(VM33)↙
==5 ;

                        fprintf(s,'loadcase %3d %3d %3d %3d %3d\n',i, j, k, l, m);

                        %Counts which load cases that are used
                            counter(i,1)=counter(i,1) + 1;
                            counter(j,1)=counter(j,1) + 1;
                            counter(k,1)=counter(k,1) + 1;
                            counter(l,1)=counter(l,1) + 1;
                            counter(m,1)=counter(m,1) + 1;
                        end
                    end
                end
            end
        end
    end
end

close(h)
```

Appendix E

Load case results for each Load peak measurement

In this chapter we will present tables the load cases that gives positive load factors for each load peak presented in appendix B

Load case\Level	Level 1	Level 2	Level 3	Level 4	Level 5	Level 6
1	✓	✓	✓	✓	✓	✓
2	✓	✓	✓	✓	✓	✓
3	✓	✓	✓	✓	✓	✓
4				✓	✓	✓
5				✓	✓	✓
6	✓	✓	✓	✓	✓	✓
7	✓	✓	✓	✓		
8	✓	✓	✓			
9	✓	✓	✓			
10	✓	✓	✓			
11						
12						
13						
14						
15						
16				✓	✓	✓
17			✓	✓	✓	✓

Table E.1: Shows how many times each of the 102 load cases satisfy as a positive load factor for the peak load 35

Load case\Level	Level 1	Level 2	Level 3	Level 4	Level 5	Level 6
1	✓	✓	✓	✓	✓	✓
2	✓	✓	✓	✓	✓	✓
3	✓	✓	✓	✓	✓	✓
4					✓	✓
5					✓	✓
6	✓	✓	✓	✓	✓	
7	✓	✓	✓	✓		
8	✓	✓	✓			
9	✓	✓	✓			
10	✓	✓	✓			
11				✓	✓	✓
12					✓	✓
13						
14						
15						
16				✓	✓	✓
17		✓	✓	✓	✓	✓

Table E.2: Shows how many times each of the 102 load cases satisfy as a positive load factor for the peak load 13

Load case\Level	Level 1	Level 2	Level 3	Level 4	Level 5	Level 6
1	✓	✓	✓	✓	✓	✓
2	✓	✓	✓	✓	✓	✓
3	✓	✓	✓	✓	✓	✓
4	✓		✓	✓	✓	✓
5	✓			✓	✓	✓
6	✓	✓	✓	✓	✓	✓
7	✓	✓	✓	✓		
8	✓	✓	✓			
9	✓	✓	✓			
10	✓	✓	✓			
11						
12						
13						
14						
15						
16			✓	✓	✓	✓
17		✓	✓	✓	✓	✓

Table E.3: Shows how many times each of the 102 load cases satisfy as a positive load factor for the peak load 11

Load case\Level	Level 1	Level 2	Level 3	Level 4	Level 5	Level 6
1	✓	✓	✓	✓	✓	
2		✓	✓	✓	✓	✓
3		✓	✓	✓	✓	✓
4			✓	✓	✓	✓
5			✓	✓	✓	✓
6		✓	✓	✓	✓	✓
7		✓		✓	✓	
8	✓	✓				
9		✓				
10		✓		✓	✓	✓
11			✓	✓	✓	✓
12			✓	✓	✓	✓
13			✓	✓	✓	✓
14				✓	✓	✓
15						
16						
17		✓				

Table E.4: Shows how many times each of the 102 load cases satisfy as a positive load factor for the peak load 9

Load case\Level	Level 1	Level 2	Level 3	Level 4	Level 5	Level 6
1	✓	✓	✓	✓	✓	✓
2	✓	✓	✓	✓	✓	✓
3	✓	✓	✓	✓	✓	✓
4		✓	✓	✓	✓	✓
5			✓	✓	✓	✓
6	✓	✓	✓	✓	✓	
7	✓	✓	✓	✓		
8	✓	✓				
9	✓	✓				
10	✓	✓				
11		✓	✓	✓	✓	✓
12	✓	✓	✓	✓	✓	✓
13	✓	✓	✓	✓	✓	✓
14	✓	✓	✓	✓	✓	✓
15	✓	✓	✓	✓	✓	✓
16	✓	✓	✓	✓	✓	✓
17	✓	✓	✓	✓	✓	✓

Table E.5: Shows how many times each of the 102 load cases satisfy as a positive load factor for the peak load 15

Load case\Level	Level 1	Level 2	Level 3	Level 4	Level 5	Level 6
1	✓	✓	✓	✓	✓	✓
2	✓	✓	✓	✓	✓	✓
3	✓	✓	✓	✓	✓	✓
4	✓	✓	✓	✓	✓	✓
5	✓	✓	✓	✓	✓	✓
6		✓	✓	✓	✓	✓
7				✓		
8						
9						
10						
11	✓	✓	✓	✓	✓	✓
12	✓	✓	✓	✓	✓	✓
13		✓	✓	✓	✓	✓
14	✓	✓	✓	✓	✓	✓
15	✓	✓	✓	✓	✓	✓
16	✓	✓	✓	✓	✓	✓
17	✓	✓	✓	✓	✓	✓

Table E.6: Shows how many times each of the 102 load cases satisfy as a positive load factor for the peak load 38

Load case\Level	Level 1	Level 2	Level 3	Level 4	Level 5	Level 6
1	✓	✓	✓	✓	✓	✓
2	✓	✓	✓	✓	✓	✓
3	✓	✓	✓	✓	✓	✓
4	✓			✓	✓	✓
5				✓	✓	✓
6	✓	✓	✓	✓	✓	✓
7	✓	✓	✓	✓		
8	✓	✓	✓			
9	✓	✓	✓			
10	✓	✓	✓			
11				✓	✓	✓
12				✓	✓	✓
13		✓	✓	✓		
14		✓	✓	✓		
15			✓	✓	✓	✓
16	✓	✓	✓	✓	✓	✓
17	✓	✓	✓	✓	✓	✓

Table E.7: Shows how many times each of the 102 load cases satisfy as a positive load factor for the peak load 2

Load case\Level	Level 1	Level 2	Level 3	Level 4	Level 5	Level 6
1	✓	✓	✓	✓	✓	✓
2	✓	✓	✓	✓	✓	✓
3	✓	✓	✓	✓	✓	✓
4				✓	✓	✓
5					✓	✓
6	✓	✓	✓	✓	✓	✓
7	✓	✓	✓	✓		
8	✓	✓	✓			
9	✓	✓	✓			
10	✓	✓	✓			
11					✓	✓
12						
13						
14						
15						
16				✓	✓	✓
17			✓	✓	✓	✓

Table E.8: Shows how many times each of the 102 load cases satisfy as a positive load factor for the peak load 23

Load case\Level	Level 1	Level 2	Level 3	Level 4	Level 5	Level 6
1	✓	✓	✓	✓	✓	✓
2	✓	✓	✓	✓	✓	✓
3		✓	✓	✓	✓	✓
4		✓	✓	✓	✓	✓
5		✓	✓	✓	✓	
6			✓	✓	✓	
7				✓	✓	
8						
9						
10					✓	✓
11	✓	✓	✓	✓	✓	✓
12	✓	✓	✓	✓	✓	✓
13	✓	✓	✓	✓	✓	✓
14	✓	✓	✓	✓	✓	✓
15	✓	✓	✓	✓	✓	✓
16	✓	✓	✓	✓	✓	✓
17	✓	✓	✓	✓	✓	✓

Table E.9: Shows how many times each of the 102 load cases satisfy as a positive load factor for the peak load 19

Load case\Level	Level 1	Level 2	Level 3	Level 4	Level 5	Level 6
1	✓	✓	✓	✓	✓	✓
2			✓	✓	✓	
3						
4						
5						
6	✓	✓	✓	✓		
7	✓	✓	✓	✓		
8	✓	✓	✓			
9	✓	✓	✓			
10	✓	✓	✓			
11			✓	✓	✓	✓
12			✓	✓	✓	✓
13	✓	✓	✓	✓	✓	✓
14	✓	✓	✓	✓	✓	✓
15	✓	✓	✓	✓	✓	✓
16	✓	✓	✓	✓	✓	✓
17	✓	✓	✓	✓	✓	✓

Table E.10: Shows how many times each of the 102 load cases satisfy as a positive load factor for the peak load 5

Load case\Level	Level 1	Level 2	Level 3	Level 4	Level 5	Level 6
1	✓	✓	✓	✓	✓	✓
2	✓	✓	✓	✓	✓	✓
3						
4						
5						
6	✓	✓	✓	✓		
7	✓	✓	✓	✓		
8	✓	✓	✓			
9	✓	✓	✓			
10	✓	✓	✓			
11			✓	✓	✓	✓
12			✓	✓	✓	✓
13	✓	✓	✓	✓	✓	✓
14	✓	✓	✓	✓	✓	✓
15	✓	✓	✓	✓	✓	✓
16	✓	✓	✓	✓	✓	✓
17	✓	✓	✓	✓	✓	✓

Table E.11: Shows how many times each of the 102 load cases satisfy as a positive load factor for the peak load 33

LC\Level	Level 1	Level 2	Level 3	Level 4	Level 5	Level 6
1	0,0282026	0,0375681	0,0280674	0,0274483	0,0260677	0,0335006
2	0,0386846	0,0436978	0,0496764	0,0528296	0,0522497	0,0495845
3	0,0519981	0,0612692	0,0895362	0,1039233	0,1079068	0,0880182
4	0,0610019	0,1095139	0,1315726	0,1122833	0,1214605	0,1091607
5	0,0709330	0,1639067	0,1823974	0,1367975	0,1247738	0,1255814
6	0,2556103	0,3531200	0,4711005	0,5722217	0,3967022	0,0615607
7	1,1504221	1,5660795	1,3759851	0,4132889	0,4032385	0
8	1,4838119	2,1253879	1,5758464	0	0	0
9	1,0760835	1,3009026	0,7720590	0	0	0
10	0,2172806	0,2770516	0,1321768	0,0797229	0,2121643	0,1559410
11	0,1644850	0,3445597	0,4411197	0,4399819	0,3809317	0,2743207
12	0,1133800	0,2444306	0,2509472	0,2657358	0,2264328	0,1760447
13	0,0586140	0,0561884	0,0822756	0,0990511	0,1005534	0,0753691
14	0,0330388	0,0324138	0,0422292	0,0417304	0,0438179	0,0381285
15	0,0278324	0,0278218	0,0219085	0,0227912	0,0249724	0,0288992
16	0,0203666	0,0195257	0,0126022	0,0082796	0,0101020	0,0137045
17	0,0177051	0,0113637	0,0079705	0,0071923	0,0086307	0,0119306

Table E.12: Shows the average load factors for each of the 102 load cases that satisfies as a positive load factor of the 11 peak loads

Appendix F

Electronic appendix

The electronic appendix in zip file contains the following

- Patran modelling file
- Excel diagrams
- Matlab codes
- Figures used in this report